

PROTON STATES OF DEFORMED NUCLEI WITH $A = 153$ TO $A = 163$

by

JOHN CHARLES TIPPETT, B.Sc.

A Thesis

Submitted to the Faculty of Graduate Studies

in Partial Fulfilment of the Requirements

for the Degree

Doctor of Philosophy

McMaster University

November 1972

DOCTOR OF PHILOSOPHY (1972)
(Physics).

McMASTER UNIVERSITY
Hamilton, Ontario.

TITLE: Proton States of Deformed Nuclei with $A = 153$ to $A = 163$

AUTHOR: John Charles Tippett, B.Sc. (University of Victoria)

SUPERVISOR: Professor D. G. Burke

NUMBER OF PAGES: x, 138

SCOPE AND CONTENTS:

Proton states of ^{153}Eu , ^{155}Eu , ^{155}Tb , ^{157}Tb , ^{159}Tb , ^{161}Tb and ^{163}Ho have been studied using the (α, t) and $(^3\text{He}, d)$ reactions. Beams of 24 MeV ^3He and 25 MeV alpha particles were produced by the McMaster University model FN tandem Van de Graaff accelerator. The reaction products were analyzed with an Enge split-pole magnetic spectrograph and detected with photographic emulsions. Ratios of the cross sections between the (α, t) and $(^3\text{He}, d)$ reactions were used as an indication of the l -values for the proton transfers, and the spectroscopic factors were extracted using DWBA calculations. Interpretation of the results is made in terms of the Unified Model.

The results of the present work confirm the assignments of the $3/2^+[411]$ and $5/2^+[413]$ Nilsson orbitals in the terbium isotopes. The $I = 11/2$ members of the $5/2^- [532]$ and $7/2^- [523]$ orbitals are identified in ^{161}Tb and ^{159}Tb and their assignments confirmed in ^{157}Tb and ^{155}Tb . It is necessary to invoke appreciable Coriolis mixing between these two orbitals in order to describe the observed rotational level spacings and the spectroscopic strengths. The assignment of the $7/2^+[404]$ orbital is confirmed in ^{155}Tb and ^{157}Tb and this orbital is identified

in ^{159}Tb and ^{161}Tb . Previous assignments of the $1/2^+[411]$ particle state with vibrational admixtures are confirmed in ^{157}Tb and ^{159}Tb and the state is identified in ^{161}Tb . The present results support the earlier evidence for the existence of a second fragment of the $1/2^+[411]$ orbital in ^{159}Tb and suggest the presence of a similar state in ^{157}Tb . The assignment of the $5/2^+[402]$ orbital is made and tentative assignment of the $1/2^-[541]$ orbital is considered for each of the terbium isotopes. In ^{163}Ho , the assignments of the $7/2^-[523]$ and $7/2^+[404]$ orbitals are confirmed, and strong evidence for the assignment of the $3/2^+[411]$, $1/2^+[411]$, $5/2^+[402]$ and $1/2^-[541]$ orbitals is found. In the europium isotopes, the assignments of the $5/2^+[413]$, $3/2^+[411]$ and $5/2^-[532]$ orbitals are confirmed, and evidence for the assignment of the $7/2^-[523]$, $1/2^+[411]$, $7/2^+[404]$ and $1/2^-[541]$ orbitals is considered.

ACKNOWLEDGEMENTS

I would like to thank Dennis Burke, my supervisor, for his direction and guidance in my research, and for much of my present enthusiasm for nuclear spectroscopy.

Thanks are also due to the members of my supervisory committee, Drs. J. Kuehner and G. Keech for their patience and co-operation.

I am grateful for the help and consideration given to me by many of my colleagues, especially:

Erle Nelson and Bob O'Neil, members of the research group, with whom I spent many hours in academic pursuits.

Don Dohan and Geoff Frank, who suffered with me in the same office, but who always had sincere interest in my endeavours.

Bev Kenyon and Martin Anderson, with whom I spent many evenings working at the university.

I am grateful for the assistance given to me during my experiments by Phil Ashbaugh and all the members of the operations group of the tandem laboratory. I would like to thank Mrs. D. Vince and Mrs. J. Prestwich for counting the photographic plates.

I am grateful for the assistance of Mrs. E. Williams in the final preparation of this manuscript.

Finally, I wish to thank the governments of Ontario and Canada for their benevolence.

TABLE OF CONTENTS

<u>CHAPTER</u>		<u>PAGE</u>
I	INTRODUCTION	1
II	THEORETICAL DESCRIPTION	5
	II.1 Unified Model	5
	a Deformed Single Particle States	7
	b Pairing Effects	10
	c Rotational States	12
	d Vibrational States	14
	e Mixing Phenomena	16
	II.2 Proton Transfer Reactions on Deformed Even-Even Nuclei	19
	a Basic Spectroscopic Information	20
	b Spectroscopic Information and the Unified Model	30
	II.3 Calculations	34
III	EXPERIMENTAL CONSIDERATIONS	41
	III.1 Outline of the Experiment	41
	III.2 Target Preparation	41
	III.3 F N Accelerator	43
	III.4 Enge Spectrograph	45
	III.5 Experimental Investigations	48
	III.6 Extraction of Cross Sections and Energies	49
	III.7 Energy Resolution Considerations	71

TABLE OF CONTENTS (continued)

<u>CHAPTER</u>		<u>PAGE</u>
IV	INTERPRETATION	74
IV.1	^{155}Tb , ^{157}Tb , ^{159}Tb and ^{161}Tb	74
	a The $3/2^+$ [411] orbital	75
	b The $5/2^+$ [413] orbital	75
	c The $5/2^-$ [532] and $7/2^-$ [523] orbitals	78
	d The $1/2^+$ [411] orbital	82
	e The $7/2^+$ [404] orbital	86
	f The $5/2^+$ [402] orbital	87
	g The $1/2^-$ [541] orbital and fragments of the $1/2^+$ [411] orbital	89
	h Proton studies of terbium	95
IV.2	^{163}Ho	97
	a The $7/2^-$ [523] orbital	98
	b The $7/2^+$ [404] orbital	98
	c The $1/2^+$ [411] and $3/2^+$ [411] orbitals	101
	d Other Levels	102
IV.3	^{153}Eu and ^{155}Eu	104
	a The $5/2^+$ [413] orbital	104
	b The $5/2^-$ [532] orbital	106

TABLE OF CONTENTS (continued)

<u>CHAPTER</u>		<u>PAGE</u>
	c The $3/2^+$ [411] orbital	109
	d The $1/2^+$ [411] orbital	109
	e Other Levels	112
V	SUMMARY	115
APPENDIX	DWBA Theory	123
REFERENCES		134

List of Figures

<u>Number</u>		<u>Page</u>
1	Nilsson Diagram for $50 < Z < 80$	9
2	Calculated angular distribution for the $(^3\text{He},d)$ reaction at $E = 24$ MeV and $Q = -0.5$ MeV	23
3	Calculated and experimental angular distributions for the (α,t) reaction on ^{152}Sm , $E = 25$ MeV	24
4	Calculated and experimental angular distributions for the (α,t) reaction on ^{154}Sm , $E = 25$ MeV	25
5	Theoretical Q value dependence of the cross sections for the ℓ value transferred in the $(^3\text{He},d)$ reaction	27
6	Theoretical Q value dependence of the cross sections for the ℓ value transferred in the (α,t) reaction	28
7	Q dependence of the (α,t) to $(^3\text{He},d)$ cross section ratio- calculated and experimental	29
8	Effects of Coriolis mixing for the $5/2^- [532]$ and $7/2^- [523]$ orbitals in ^{159}Tb	39
9	Diagram of the beam optics	46
10	Diagram of the Enge Spectrograph	47
11	Spectra of ^{155}Tb from (α,t) and $(^3\text{He},d)$ reactions	51
12	Spectra of ^{157}Tb from (α,t) and $(^3\text{He},d)$ reactions	52
13	Spectra of ^{159}Tb from (α,t) and $(^3\text{He},d)$ reactions	53
14	Spectra of ^{161}Tb from (α,t) and $(^3\text{He},d)$ reactions	54
15	Spectra of ^{163}Ho from (α,t) and $(^3\text{He},d)$ reactions	55
16	Spectra of ^{153}Eu from (α,t) and $(^3\text{He},d)$ reactions	56
17	Spectra of ^{155}Eu from (α,t) and $(^3\text{He},d)$ reactions	57

List of Figures (continued)

<u>Number</u>		<u>Page</u>
18	Energies of the $5/2^-$ [532] and $7/2^-$ [523] orbitals in the nuclei studied	117
19	Energies of the $5/2^+$ [413] and $7/2^+$ [404] orbitals in the nuclei studied	118
20	Energies of the $3/2^+$ [411] and $5/2^+$ [402] orbitals in the nuclei studied	119
21	Energies of the $1/2^+$ [411] orbital in the nuclei studied	120
22	Energies of the $1/2^-$ [541] orbital in the nuclei studied	121

List of Tables

<u>Number</u>		<u>Page</u>
1	DWBA parameters used	36
2	Percentage abundance of isotopes in targets	42
3	Experiments done in the study	50
4	(α ,t) reaction Q-values	59
5	Energy and cross section of levels in ^{155}Tb	60
6	Energy and cross section of levels in ^{157}Tb	62
7	Energy and cross section of levels in ^{159}Tb	64
8	Energy and cross section of levels in ^{161}Tb	66
9	Energy and cross section of levels in ^{163}Ho	68
10	Energy and cross section of levels in ^{153}Eu	69
11	Energy and cross section of levels in ^{155}Eu	70
12	Spectroscopic information for the $3/2^+[411]$ and $5/2^+[402]$ orbitals in the terbium isotopes	76
13	Spectroscopic information for the $5/2^+[413]$ and $7/2^+[404]$ orbitals in the terbium isotopes	77
14	Spectroscopic information for the $5/2^-[532]$ and $7/2^-[523]$ orbitals in the terbium isotopes	81
15	Spectroscopic information for the $1/2^+[411]$ orbital and fragment in the terbium isotopes	84
16	Spectroscopic information for the $1/2^-[541]$ orbital in the terbium isotopes	91
17	Spectroscopic information for states in ^{163}Ho	99
18	Spectroscopic information for the $5/2^+[413]$ orbital in the europium isotopes	105
19	Spectroscopic information for the $3/2^+[411]$ orbital in the europium isotopes	107
20	Spectroscopic information for the $5/2^-[532]$ and $7/2^-[523]$ orbitals in the europium isotopes	108

CHAPTER I

INTRODUCTION

To the nuclear spectroscopist, there are two important aspects of the study of nuclear excitations. The first is the knowledge of the properties of these excited states, most especially, their energies, their angular momenta as well as their population intensities (which depend on the nature of the study). The second aspect is the description of these states in terms of some simple nuclear model. With such a description, one can evaluate and understand the systematic trends of the nuclear properties without clouding the picture by a complex theoretical formalism that requires a detailed description of the two-body nuclear force.

The study of the nuclear states of ^{153}Eu , ^{155}Eu , ^{155}Tb , ^{157}Tb , ^{161}Tb and ^{163}Ho in this work is done using both the $(^3\text{He},d)$ and (α,t) reactions. In the $(^3\text{He},d)$ reaction, ions of helium-3 are projected at the target nuclei, and the numbers and energies of the outgoing deuterons are measured at various angles with respect to the incident beam direction. In the (α,t) reaction, helium-4 ions are used as the projectiles, and the outgoing tritons are studied. In both reactions, the residual nuclei contain one more proton than the target nuclei, and are generally left in excited states. The measurements of the energies of the outgoing particles allow one to determine the energies of the excited states in which the residual nuclei are left. The variation in the yield of the reaction product with angle, as well as the differences in intensities between the two reactions, provides information that can

be used to determine the angular momentum transferred to the nucleus for each state populated. This information, together with data from other studies (for example, gamma decay scheme works) can often be used for a positive identification of the excited states. The success of this spectroscopic technique is attested by the recent works of Lu and Alford (1971), Price et al. (1971) and O'Neil et al. (1971) who have studied levels in rhenium, iridium and lutetium isotopes respectively. The principles on which the technique is based are outlined in section II.2.

The character of the low-lying (up to about one MeV excitation) spectra in odd-A deformed rare earth nuclei ($151 < A < 191$) is in general well described by the Unified Model. The review article by Bunker and Reich (1971) considers much of the experimental information about these nuclei in terms of this model. Simply, the Unified Model combines the single particle and collective picture of nuclear excitations.

In the single particle picture, the odd-A nucleus is described by a central potential in which the odd nucleon moves. This average potential is generated by the nuclear force due to all the other nucleons. There are two properties of the nuclear force that are found to be important for deformed rare earth nuclei but are not described by the average central potential. The phenomenological quadrupole force is considered to be an important part of the long range two particle interaction, that is not accounted for by a central force. This non-central force is simply derived from a mathematical expression for the general two body force (Preston, 1961, chap. 9) and can be thought of as one which depends not only on the separation of the two interacting nucleons,

but their position in the nucleus as well. The inclusion of this force in the expression for the central potential can lead to a spheroidal potential. The odd nucleon is assumed to move in this deformed potential, which is the shape of the deformed nucleus. The other property of the nuclear force, to be included in the single particle description, is that of pairing. This is an effect which induces nucleons to travel in pairs with a total angular momentum of zero. The ground state angular momentum of zero for all even-even nuclei (even Z and even N) is evidence of this effect. The pairing force distorts the energies expected for single particle excitations but it simplifies the nature of the spectra as it does not allow particle pairs to be broken for the low energy excitations.

The two main collective effects are rotations and vibrations. The characteristic energies of a rotational mode of excitation are often observed in deformed nuclei (Bunker and Reich, 1971). These excitations are described by rotations of the whole nucleus and are generally assumed to be independent of the single particle motions. The vibrations, which are described as oscillations in the shape of the nucleus, are attributed to the same long range forces that generate the static distortion in deformed nuclei.

In the Unified Model, both single particle and collective effects are expected to be observed in the nuclear excitations. As well, there are couplings between the various phenomena which can distort the properties of the nuclear states. If these couplings are strong, identification of the states in terms of the model is often very difficult.

In this work, the properties of the states in ^{153}Eu , ^{155}Eu , ^{155}Tb , ^{157}Tb , ^{159}Tb , ^{161}Tb and ^{163}Ho were studied in terms of the Unified Model. Most of these nuclei have not been previously investigated using proton transfer reactions. In this mass region, the states of odd-N nuclei (many of which have been studied by neutron transfer reactions such as (d,p) or (d,t)) are found to be difficult to describe in terms of the simple Unified Model. For many states, the effect of the complex mixing phenomena, which is normally assumed to be small, was found to be appreciable. The purpose of the present investigation is to identify the low lying nuclear levels that are populated by the proton transfer reactions, and to discover how well they can be described by the Unified Model.

II Theoretical Description

II.1 The Unified Model

The nature of the nuclear states of low excitation (< 1 MeV) which are generally observed for the deformed rare earth region, suggests that the Hamiltonian for the Unified Model should be written as:

$$H = \sum_i H_{i \text{ deformed single particle}} + H_{\text{pairing}} + H_{\text{rotational}} + H_{\text{vibrational}} + H_{\text{mixing}} \quad (1)$$

The deformed single particle, pairing, rotational and vibrational parts of the Hamiltonian are considered to be independent of each other and all coupling terms are placed in H_{mixing} . The solutions of this Hamiltonian are expected to describe the general characteristics of the states of deformed rare earth nuclei.

The Hamiltonian of the Unified model is an approximation of the general Hamiltonian for the two body interaction with N nucleons:

$$H' = \sum_i^N T_i + \sum_{i < j}^N V_{ij} \quad (2)$$

T_i is the kinetic energy of particle i

V_{ij} is the general interaction between particles i and j

Exact solution of (2) is not possible, partly because the two nucleon interaction V_{ij} is not well understood, but mainly because of the mathematical complexity of this many particle problem. The success of the model approach as an approximation to the general Hamiltonian is demonstrated by the spherical Shell Model (Preston 1963, Chap. 7)

on which the Unified Model is founded. The basic assumption of the Shell Model is that the two-particle potentials can be replaced by an average single-particle central potential with a spin-orbit term ($\vec{l} \cdot \vec{s}$). This model is used to predict the "magic numbers" (Evans, 1955, Chap. 11). Nuclei with a "magic" number of nucleons (protons or neutrons) have among other distinctive properties, large nucleon binding energies which are characterized by "closed shells" in the Shell Model. Refinements to the simple model attempt to account for the residual interactions not described by the average potential, and have mainly followed two different approaches. The first is the microscopic description of the residual two nucleon force. This approach, which is the basis of the "modern" Shell Model, requires prohibitive calculations for all but the simplest nuclear configurations. Generally, the nucleus is assumed to have an inert core (a closed nuclear shell) and a few extra-core, interacting nucleons. A basis of spherical, non-interacting states is used and the total Hamiltonian, with the assumed residual interaction, is diagonalized (solved for the wave functions and energies in terms of the basis states) (see French et al. 1969). The alternate approach is to include more of the residual interactions in a Hamiltonian that can still be solved exactly. The attempt is made to include those terms of the residual interaction that predict the principal properties of the observed nuclear excitations. The Unified Model, which includes the residual effects of the two nucleon quadrupole and pairing forces as well as the vibrational and rotational forms of collective motion, has been very successful in describing states of deformed rare earth nuclei

(see Bunker and Reich, 1971).

II.1a Deformed Single Particle States

The inclusion of the residual two nucleon quadrupole interaction in the average central Shell Model potential leads to H_{DSP} , the single particle Hamiltonian with a deformed average potential. A number of H_{DSP} 's have been proposed (Ogle et al. 1971), but one of the simplest is that used by Nilsson (1955). The Hamiltonian includes an harmonic oscillator potential with a quadrupole deformation that is axially symmetric. As expressed by Chi (1966):

$$H_{\text{DSP}} = \frac{P^2}{2m} + V(r) + C\vec{l} \cdot \vec{s} + D\vec{l} \cdot \vec{l} \quad (3)$$

where P and m are the momentum and mass of the particle respectively, and

$$V(r) = \frac{1}{2} m\omega_0^2 r^2 (1 - 2\beta Y_{20}(\theta, \phi)), \quad (3)$$

$Y_{20}(\theta, \phi)$ is the "quadrupole" spherical harmonic

(defined in Messiah, 1966, Appendix B.),

β is a measure of the quadrupole deformation and is

$\approx \delta/0.95$ where δ is the deformation parameter used by

Nilsson,

C , D and ω_0 are chosen to reproduce the spherical shell model energy levels ($\beta=0$) and are related to κ and μ , the parameters usually quoted (Chi, 1966).

A solution of the Hamiltonian yields states with good π (parity) and K (the total angular momentum projection on the nuclear symmetry axis). Moreover, states of different N , the major oscillator quantum number,

are assumed not to mix. These states are also identified by quantum numbers which are good only for large deformation ($\beta \rightarrow \infty$): n_3 the number of nodes in the wave function along the symmetry axis and Λ the orbital angular momentum projection on the symmetry axis. Thus $\chi_\Omega = \Omega^\pi [Nn_3\Lambda]$. From the symmetry of the nuclear system, the intrinsic state χ_Ω and its conjugate state $\chi_{-\Omega}$ are degenerate. One normally considers the Nilsson orbitals with Ω positive, so that each orbital can contain two particles. The deformed states are conveniently expanded in terms of spherical oscillator states of good j and l (total and orbital angular momenta) by:

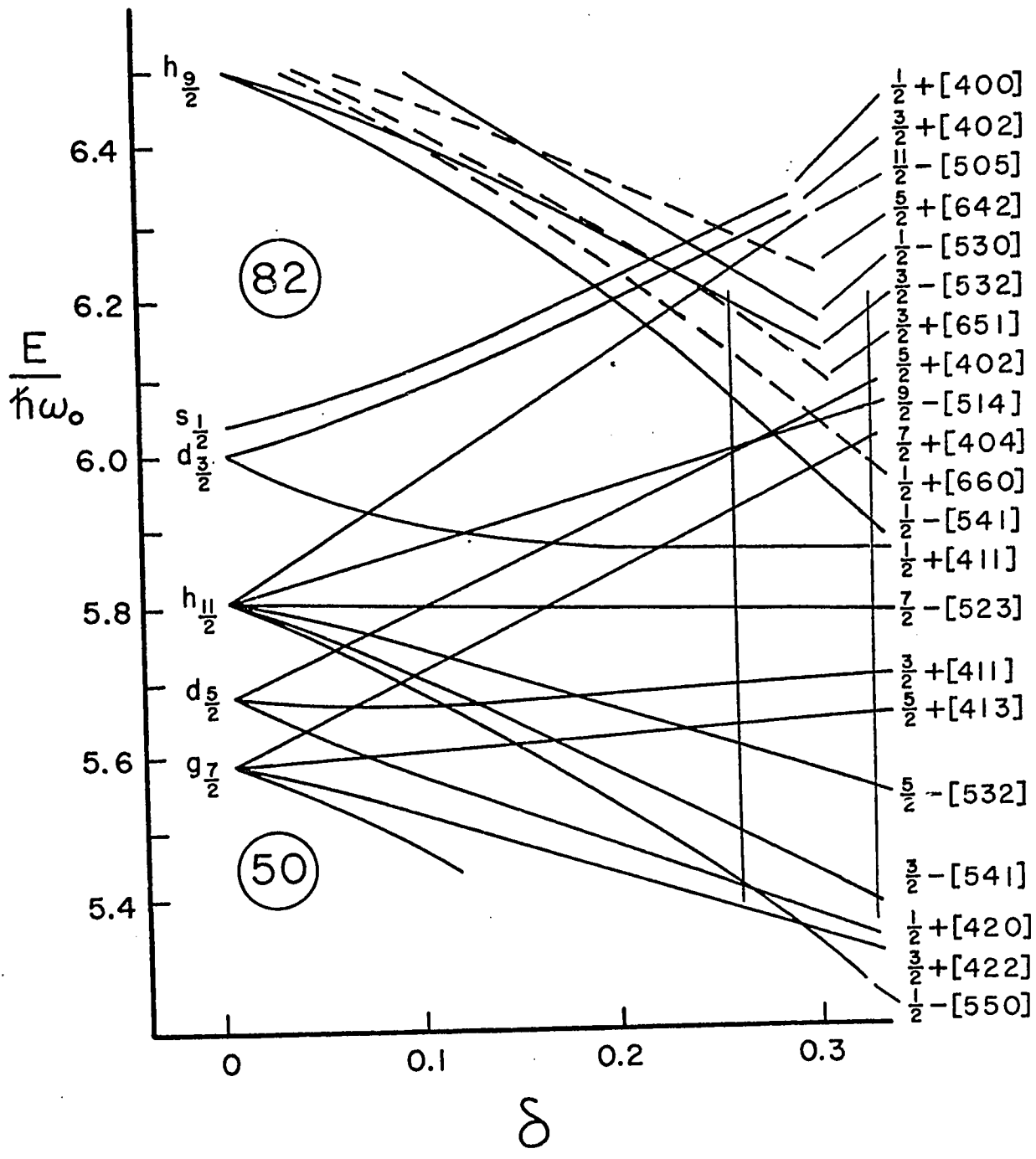
$$\chi_{sp}^\Omega = \sum_j C_{jl}^\Omega \phi_{jl}^{N\Omega} \quad (4)$$

Alternate definitions of the deformed single particle potential are discussed by Ogle et al. (1971). Potentials with a Wood-Saxon shape have been used instead of the harmonic oscillator, a radial dependence has been introduced in the $\vec{l} \cdot \vec{s}$ and $\vec{l} \cdot \hat{l}$ terms, and deformations with a Y_{40} term as well as the Y_{20} term (eqn. 3) are used. The principal properties of the single particle states are generally quite similar for the different potentials. However, the $\Delta N=2$ mixing which is neglected for most of these calculations, has been observed to be underestimated when it is calculated using the Nilsson wavefunctions (Anderson, 1968). In the present study of the proton states between $Z=63$ and $Z=67$, this mixing is not expected to be important. In Fig. 1, from calculations of Gustafson et al. (1967), the single particle energies are displayed as functions of the deformation, for the proton states.

6

Figure 1

Nilsson diagram for $50 < Z < 80$, adapted from Gustafson et al. (1967).
 $\kappa = 0.0637$ and $\mu = 0.6$. The vertical lines enclose the deformation
region of interest.



II.1b Pairing Effects

Nucleons tend to pair together in conjugate states (time reversed states) because of the so-called pairing force. This phenomenological force is an approximation to the short range component of the residual interaction, not described by the average deformed potential (Bes and Sorensen, 1969). This interaction can be written as:

$$V'_{ij} \approx G \delta(\vec{r}_i - \vec{r}_j) \delta(\bar{\alpha}_i = \alpha_j) \quad (5)$$

where particle i is in state α_i and the delta function $\delta(\bar{\alpha}_i = \alpha_j)$ requires that particle j be in the time reversed state of particle i , $\delta(\vec{r}_i - \vec{r}_j)$ defines the short range nature of the interaction.

This expression assumes that the short range residual interaction is independent of the state (G is constant), and is only effective between conjugate pairs of states. It is best treated in terms of Second Quantization (see Davydov, 1966) where the Hamiltonian is written:

$$H = \sum_i e_i a_i^\dagger a_i + G/2 \sum_{i,j} a_i^\dagger \bar{a}_{\bar{i}}^\dagger a_j a_{\bar{j}} \quad (6)$$

a_i^\dagger is a creation operator for a particle in state i

(i is a deformed single particle state),

a_i is the corresponding annihilation operator,

\bar{i} is the conjugate state of i ,

e_i is the energy of the single particle state i .

Application of the BCS theory of superconductivity (Bardeen et al. 1957) to the nuclear Hamiltonian (6), suggests a canonical

transformation from a basis of particles that interact, through the pairing force, to a system of non-interacting quasi-particles. The transformation can be written $\alpha_i^\dagger = Ua_i^\dagger - Va_i$, where α_i^\dagger is the quasi-particle creation operator. Ogle et al. (1971) and Bes and Sorensen (1969) have good presentations of the pairing theory and the BCS approximation. In the quasi-particle formalism, the ground state wave function of an even-even nucleus is written:

$$\phi_{ee} = \prod_{\nu} (U_{\nu} + V_{\nu} a_{\nu}^{\dagger} a_{\nu}^{\dagger}) |o\rangle \quad (7)$$

ν is an index over all the single particle states

(not including the conjugate states),

U_i^2 is the probability that state i is empty,

V_i^2 is the probability that state i contains a pair of particles,

$|o\rangle$ is the quasi-particle vacuum.

For an odd A nucleus, the single quasi-particle wave function is written:

$$\chi_i = \psi_i \phi_c \quad \text{and} \quad \phi_c = \prod_{\nu \neq i} (U_{\nu} + V_{\nu} a_{\nu}^{\dagger} a_{\nu}^{\dagger}) |o\rangle \quad (8)$$

where ψ_i is the single particle state (χ^{Ω} in eqn. 4).

The energy of quasi-particle state i is given by:

$$\epsilon_i = [(e_i - \lambda)^2 + \Delta^2]^{1/2} \quad (9)$$

where e_i is the single particle energy of the state,

$$\Delta = G \sum_k U_k V_k \quad \text{and is called the diffuseness parameter,} \quad (10)$$

$$V_i = 1/2 [1 - (e_i - \lambda)/\epsilon_i]^{1/2}, \quad (11)$$

λ is the Fermi energy (usually near the energy of the highest occupied single particle state) and is adjusted so that:

$$\sum_{\nu} 2V_{\nu}^2 = N \text{ the total number of nucleons.} \quad (12)$$

The pairing force generates a diffuse Fermi surface. That is, even in the ground state of the nucleus, paired particles appear with small probabilities in intrinsic states that would have been excited states without pairing. The effect of pairing is to compress the expected energy spacings between the low lying single particle states (eqn. 9). The pairing strength G is normally determined from the odd-even mass difference in nuclei (which should be $\approx 2\Delta$). To describe a single quasi-particle state, the U 's and V 's for all the other single particle states should be calculated consistent with equations (9) and (12). The state occupied by the quasi-particle is "blocked", i.e. no U or V is defined for it. The evaluation of the U 's and V 's is an iterative procedure, and a complete set of these parameters should be calculated for each single quasi-particle state. This procedure, and the principle of "blocking" is considered in detail by Ogle *et al.* (1971). It is difficult to calculate the U 's and V 's of each single particle state for all single quasi-particle excitations. For simplicity, the U 's and V 's of the single particle states were assumed to be independent of the location of the single quasi-particle.

II.1c Rotational States

If the nucleus has a deformed shape, energy can be put into rotation of the nucleus as a whole. The total rotational Hamiltonian

can be written:

$$H'_{\text{rot}} = \hbar^2 (R_x^2/2\mathcal{I}_x + R_y^2/2\mathcal{I}_y + R_z^2/2\mathcal{I}_z) \quad (13)$$

where R_i is the angular momentum of the rotating body about the i axis,

\mathcal{I}_i is the moment of inertia about the i axis,

$$\vec{I} = \vec{R} + \vec{j}$$

\vec{I} is the total angular momentum and

\vec{j} is the intrinsic spin of the nucleus.

If the nucleus is assumed to have axial symmetry (about the z axis), there can be no rotation about the z axis, and $\mathcal{I}_x = \mathcal{I}_y = \mathcal{I}$.

Eqn. (13) then reduces to

$$\begin{aligned} H'_{\text{rot}} &= \hbar^2/2\mathcal{I} [(\vec{I}-\vec{j})^2 - (I_z-j_z)^2] \\ &= \hbar^2/2\mathcal{I} [(I+1)I - \Omega^2 + H_{\text{rpc}} + \hbar^2/2\mathcal{I} (\vec{j}^2)] \\ &= H_{\text{rot}} + H_{\text{rpc}} + \hbar^2/2\mathcal{I} (\vec{j}^2) \end{aligned} \quad (14)$$

where Ω is the projection of \vec{j} (and \vec{I}) on z the symmetry axis and $H_{\text{rpc}} = -\hbar^2/2\mathcal{I} [I_+j_- + I_-j_+]$ (15)

where $I_{\pm} = I_x \pm iI_y$ $j_{\pm} = j_x \pm j_y$ (here $i = \sqrt{-1}$)

H_{rot} is the rotational Hamiltonian in (1). The development of equations (14) and (15) from (13) can be found in Preston (1963) Chap. 10.

As H_{rpc} couples the particle motion (\vec{j}) to the rotation of the whole nucleus (\vec{I}), it is included in the H_{mixing} of (1). It is normally assumed to be small (the adiabatic approximation).

For a deformed nucleus with an intrinsic quasi-particle state χ_{Ω} , the total antisymmetrized wavefunction of the Hamiltonian $H_{\text{DSP}} + H_{\text{rot}}$ can be written

$$\Phi_{M\Omega}^I = [(2I+1)/16\pi^2]^{1/2} [\chi_{\Omega}^I D_{M\Omega}^I + (-1)^{I+\Omega} \chi_{-\Omega}^I D_{M-\Omega}^I] \quad (16)$$

where the $D_{M\Omega}^I$'s are the rotation matrices (Preston 1963, Appendix A),

The energies of the wavefunctions (16) are:

$$E(I\Omega) = \epsilon_{\Omega} + \hbar^2/2\mathcal{I} [I(I+1) - 2\Omega^2 + \delta_{\frac{1}{2},\Omega} a (-1)^{I+1/2} (I+1/2)] \quad (17)$$

where ϵ_{Ω} is the energy of the intrinsic state (with the $\hbar^2/2\mathcal{I} \langle \vec{j}^2 \rangle$ term from (14) included),

a is the decoupling parameter and arises from the inclusion of H_{rpc} in the Hamiltonian for the $\Omega = 1/2$ states.

It can be evaluated from the amplitudes of states $\phi_{j\ell}^{N\Omega}$ in (4).

The $(\hbar^2/2\mathcal{I}) \langle \vec{j}^2 \rangle$ term in (14) which could be included in the intrinsic state Hamiltonian is normally neglected. Its main effect is an energy shift of $\hbar^2/2\mathcal{I} \langle \vec{j}^2 \rangle$ for the state, where the \vec{j}^2 is averaged over the j components of the intrinsic state.

Equation (17) shows that for one intrinsic state, a large number of rotational states with $I \geq \Omega$ are formed. Experimentally, only the relative energies of the members of a rotational band are of interest, and these are used to determine $\hbar^2/2\mathcal{I}$, the rotational parameter. It is typically about 11 keV for the nuclei studied.

II.1d Vibrational States

Vibrational states have been observed in even-even nuclei, and their existence is attributed to part of the long range residual interaction in the nuclear force:

$$v(i,j) = \sum_{\text{res}} \sum_{\ell} v_{\ell}(r_i r_j) P_{\ell}(\cos\theta_{ij}) \quad (18)$$

The quadrupole ($\ell=2$) and octupole ($\ell=3$) terms are considered important for the vibrations. The Hamiltonian for the vibrations is thus assumed to be

$$H_0 = -\chi \sum_{i < j} \sum_{\mu} (-1)^{\mu} \hat{O}_{L\mu}(i) \hat{O}_{L-\mu}(j) \quad (19)$$

$$\text{For the quadrupole term } \hat{O}_{L\mu}(i) = r_i^2 Y_{2\mu}(\theta_i, \phi_i)$$

In the introduction, it was mentioned that the quadrupole interaction leads to the deformed potential, and consequently a deformed nucleus. As well as a static deformation, the interaction is expected to generate dynamic deformations, i.e. vibrations. To study vibrations, the solutions to (19), the microscopic approach of the Random Phase Approximation is normally used. The most detailed calculations have been done by Soloviev and co-workers (see Soloviev and Fedotov, 1971).

The approach to the solution of (19) is to consider boson-like pairs of quasi-particles in states that couple to an angular momentum L and its projection on the symmetry axis M . The vibrational excitation, a phonon, can be described as a linear combination of all the quasi-particle pairs coupling to L and M ($M = \Omega_i + \Omega_j$ and

$$L = |\Omega_i \pm \Omega_j|):$$

$$P_L^{M\dagger} = \sum_{\nu} [X_{\nu}^{LM} A_{\nu}^{LM\dagger} - Y_{\nu}^{LM} A_{\nu}^{LM}] \quad (20)$$

$$\text{and } H_0 P_L^{M\dagger} = W P_L^{M\dagger}$$

W is the excitation energy of the phonon

$A_{\nu}^{LM\dagger}$ is the creation operator for a boson-like

quasi-particle pair from states i and j coupling

to L and M

For the quadrupole interaction, the Hamiltonian (19) can be approximated by:

$$H = \chi \sum_{\nu\nu'} q_{\nu} q_{\nu'} (A_{\nu}^{\dagger} + A_{\nu}) (A_{\nu'}^{\dagger} + A_{\nu'}) \quad (21)$$

$$\text{where } q_{\nu} = \langle i | r_{ij} Y_{20} | j \rangle$$

χ , the strength of the quadrupole interaction can be estimated from the nuclear model but is normally determined empirically

These equations can be solved for W and the coefficients X^{LM} and Y^{LM} (20) which are the amplitudes of the two quasi-particle bosons in the phonon.

For odd-A nuclei, it is tempting to suppose that the vibrational excitations would be independent of the single-quasi-particle states, so that a general intrinsic wavefunction could be written:

$$\psi_K = P_L^M \psi_i^{\Omega} \phi_c \quad (22)$$

$$\text{where } K = M \pm \Omega$$

ψ and ϕ_c are defined by equation (8)

P_0 represents no vibration.

Unfortunately, if P_L^M is calculated from the even-even nucleus, it may contain paired components of the state which is singly occupied in the odd-A nucleus. Thus the components for the phonon for the odd-A case should be recalculated. The most serious problem though, is the particle vibrational coupling which will be discussed in section II.1e. Good outlines of the microscopic approach to vibrations are found in the articles by Bes and Sorensen (1969) and Ogle *et al.* (1971).

II.1e Mixing Phenomena

Mixing of the nuclear states is a consequence of the way in

which the model Hamiltonian is chosen. In order to have parts of the Hamiltonian separable, one assumes that the coupling between these parts are small. For the phenomenological Hamiltonian of the Unified Model, this is generally the case. Of all the mixing phenomena, in the present study, only the rotational particle coupling and the vibrational particle coupling are found to be important for most of the low lying states of the nuclei.

The rotational particle coupling, which is more commonly known as Coriolis mixing, is defined by equation 15. Physically, it appears to be a pseudo force that affects a particles' motion in a rotating coordinate system. Its effect on the single particle states is to mix those which differ in K by ± 1 . This effect can be calculated by diagonalizing the model Hamiltonian (with H_{rpc} included) in the single quasi-particle representation, to generate a new set of basis states. The matrix element for states differing in K by ± 1 is written as:

$$\langle \mu | H_{rpc} | \nu \rangle = \frac{-\hbar^2}{2\mathcal{I}} [(I_{+}^{-}K)(I_{+}K+1)]^{1/2} \sum_j C_{j\ell}^{\mu} C_{j\ell}^{\nu} [(j_{+}^{-}K)(j_{+}K+1)]^{1/2} \hat{\theta} \quad (23)$$

where $\mu = (I, M, K)$ and $\nu = (I, M, K \pm 1)$

The intrinsic single particle part of states ν and μ is decomposed into the spherical components $C_{j\ell}$
eqn. (4)

$$\hat{\theta} = (U_{\mu}^{\nu} U_{\nu}^{\mu} + V_{\mu}^{\nu} V_{\nu}^{\mu}) \prod_{i \neq \mu, \nu} (U_i^{\nu} U_i^{\mu} + V_i^{\nu} V_i^{\mu}) \quad (24)$$

The superscript on the U's and V's denotes the single quasi-particle state for which the U's and V's of the single particle states are calculated. One usually

assumes that the pairing amplitudes of the single particle states are independent of the single quasi-particle excitations and thus

$$\hat{\theta} = \sum_{\mu} U_{\mu} U_{\mu} + \sum_{\mu} V_{\mu} V_{\mu} \quad (25)$$

Experimentally, the mixing between bands is often found to be less than that predicted (using eqns. 23 and 25). One usually applies an empirical attenuation factor to the Coriolis matrix element (23). (See for example Løvnhøiden et al. (1972)). This was done in the present study. It is not certain if there is any theoretical justification for this attenuation in the Coriolis mixing. It is possible that the product term in (24), which is assumed equal to one, may be considerably less than unity. Unfortunately, this is difficult to calculate.

The effect of Coriolis mixing is to "push apart" states of the same I but with K differing by ± 1 . Unless the states are very strongly mixed, they are normally assigned the usual Nilsson labels. The mixing becomes stronger for the higher spin states, and is also the strongest between members of orbitals which originate from the same spherical Shell Model orbital. The spectroscopic strengths of the states in the single particle transfer reactions are affected by Coriolis mixing. This effect will be discussed in section II.2.

The vibrational particle coupling arises from terms neglected in the vibrational Hamiltonian (21), that contain both boson-like operators ($A_{\nu}^{LM\dagger}$) and quasi-particle annihilation and creation operators (α_{ν}^{\dagger}). If these terms are included, they will mix single particle states and vibrational states which have the same parity,

total angular momentum (I) and angular momentum projection (Ω).

The mixing will be strong if there is a large multipole matrix element $\langle i | 0_{LM} | j \rangle$ between the single quasi-particle state and the base state of the vibration. Calculations have been done by Soloviev and Fedotov, 1971, and in some instances this mixing is predicted to be very large. Unfortunately, accurate descriptions of the microscopic structure of the vibrations are not possible, and because of the approximate nature of the calculations, the description of the vibrational states is not always successful. Moreover, when the particle vibrational coupling is taken into account, it is usually too difficult to calculate the effect of Coriolis mixing as well. If both effects are expected to be strong, interpretation of the states in terms of the model may not be possible.

There are other possible forms of mixing that are not considered to be important in the present studies. $\Delta N=2$ mixing of the Nilsson states, which has been found important in other cases (Anderson, 1968), was mentioned in section II.1a. The approximate solution of the single particle and pairing Hamiltonian in the BCS formalism neglects terms that would couple one-quasi-particle to three-quasi-particle states. Three-quasi-particle excitations are not expected below the pairing gap (which is about 1 MeV in the deformed region). Thus, for the present study, these other forms of mixing are expected to be negligible.

II.2 Proton Transfer Reactions on Deformed Even-Even Nuclei

The basic and model dependent spectroscopic information that one is expected to obtain from a proton transfer reaction on an

even-even target nucleus is discussed in this section.

II.2a Basic Spectroscopic Information

The basic spectroscopic information is that obtained without the use of the nuclear model (eg. the Unified Model). This information includes the energies and cross sections of the levels populated in the present study. It also includes the spins and parities of these levels, although in the present work, these are determined by model dependent arguments.

The energies of the levels excited in the present type of experiment can be obtained directly. This is unlike gamma decay studies, where only the energies of the transitions between the levels are measured. If the reaction is written $A(a,b)B$ where A and B are the target and residual nuclei, and a and b are the incident and scattered particles, the conservation of energy in the center of mass system can be written:

$$E_a = E_b + Q \quad (26)$$

where Q is called the reaction Q -value.

The energy of an excited state populated in nucleus B is given by $E = Q_{gs} - Q$ where Q_{gs} is the Q -value of the reaction to the ground state of nucleus B . Thus by measuring the energy of particle b , one can determine the energy of the state in which the residual nucleus B was left.

The other basic information that is obtained from the reaction, is the intensity of the scattered particles relative to that of the incident particles. These relative intensities can vary with angle, and are normally expressed as differential cross sections

defined by equation A.1. Nuclear information can often be extracted from angular distributions of the differential cross sections, if they are compared with those predicted by the DWBA calculations (outlined in the Appendix). Equation A.22 for a single particle transfer into an even-even target nucleus where $J_A=0$ (and therefore $J_B=j$) can be written:

$$\frac{d\sigma}{d\Omega} = N\beta_{j\ell}^2 \sigma_{DW}^{\ell sj}(\theta) \quad (27)$$

where $\sigma_{DW}^{\ell sj}(\theta)$ is calculated by DWUCK (Kunz, 1967),

and j is now the total spin of the final state.

For many reactions, the angular distribution has a shape that is characteristic of the ℓ -value transferred. Often this feature, together with other experimental information and model dependent arguments, has been used to infer the total angular momenta (I) of the final states populated (see for example, the study using the (d,p) reaction by Hjorth et al., 1965). For the (α ,t) and (^3He ,d) reactions at the incident particle energies available for the present studies, the angular distributions are not very characteristic of the ℓ -values transferred.

In the (^3He ,d) reaction, this effect can be attributed to the high Coulomb barrier which makes the penetration of the ^3He particle difficult. At higher energies, the angular distributions become more distinctive. As well as the coulomb barrier, the lack of structure in the (α ,t) reaction can be attributed to an angular momentum mismatch (Stock et al. 1967). This mismatch is a result of the large negative Q -value for the (α ,t) reaction, which requires a large change in momentum in the reaction. In a semi-classical

picture (Butler et al., 1958) the large momentum change which is expected to occur at the nuclear surface tends to "prefer" large angular momentum transfers ($l \sim 7$), that are generally not "matched" by the l -value of the available nuclear states. The angular momentum mismatch introduces a problem for the calculation of the cross sections. Normally, one uses Optical Model parameters, which are determined by fitting the elastic scattering angular distributions of the particles, to calculate the incident and scattered particle distorted waves. The major contributions to both the elastic scattering and the reaction are usually found to be due to only a few partial waves (eqn. A.14) in both incident and outgoing channels (Hooper, 1966). For the mismatch case, this localization of the partial wave amplitudes does not occur, and the best set of optical parameters to fit the reaction data are not necessarily those obtained from a fit to elastic scattering data. In Fig. 2, some typical calculations for the angular distributions of the ($^3\text{He},d$) reaction at $E_{^3\text{He}} = 24$ MeV are shown; the calculations are discussed in Section II.3. Figures 3 and 4 compare some experimental angular distributions of the tritons from the (α,t) reaction with the results from the DWBA calculations.

Although the shapes of the angular distributions from the (α,t) and ($^3\text{He},d$) reactions are quite insensitive to the l -value transferred, the intensity dependence on the l transferred is different for the two reactions. For the ($^3\text{He},d$) reaction, the cross section decreases with increasing l -value, whereas in the (α,t) reaction the cross sections are similar for most l -values ($l \leq 6$).

Figure 2

DWBA calculations of the deuteron angular distributions for l -value transfers of 0, 1, 2, 3, 4 and 5 in the $^{154}\text{Sm}(^3\text{He},d)^{155}\text{Eu}$ reaction at $E(^3\text{He}) = 24$ MeV and Q -value = -0.5 MeV.

The cross sections have been multiplied by arbitrary factors for display purposes.

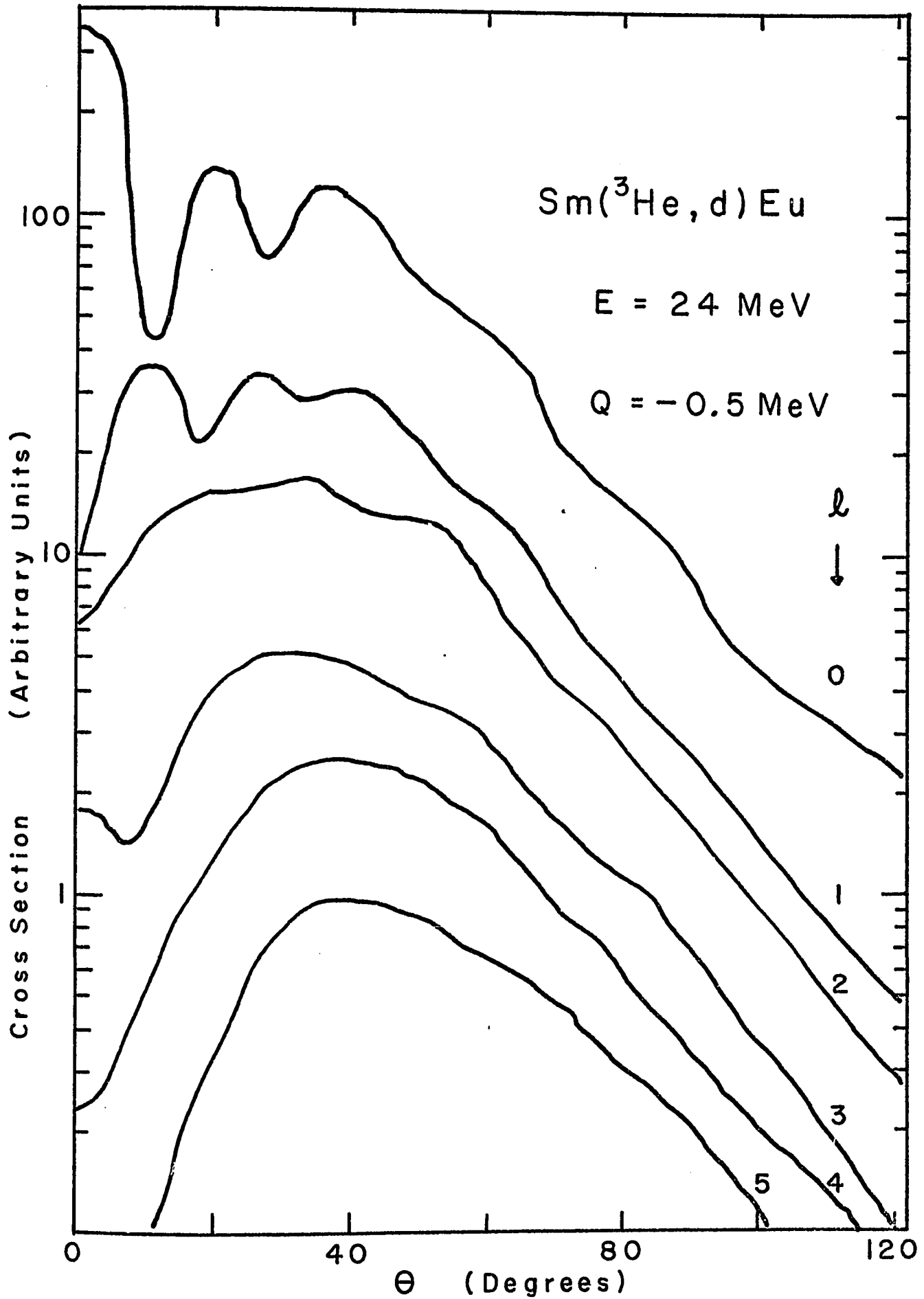


Figure 3

Triton angular distributions for the $^{152}\text{Sm}(\alpha, t)^{153}\text{Eu}$ reaction at $E(\alpha) = 25$ MeV. The $\ell = 0, 1$ and 3 curves are from the DWBA calculations for a Q-value of -14 MeV, and have been multiplied by arbitrary constants for display purposes. The $\ell = 2, 4$ and 5 curves, calculated by the DWBA program are compared with the measured triton angular distributions for population of the 173 keV level ($5/2 \ 3/2^+[411]$ state) - \ast , the 85 keV level ($7/2 \ 5/2^+[413]$ state) - \circ , and the 322 keV level ($11/2 \ 5/2^-[532]$ state) - \bullet respectively in ^{153}Eu . (See table 10).

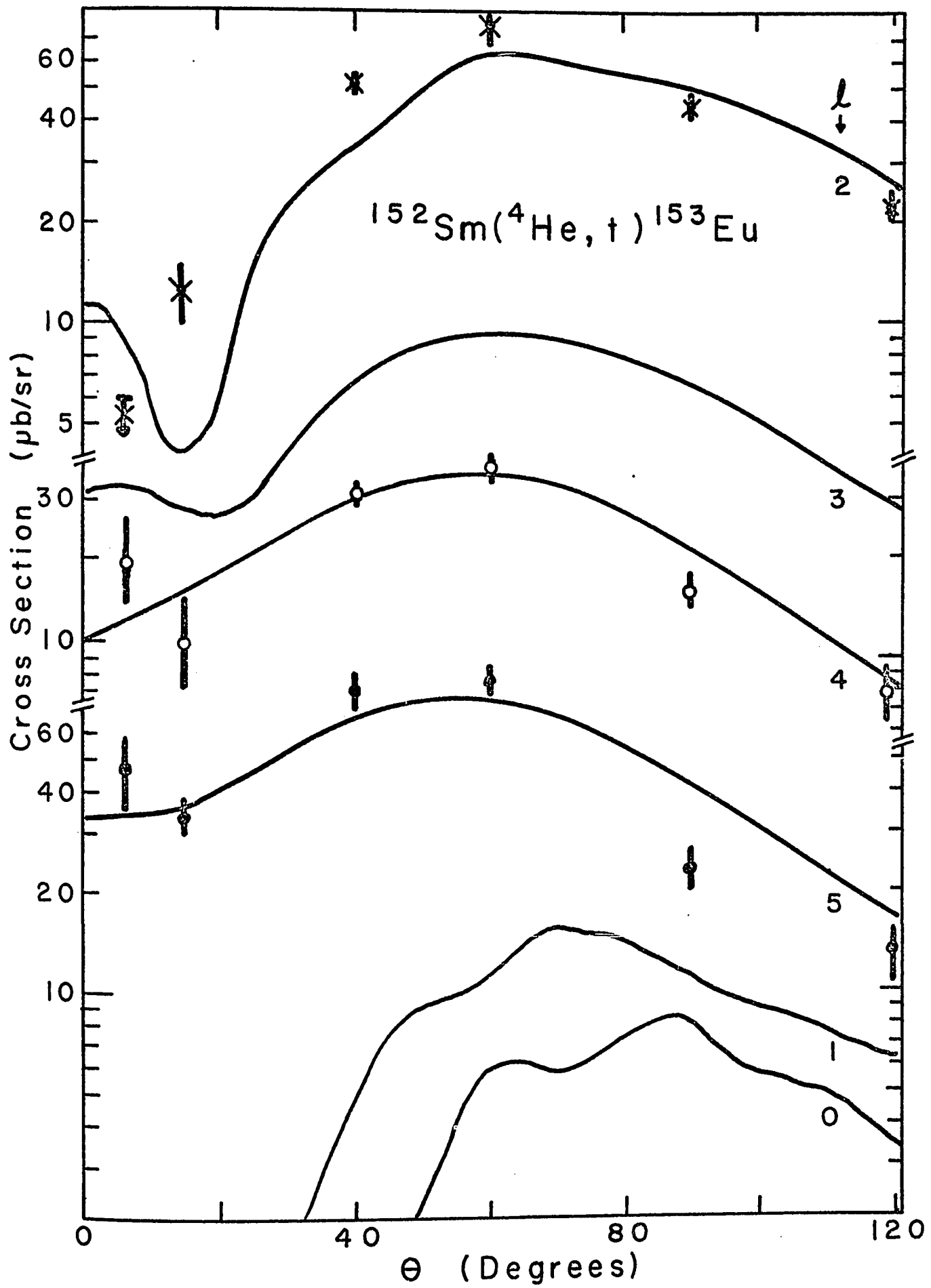
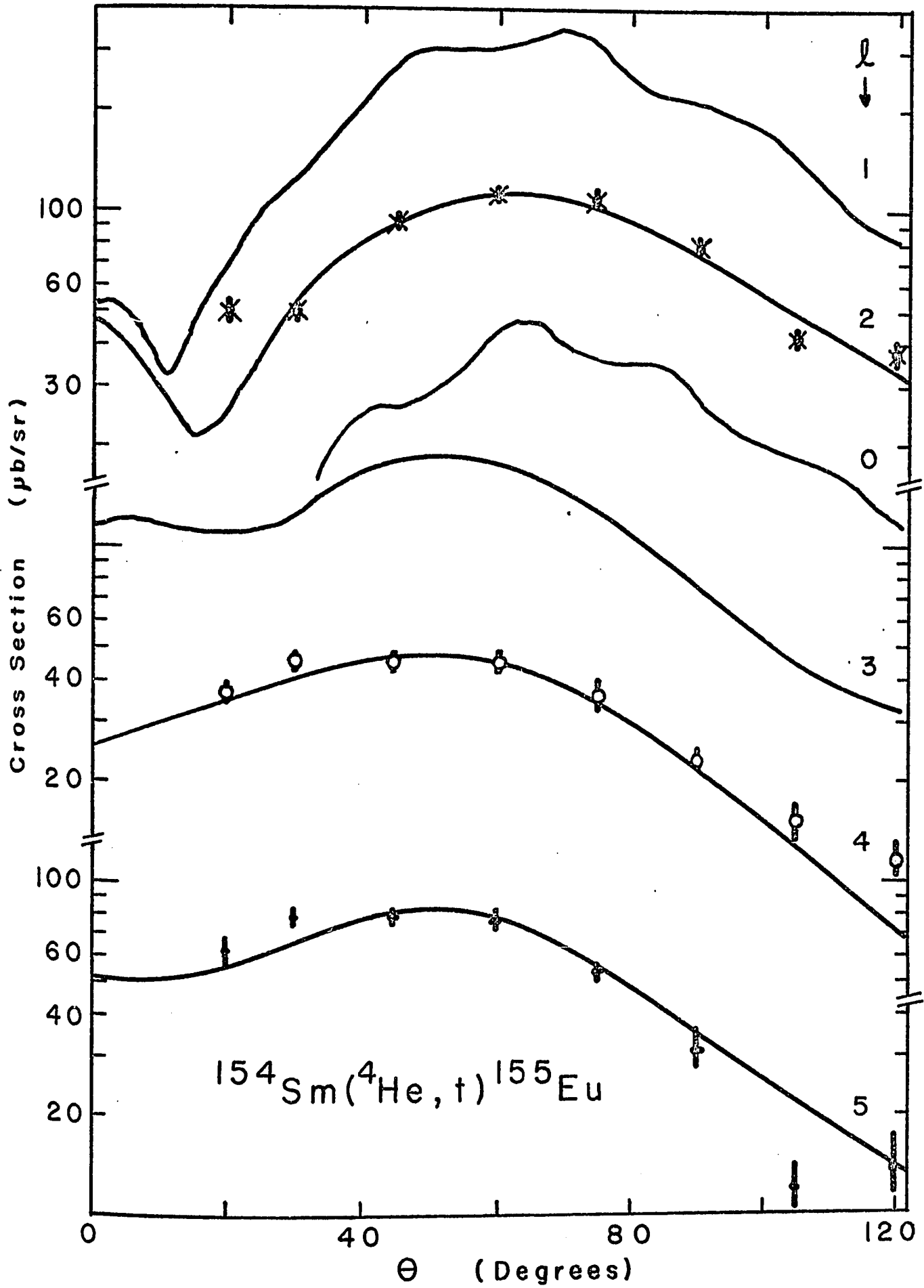


Figure 4

Triton angular distributions for the $^{154}\text{Sm}(\alpha, t)^{155}\text{Eu}$ reaction at $E(\alpha) = 25$ MeV. The $\ell = 0, 1$ and 3 curves are from the DWBA calculations for a Q-value of -13 MeV, and have been multiplied by arbitrary constants for display purposes. The $0 < \theta < 30^\circ$ part of the $\ell = 0$ curve has been omitted; the intensity decreases several orders of magnitude from $\theta = 30^\circ$ to $\theta = 0^\circ$. The $\ell = 2, 4$ and 5 curves, calculated from the DWBA program are compared with the measured triton angular distributions for population of the 307 keV level ($5/2 \ 3/2^+[411]$ state) - \star , the 78 keV level ($7/2 \ 5/2^+[413]$ state) - \circ , and the 356 keV level ($11/2 \ 5/2^-[532]$ state) - \bullet respectively in ^{155}Eu . (See table 11).



Figures 5 and 6 which are calculations of the Q value dependence of the differential cross sections for the ($^3\text{He},d$) and (α,t) reactions respectively, show the dependence of these cross sections on the ℓ -value.

Thus if one considers the ratio of the differential cross sections in the (α,t) reaction to those in the ($^3\text{He},d$) reaction, for a given excited state in the residual nucleus, from (27)

$$\frac{d\sigma/d\Omega (\alpha,t)_\theta}{d\sigma/d\Omega (^3\text{He},d)_{\theta'}} = \frac{N(\alpha,t) \sigma^{\ell sj}(\theta)}{N(^3\text{He},d) \sigma^{\ell sj}(\theta')} \quad (28)$$

This ratio is independent of the nuclear structure, but is sensitive to the ℓ transferred. A typical plot of the calculated ratios as a function of Q value for several ℓ -values is shown in Fig. 7 along with some experimental ratios.

For convenience, the expression (28) will be called the cross section ratio. In view of the experimental and theoretical uncertainties, the cross section ratio is useful in estimating the ℓ -value transferred, but cannot be used alone to determine it exactly.

The lack of fine structure in the angular distributions (see figures 2, 3 and 4) suggests that confidence can be placed in a ratio obtained from experiments at one angle in the (α,t) reaction and one angle in the ($^3\text{He},d$) reaction. Normally the cross sections are measured at several angles for each reaction to avoid confusion due to impurities in the target.

For a given ℓ -value transferred, the sensitivity of the differential cross sections to the j -value transferred depends only

Figure 5

The calculated Q-value dependence of the cross section at $\theta = 30^\circ$ for different l -values in the $^{154}\text{Gd}(^3\text{He},d)^{155}\text{Tb}$ reaction. The curves are calculated for $U^2 C_{j\ell}^2 = 1$ [$\beta_{j\ell}^2 = 2/(2j+1)$]. For comparison with Fig. 6, the ground state Q-value for the $^{152}\text{Sm}(^3\text{He},d)^{153}\text{Eu}$ reaction is indicated. The calculated cross sections have a similar Q dependence but can be up to 25% greater for reactions on ^{152}Sm compared with ones on ^{154}Gd .

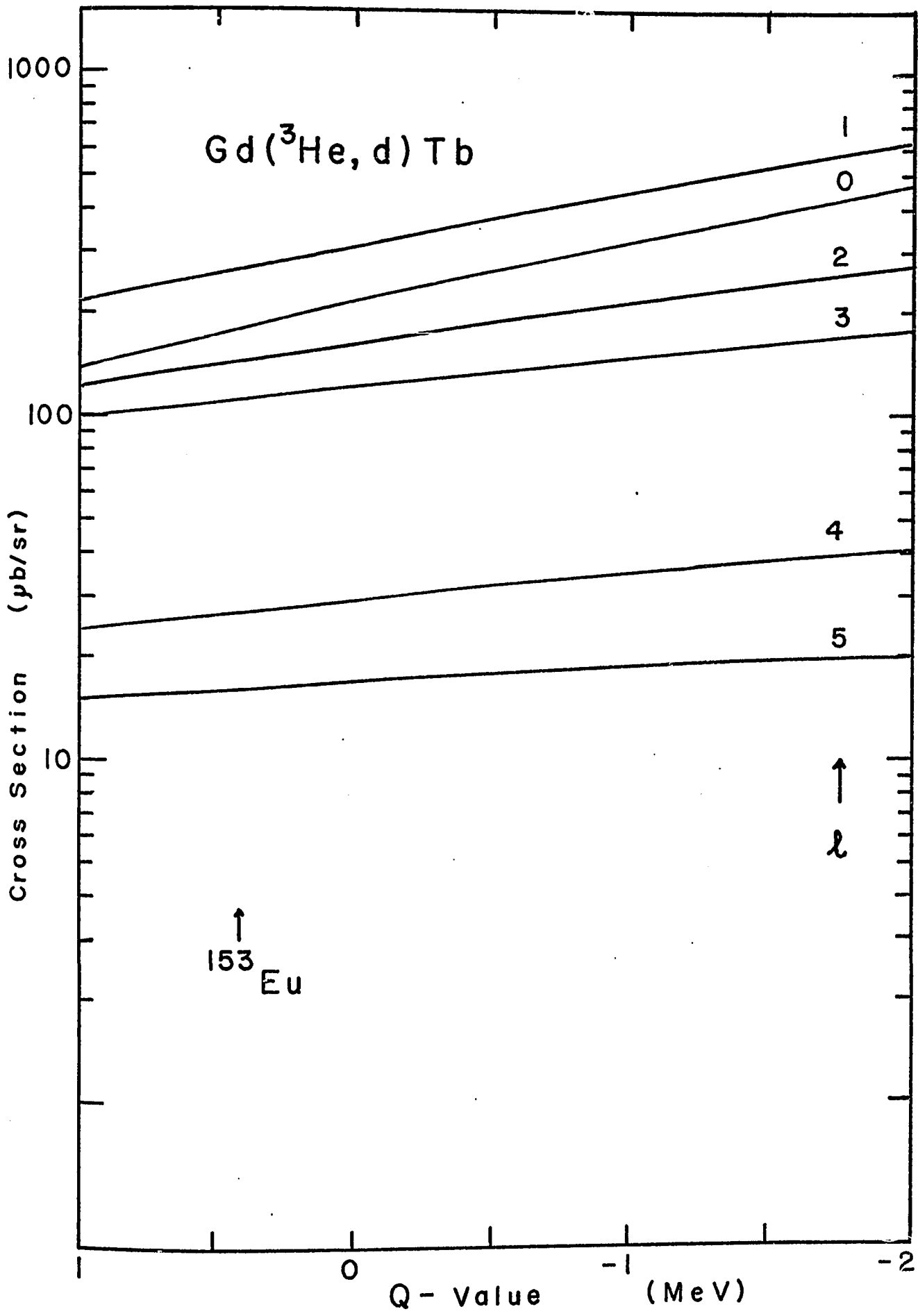


Figure 6

The calculated Q-value dependence of the cross section at $\theta = 60^\circ$ for different ℓ -values in the $^{152}\text{Sm}(\alpha, t)^{153}\text{Eu}$ reaction. The curves are calculated for $U^2 C_{j\ell}^2 = 1$ [$\beta_{j\ell}^2 = 2/(2j+1)$]. For comparison with Fig. 5, the ground state Q-value for the $^{152}\text{Sm}(\alpha, t)^{153}\text{Eu}$ reaction is indicated.

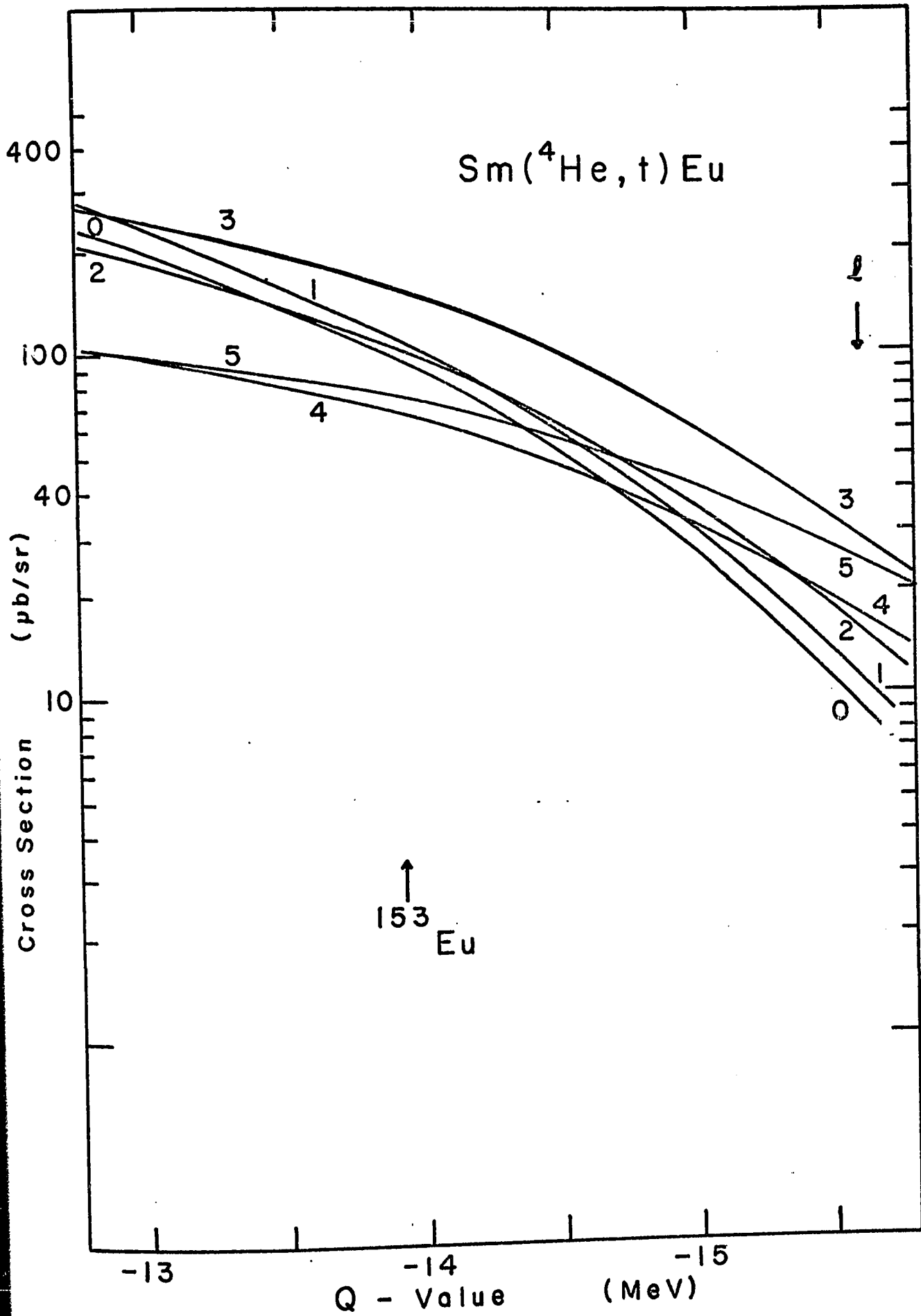
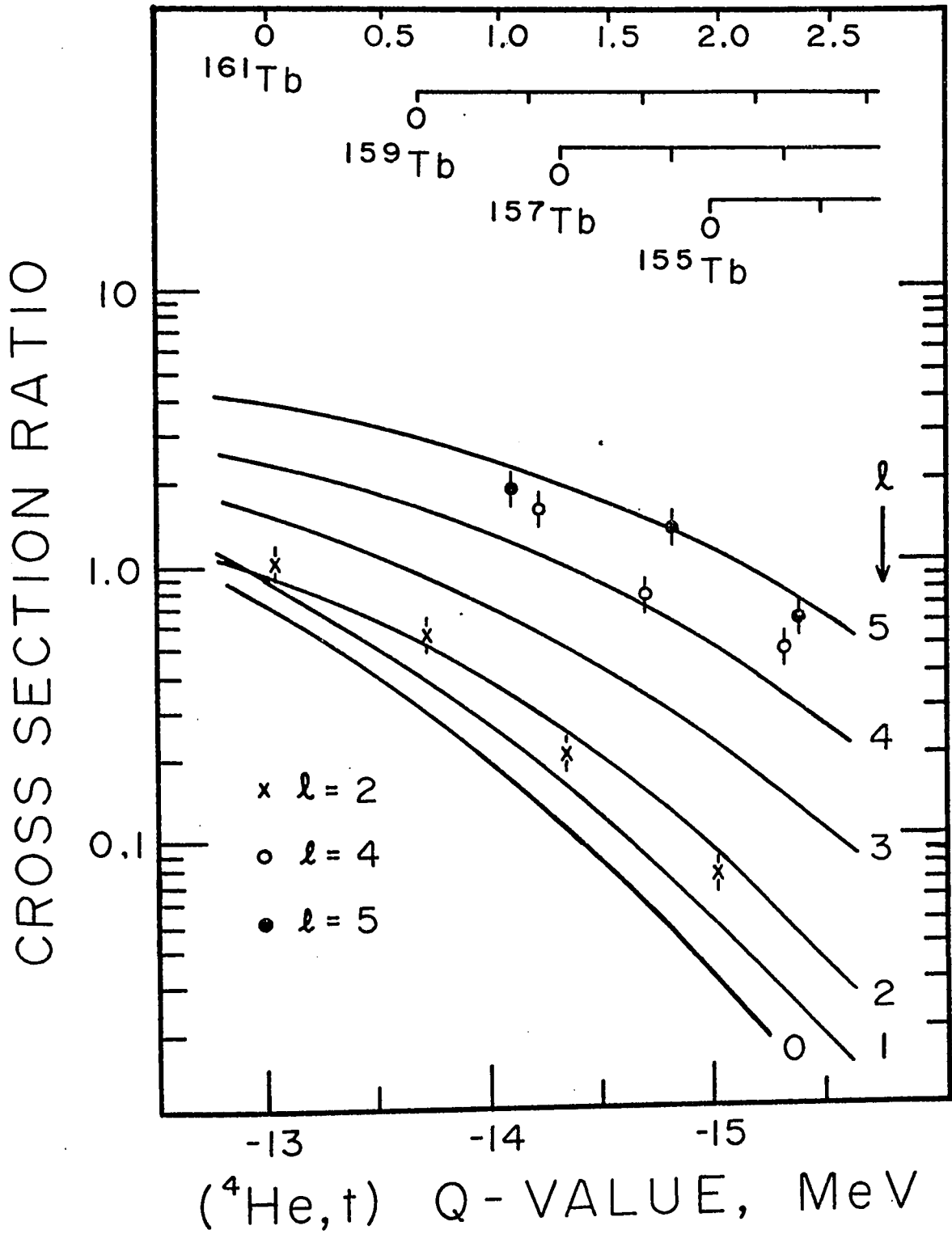


Figure 7

The ratio of the (α, t) cross section at $\theta = 60^\circ$ and $E = 25$ MeV to the $({}^3\text{He}, d)$ cross section at $\theta = 30^\circ$ and $E = 24$ MeV for the terbium isotopes. The solid lines are from the DWBA calculations. The $\ell = 2$ points are from the $5/2\ 3/2^+[411]$ state in each isotope (table 12), the $\ell = 4$ points are from the $7/2\ 5/2^+[413]$ state (table 13) and the $\ell = 5$ points, from the $11/2$ member of the mixed $7/2^- [523]$ and $5/2^- [532]$ orbitals (table 14). The $\ell = 4$ and $\ell = 5$ points are obscured by the ${}^{13}\text{C}({}^3\text{He}, d){}^{14}\text{N}(\text{g.s.})$ reaction for the ${}^{161}\text{Tb}$ isotope.

EXCITATION ENERGY, MeV



on the bound state spin orbit strength, and the calculations show that it affects the differential cross sections in both reactions as a constant multiplicative factor. It is thus important only for the determination of the absolute spectroscopic factors.

II.2b Spectroscopic Information and the Unified Model

If the spin (total angular momentum) of a state populated in the proton transfer reaction is known, the spectroscopic factor $\beta_{j\ell}^2$ (eqn. 27) can be extracted from the measured and calculated cross sections. For the present work it is desirable to interpret $\beta_{j\ell}^2$ in terms of the Unified Model.

The spectroscopic factor for proton transfer on an even-even target can be written from A.7:

$$\beta_{j\ell}^2 = \left(\int \phi_A \phi_x^{j\ell m} \phi_B^{J_B M_B} \right)^2 \quad (29)$$

where $J_A = M_A = 0$ and $J_B = j$

$$M_B = m$$

and $\phi_x^{j\ell m}$ is the bound state wave function of the proton.

The nuclear wave functions ϕ_A and $\phi_B^{J_B M_B}$ can be written as in eqn. (16):

$$\phi^{IM} = [(2I+1)/16\pi^2]^{1/2} [\theta_\Omega D_{M\Omega}^I + (-1)^{I+\Omega} \theta_{-\Omega} D_{M-\Omega}^I] \phi'_c$$

where $\theta_\Omega = (P_L \chi_{M,\Omega})$ P_L the phonon operator and $\chi_{M,\Omega}$,

the intrinsic quasi-particle state are coupled to projection Ω

ϕ'_c is the BCS core wavefunction for a quasi-particle

in state $\chi_{M,\Omega}$,

For the even-even target, there are no vibrational phonons or intrinsic

single quasi-particle states:

$$\phi_A = [1/8\pi^2]^{1/2} \phi_c \quad (30)$$

To evaluate (29), the bound state wave function $\phi_x^{j\ell m}$, which is defined in the laboratory system, must be expressed in terms of the body fixed (nuclear) axis. This is done by using the rotational D functions:

$$\phi_x^{j\ell m} = \sum_{\Omega'} \phi_x^{j\ell\Omega'} D_{m\Omega'}^j \quad (31)$$

Thus:

$$\beta_{j\ell} = \int \frac{\phi_c^*}{[8\pi^2]^{1/2}} \sum_{\Omega'} \phi_x^{j\ell\Omega'} D_{m\Omega'}^j \frac{(2j+1)^{1/2}}{(16\pi^2)^{1/2}} [\theta_{\Omega} D_{m\Omega}^j + (-1)^{j+\Omega} \theta_{-\Omega} D_{m-\Omega}^j] \phi_c' \quad (32)$$

Integrating over the angular coordinates of the nucleus (which affects only the D functions) gives:

$$\beta_{j\ell} = \frac{\langle \phi_c | \phi_c' \rangle}{\sqrt{2} (2j+1)^{1/2}} \int [\phi_x^{j\ell\Omega} \theta_{\Omega} + (-1)^{j+\Omega} \phi_x^{j\ell-\Omega} \theta_{-\Omega}] \quad (33)$$

The integral $\int \phi_x^{j\ell\Omega} \theta_{\Omega}$ over the internal coordinates selects out of θ_{Ω} only the pure single particle component with good j and ℓ . Thus intrinsic states that are vibrations have zero contribution to the spectroscopic factor. If θ_{Ω} is a pure single particle state, from the expansion of the state in terms of ones with good j and ℓ , (4), the integral is equal to $C_{j\ell}$. From the symmetry properties of $\theta_{-\Omega}$, the second term in the integral of (33) is also $C_{j\ell}$. Since

$$\phi_c' = \prod_{\nu \neq \mu} |U_{\nu} + V_{\nu} a_{\nu}^{\dagger} a_{\nu}^{\dagger}| 0 \rangle \quad (\text{where } \mu \text{ represents the intrinsic state } \theta_{\Omega}),$$

the term $\langle \phi_c | \phi_c' \rangle = U_{\mu}$

Thus

$$\beta_{j\ell} = \frac{\sqrt{2} C_{j\ell} U_{\mu}}{(2j+1)^{1/2}} \quad (34)$$

and the cross section from (27) can be written:

$$\frac{d\sigma}{d\Omega} = N \frac{2C_{j\ell}^2 U^2 \sigma_{DW}^{sj}}{2j+1} \quad (35)$$

The significance of (35) is that for a state of spin $I (=j)$ which is a rotational member of a band based on the single quasi-particle orbital $\chi_{\Omega} = \Omega^{\pi} [Nn_3\Lambda]$ with pairing parameter U , the spectroscopic strength for its population will be proportional to $C_{j\ell}^2 U^2$, where the $C_{j\ell}$ is the amplitude of the spherical state with good j and ℓ in the orbital χ_{Ω} .

This can be valuable for assigning states in the deformed nuclei. The $C_{j\ell}^2$'s are often characteristic of a certain Nilsson orbital, and by examining the relative energy spacings and the intensities of the levels (the 'fingerprint') from the experiment, it is often possible to interpret these levels as rotational members based on an intrinsic Nilsson orbital. The absolute intensity of the states populated in a band is governed by the U^2 (the 'emptiness') of the intrinsic state. As predicted by (35), one would expect that the greater the probability of the state being empty (U^2), the greater the probability of putting a particle into that state, and therefore, the greater the cross section.

It should be noted that the $C_{j\ell}$ measured by the stripping reaction is not consistent with that determined from the Nilsson model. The spherical states (of good j and ℓ) from which the intrinsic Nilsson state is expanded, are those for an harmonic oscillator. In the cross section calculation (DWBA), the spherical state is generated from a spherical Wood-Saxon potential with a binding energy

that depends only on the Q-value. It would be better to calculate the Nilsson $C_{j\ell}$ coefficients using the Wood-Saxon potential, although strictly one should perform a coupled channel calculation between these spherical components of the intrinsic state. This was done by Rost (1967), and the results were not significantly different from the Nilsson prediction. Moreover, in the reaction theory, the energy of the transferred particle in the average potential of the nucleus is determined from its binding energy. This neglects the effects of the residual interaction on the binding energy. The problem has been considered by Pinkston and Satchler (1965), and in deformed nuclei, where the effects of the strong residual interactions are included in the description of the deformed single quasi-particle states, it is not expected to be serious. For the present study, in view of the previous discussions, and the uncertainties in the theoretical and experimental cross sections, the $C_{j\ell}$'s from the Nilsson Model (Chi, 1966) are used.

In the calculation of the spectroscopic factor, it was indicated that the stripping amplitude into a vibrational state is zero. Consistent with the picture of the direct reaction mechanism, this simply implies that collective motions such as vibrations should not be populated by single particle transfer reactions. Empirically, this is generally found to be the case. It should be pointed out nevertheless, that one of the assumptions in the DWBA stripping formalism is that the term in the interaction potential (v in eqn. A.4) connecting the scattered particle with the core nucleons can be neglected. It is this term that could cause vibrational excitations in

stripping. Population of a state which has vibrational components is expected though, if it also has some single particle strength. This would result from the vibrational particle coupling discussed in section II.1e. The spectroscopic strength of a rotational member of the band built on the mixed state should be $2 C_{j\ell}^2 U^2 a_\alpha^2 / (2j+1)$ where a_α is the amplitude of the single quasi-particle state $|\alpha\rangle$ in the mixed vibrational state. In this case, the single particle transfer reaction can measure the magnitude of the single particle component in the mixed state.

Coriolis mixing also affects the measured spectroscopic strength. If the mixed state $\chi^I = \sum_U a_U \theta_U^I$, where θ_U^I is the I spin rotational member of the single quasi-particle state $|u\rangle$, it is simple to show that

$$\beta_{I\ell} = \frac{2}{2I+1} \left(\sum_U a_U C_{j\ell}^U U^U \right) \quad \text{where } (j=I) \quad (36)$$

The spectroscopic factor $\beta_{I\ell}^2$ depends sensitively on the signs of the a_U 's and $C_{j\ell}^U$'s. In the cases where the mixing is strong between only two states, one finds a shift of the spectroscopic strength to the state of lower excitation. For simplicity, the square of the term in brackets of (36) will be called the $U^2 C_{j\ell}^2$ for the state, regardless of how mixed it may be. Figure 8 demonstrates the effect that the strong mixing of members of the $5/2^- [532]$ and the $7/2^- [523]$ orbitals has on their spectroscopic strengths and energies.

II.3 Calculations

For the present work, the DWBA calculations were performed using the computer code DWUCK, written by Kunz (1967). Sets of

calculations were done for most of the reactions studied: Angular distributions for $\ell = 0, 1, 2, 3, 4$ and 5 were calculated for three or four Q -values that spanned the region of interest. The parameters used are shown in table 1, and are those used by Lu and Alford (1971). However, no lower cut-off was used in the radial integral. For the (α, t) and $({}^3\text{He}, d)$ reactions, there has been some uncertainty in the values of N , the normalization constant for the DWBA calculation (eqn. A.23). Kunz gives values of $N = 4.42$ and $N = 46$ for the $({}^3\text{He}, d)$ and (α, t) reactions respectively, whereas Hering *et al.* (1971) suggests values of $N = 4.23$ and $N = 35.1$ respectively. These normalizations are affected by finite range corrections (which can be made in the DWUCK program by the local energy approximation (Smith, 1967)). The suggested values of the finite range correction parameters by Kunz and Hering also differ. If the spectroscopic strength of some observed state were known, the normalization constants for the reactions could be determined empirically. As this was not the case, the value of $N = 4.42$ was arbitrarily chosen for the $({}^3\text{He}, d)$ reaction. In previous works (eg. Price *et al.* (1971)), the normalization constants for the (α, t) reactions were found to be too small. For the present studies, a value of $N=115$ was selected for the (α, t) calculations in order to obtain the same average spectroscopic strengths in both reactions for the well known $5/2 \ 3/2^+ [411]$ states of the four terbium isotopes. In the analysis, the values of $U_{j\ell}^2 C_{j\ell}^2$ extracted from the experimental data appear to be about 30% larger than those expected from the theoretical calculations. This effect is attributed to the 'arbitrary' definition of the normalization constant,

Table 1
Optical Model Parameters used in the D.W.B.A Calculations

Particle	V (MeV)	r_{oc} (fm)	r_o (fm)	a (fm)	W (MeV)	W_D (MeV)	r'_o (fm)	a' (fm)	$v_{s.o.}$ factor
α	-200	1.3	1.4	.6	-20		1.4	.6	
t	-200	1.3	1.4	.6	-50		1.4	.6	
^3He	-175	1.4	1.14	.723	-17.5		1.6	.81	
d	-111	1.25	1.05	.859		70.8	1.24	.794	
Bound State Proton	Adjusted to reproduce separation energy	1.25	1.25	.65					8.

though it is difficult to say whether or not it may also be due to limitations in the nuclear model.

From the calculated angular distributions for the different l and Q values, curves of the Q dependence at each particular reaction angle were obtained. Some typical curves are shown in figures 5 and 6. These were used to extract the $U^2 C_{j\ell}^2$'s for the assigned states. As well, theoretical curves of the cross section ratio were generated as shown in fig. 7, and were used to estimate the l -values of the transitions to the states in the residual nuclei.

Parameter variations for the DWBA calculations were undertaken in an attempt to find a better fit to the experimental angular distributions for the (α, t) reactions (shown in figures 3 and 4). These were not successful as the shape of the angular distributions seemed rather insensitive to the parameters. Fortunately, this insensitivity was also found in the calculated Q dependence, which gives some confidence to the extracted spectroscopic strengths.

The theoretical calculation of the spectroscopic strengths of the states for the nuclei in the study was made with a program written by O'Neil (1970). A Nilsson type calculation based on the approach of Chi (1966) was performed to calculate the structure of the intrinsic states. The energies of these states were then corrected for the effect of pairing (eqn. 9) and the rotational bands were constructed. The effect of Coriolis coupling was then calculated by diagonalizing the total rotational Hamiltonian (H_{rpc} included) in the single-quasi-particle basis. The resulting energies and $U^2 C_{j\ell}^2$'s of the band members could then be compared with the experimental obser-

vations. The potential well parameters of the Nilsson calculation were $\kappa=0.0637$ and $\mu=0.6$. The states considered in the calculations were the $1/2^+[420]$, $1/2^+[411]$, $3/2^+[411]$, $3/2^+[422]$, $5/2^+[413]$, $5/2^+[402]$, $7/2^+[404]$, $1/2^+[660]$, $1/2^-[550]$, $1/2^-[541]$, $3/2^-[532]$, $3/2^-[541]$, $5/2^-[532]$, $7/2^-[523]$, $9/2^-[514]$ and $11/2^-[505]$ Nilsson orbitals.

Deformations of $\delta=0.275, 0.32, 0.28, 0.31, 0.33, 0.34$ and 0.32 were used of ^{153}Eu , ^{155}Eu , ^{155}Tb , ^{157}Tb , ^{159}Tb , ^{161}Tb and ^{163}Ho respectively, as measured by Elbek (1963) for the corresponding target isotones.

In view of the theoretical limitations of the models discussed previously, these calculations were done only to determine if the observed states could be described by these models. Thus the Nilsson energies as well as the rotational parameters, the Fermi energy and the attenuation coefficient of the Coriolis matrix elements were treated as adjustable (though not free) parameters. For example, the rotational parameter was varied between 9 keV and 14 keV, the attenuation coefficient between 0.5 and 1.0, and the band head energies within several hundred keV of that predicted by the Nilsson model with pairing. The results of the calculations are discussed with the level interpretations.

The effect of the Coriolis mixing on the energies and spectroscopic strengths is demonstrated in figure 8. In these calculations, all the orbitals from the spherical $h_{11/2}$ shell (see fig.1) were included. The rotational parameter was 13.3 keV, the unperturbed bandhead energies (actually the energies of the lowest rotational member of the band) were 370 keV for the $5/2^-[532]$ orbital and 450 keV for the $7/2^-[523]$ orbital, the Fermi energy was zero and the Coriolis

Figure 8

Comparison of the calculated energies and spectroscopic strengths of the $5/2^- [532]$ and $7/2^- [523]$ orbitals, both mixed and unmixed, with the observed energies and strengths of states in ^{159}Tb . Details of the calculation are in section II.3.

5/2⁻[532] ORBITAL

UNMIXED

11/2

5/2

7/2

9/2

11/2

7/2⁻[523]

ORBITAL

UNMIXED

(Relative Scale)

7/2

9/2

MIXED STATES

11/2

$U^2 C_{j\lambda}$

5/2

7/2

9/2

7/2

9/2

11/2

7/2

9/2

OBSERVED STATES

11/2

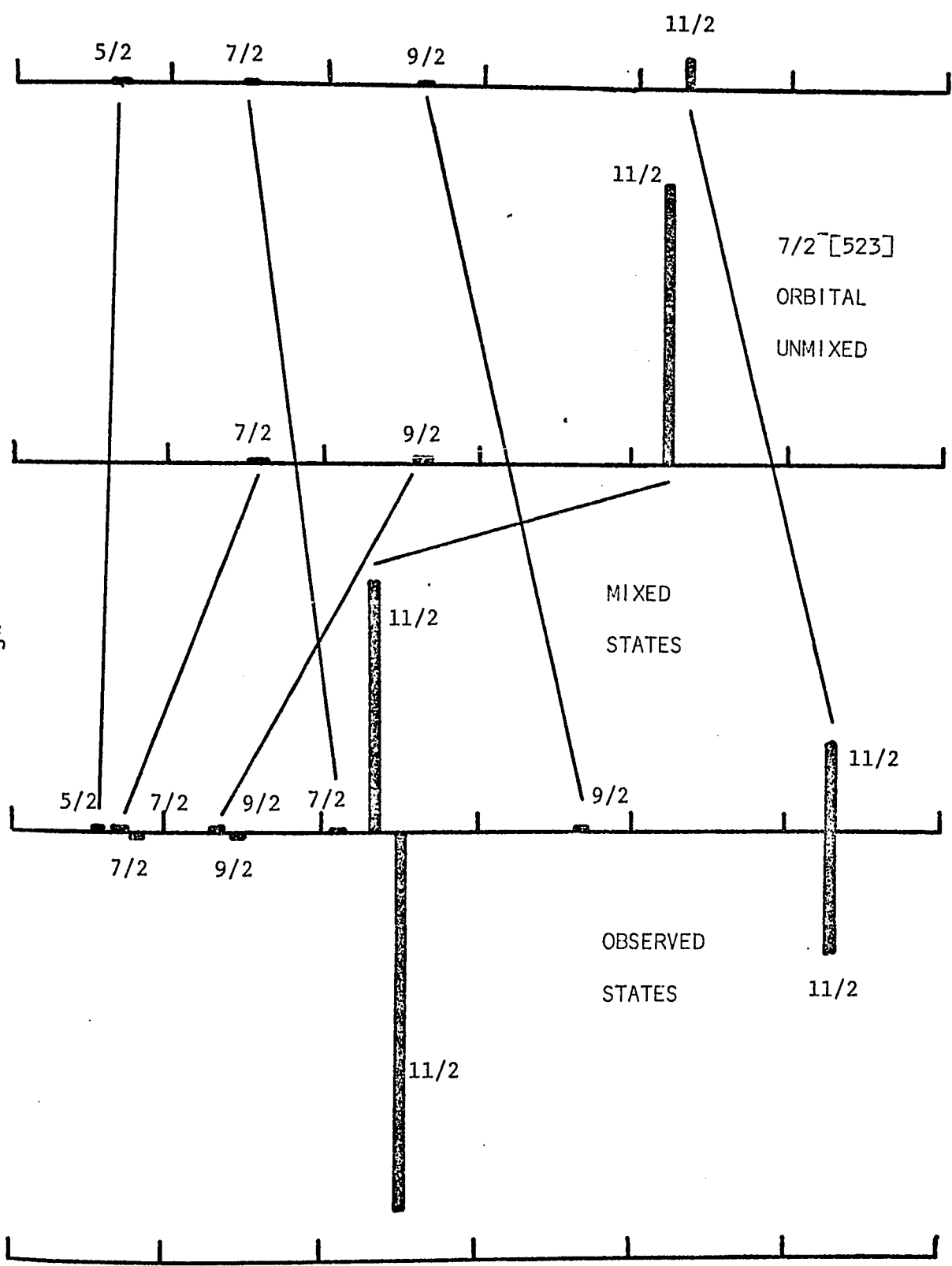
11/2

400

600

800

Excitation Energy (KeV)



attenuation coefficient was 0.77. The results of the calculations are consistent with the experimental energies and strengths shown in the lower part of fig. 8.

III Experimental Considerations

III.1 Outline of the Experiment

Thin targets of gadolinium, dysprosium and samarium were exposed to 24 MeV beams of $^3\text{He}^{++}$ and 25 MeV beams of α^{++} from the McMaster University Tandem Van de Graaff accelerator. The reaction products were analysed at various reaction angles by an Enge split-pole magnetic spectrograph and detected by photographic emulsions. The energies and relative differential cross sections of the levels populated in the residual nuclei were determined from the positions and densities of the tracks of the reaction products in the emulsions. The absolute differential cross sections were determined using a solid state particle detector placed in the target chamber to monitor the elastically scattered particles.

III.2 Target Preparation

The targets used for the experiments generally consisted of $\sim 40\mu\text{g}/\text{cm}^2$ of rare earth metal foil supported by $\sim 30\mu\text{g}/\text{cm}^2$ of carbon backing. The target manufacture was based on the process described by Westgaard and Bjornholm (1966). Oxides of ^{152}Sm , ^{154}Sm , ^{154}Gd , ^{156}Gd , ^{158}Gd , ^{160}Gd and ^{162}Dy were obtained from the Isotope Sales Division of the Oak Ridge National Laboratory. Lists of the isotopic impurities are shown in table 2. The oxides were mixed with a reducing metal (for samarium oxide, lanthanum metal was used and for the gadolinium and dysprosium oxides, thorium metal) and placed in

Table 2

Percentage Abundance of Gd Isotopes in Target

Target	152	154	155	156	157	158	160
^{154}Gd	<0.01	99.35	0.48	0.10	0.04	0.02	0.01
^{156}Gd	<0.05	0.13	1.99	93.58	2.57	1.27	0.46
^{158}Gd	<0.05	<0.05	0.25	0.56	0.81	97.59	0.81
^{160}Gd	<0.02	0.09	0.41	0.72	0.67	2.16	95.95

Percentage Abundance of Dy isotopes in Target

Target	156	158	160	161	162	163	164
^{162}Dy	<0.02	<0.02	0.08	1.22	96.26	1.75	0.69

Percentage Abundance of Sm isotopes in Target

Target	144	147	148	149	150	152	154
^{152}Sm	<0.01	0.08	0.07	0.12	0.10	99.18	0.45
^{154}Sm	-	0.04	0.04	0.19	0.04	0.39	99.30

a small tantalum crucible. The crucible was put in a vacuum chamber and heated by electron bombardment using a Varian electron gun. The evaporated metal from the reduced oxide was condensed onto the carbon substrates which were on glass slides held 3 to 4 inches above the crucible. For the samarium targets, the crucible was heated about 9 min. at 1300 °C, and for the dysprosium and gadolinium targets, temperatures of 1700 °C and 2000 °C respectively were maintained for 6 one minute intervals with a 10 minute 'cool down' period between. The intermittent heating was necessary as the higher temperatures often caused the carbon backings to disintegrate. The temperatures, measured by an optical pyrometer, may have been incorrect by several hundred degrees, but the measurements were made only to maintain similar conditions from one evaporation to another. The targets were floated off from the glass slide in distilled water and were picked up on aluminum frames, 1" square with a 1 cm. hole in the centre.

Some tests of the target purities were made. On a typical evaporated sample of samarium, a neutron activation analysis by Ungrin (1969-Thesis) indicated that there was less than 0.1% lanthanum. On a typical sample of gadolinium metal, an electron microprobe analysis indicated about 5% contamination with thorium. For a number of targets, the energies and intensities of the elastically scattered particles were measured by the spectrograph. The intensities of the particles scattered by the contaminants were consistent with those expected for these impurity concentrations.

III.3 F.N. Accelerator

The 24 MeV ^3He and 25 MeV α beams were produced by the McMaster

model F.N. Tandem Van de Graaff accelerator. The three main components of the accelerator are the ion source, the high voltage system and the beam handling system.

Negative ions of helium are generated in the duoplasmatron ion source. From a plasma, positive helium ions are extracted by voltages of ~ 20 kV. These are focussed electrically into a canal containing lithium vapour. Passing through the vapour, about 1% of the ions pick up electrons to become negatively charged. These negative ions are then electrically extracted, and focussed down the beam line towards the high voltage section of the accelerator. The energy of the beam is about 40 keV and the intensity is typically $\sim 5 \mu\text{a}$.

The high voltage terminal of the accelerator is held at +8.00 MV for the 24 MeV helium beams and at +8.33 MV for the 25 MeV helium beams. The negative ions accelerate towards a thin carbon foil in the terminal. As they pass through, for most of the ions, all the electrons are stripped off. The resulting positive ions accelerate from the terminal towards the analyzing magnet which is used to select the particle energies. The ions are magnetically focussed through sets of collimating slits before (the object slits) and after (the image slits) the analyzing magnet. The beam currents on the image slits, together with a feed back mechanism, are used to stabilize the terminal voltage.

The beam handling system from the terminal to the target is primarily concerned with directing a highly collimated beam onto the target. Doublet and triplet quadrupole magnets are used as astigmatic lenses to focus the beam from the image slits onto the target. For


the typical settings of the image slits at 1.5 mm vertical gap and 0.75 mm horizontal gap, the beam current through them is usually about 1.5 μ a. With the slits at the target chamber entrance that have a 3 mm vertical gap and a 1 mm horizontal gap, the beam current passing through the target is typically about 90% of that through the image slits. The beam entering the analyzing magnet has an energy spread which is a product of the effects of the ion source, the stripper foil straggling and the voltage stabilization of the terminal. The dispersive effect of the analyzing magnet and the switching magnet combine to produce a gradient of particle energies across the target. This spread in energy, which creates a wide beam spot on the target, is compensated for by the dispersion of the spectrograph, resulting in a narrow image at the focal plane of the instrument (figure 9 outlines the beam optics and demonstrates the dispersive effects on the beam spot size). This effect, called dispersion compensation, can be optimised by an appropriate choice of the target angle if the energy gradient in the beam spot is known.


III.4 The Enge Spectrograph


The spectrograph used to analyze the reaction products is an Enge Split-pole type, with a maximum radius of curvature of $\rho \approx 90$ cm. A detailed description of the device can be found in the paper by Spencer and Enge (1966). Figure 10 shows an outline of the magnet pole faces and some particle trajectories. The large solid angle of acceptance, as well as the high resolution of the spectrograph, are essential for the present experiments. The device is designed


Figure 9

Diagram of the beam handling system from the object slits of the analyzing magnet to the focal plane of the Enge spectrograph.

 across the beam represents a focus of the beam in the transverse horizontal direction.

 represents the magnitude of the dispersive effect of the analyzing magnet on the beam. For an aberration free system, this would be a measure of the width of the beam. The point indicates the direction of displacement (dispersion) of the higher energy parts of the beam.

 applies similarly to the switching magnet.

 applies similarly to the spectrograph.

The effect of the dispersion in the spectrograph can help to cancel the contributions from the analyzing and switching magnets.

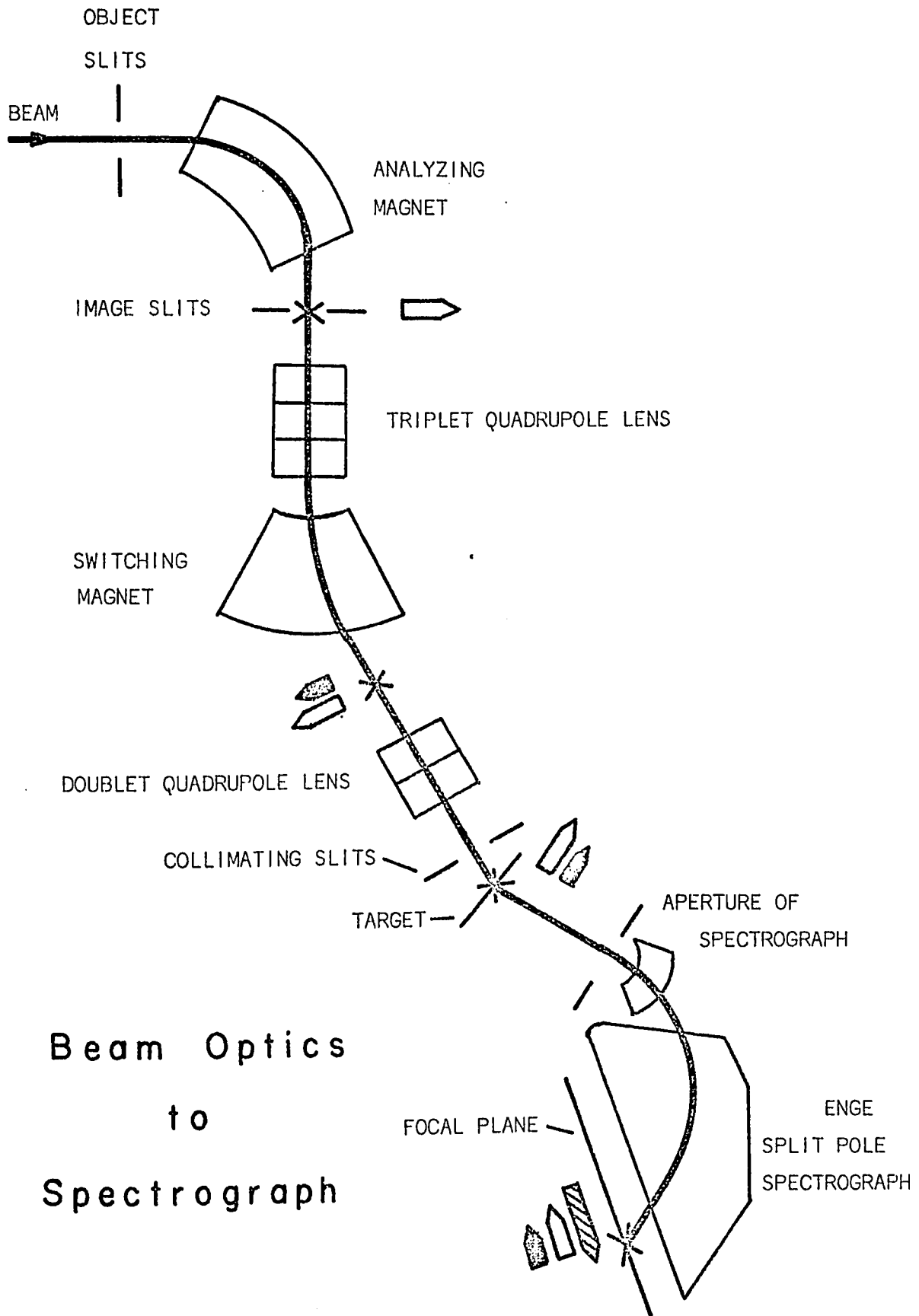
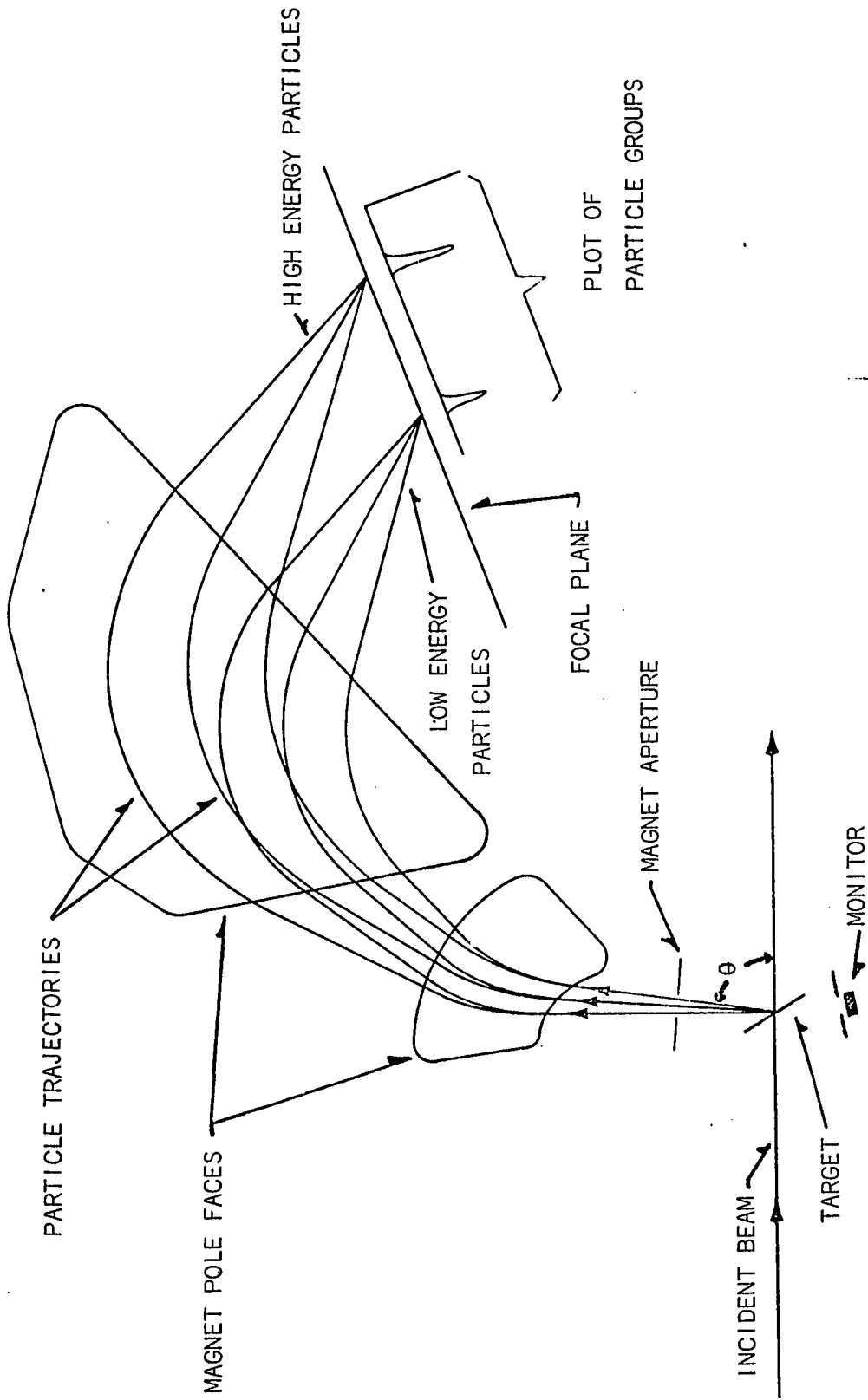


Figure 10

Outline of the Enge Split-pole Spectrograph, showing the magnet pole faces, and some particle trajectories. The position of the monitor used in the present experiments is also shown, as well as the reaction angle θ .



to have approximate second order focussing over its full momentum range $p_{\max}/p_{\min} \approx 2.8$ in the horizontal (median) plane and some vertical focusing as well. This, as well as the high dispersion ($\Delta y/\Delta p \approx 1.7$, where y is the distance along the focal plane) and low horizontal magnification ($M_H \approx 0.35$) give a high total resolving power ($p/\Delta p \approx 3000$) for an aperture of ≈ 2 msr. (milliradians). The spectrograph is designed to correct for the kinematic broadening which occurs for large acceptance angles in the horizontal plane. This broadening is a spread in the energy of the scattered particles and is due to the variation in the recoil energy loss in the target as a function of the scattering angle of the projectile. This effect, which is greater for a light mass nucleus than a heavy mass nucleus, decreases the focal length of the spectrograph (moves the focal plane closer to the magnet poles). In the present experiments, the kinematic correction is made for the rare earth masses. Thus reactions from the rare earth nuclei produce narrow peaks in the spectrum, whereas reactions with light impurities (eg. $^{13}\text{C}(^3\text{He},d)^{14}\text{N}$) produce broad peaks (see for example fig. 12). The photographic plates used for the experiments are 5 cm by 25 cm Kodak NTB50 nuclear emulsions, which are covered with aluminum foils, 0.1 mm thick, to absorb knock-on carbon nuclei and singly charged alpha particles in the (α, t) experiments, and 0.5 mm thick to absorb tritons from the $(^3\text{He}, t)$ reaction in the $(^3\text{He}, d)$ experiments.

III.5 Experimental Investigations

The experiments done for the present studies are shown in

table 3. Figures 11 to 17 show the results of typical exposures for each of the nuclei studied. As well, the angular distributions of the tritons from the (α, t) reactions on the two samarium isotopes were measured. The angular distributions for the population of the $7/2 \ 5/2^+$ [413], $5/2 \ 3/2^+$ [411] and the $11/2 \ 5/2^-$ [532] states in the residual europium isotopes are shown in figures 3 and 4, along with the calculated angular distributions discussed in section II.3.

III.6 Extraction of Cross Sections and Energies

The nuclear emulsions were developed and scanned for the tracks of the reaction product in 0.25 mm strips. The total intensities and positions of the peaks in the resulting spectra were determined both by a hand calculation of the sums and centroids of the peaks, and by a spectrum fitting program which used a skewed-Gaussian peak shape in a non-linear least squares fit. The energies of the detected particles were calculated from their positions on the photographic plate. The spectrograph was previously calibrated using a radioactive alpha particle emitter to give ρ (the radius of curvature in the magnetic field) as a function of the plate position. This, together with the strength of the magnetic field measured by an NMR (Nuclear Magnetic Resonance) fluxmeter is sufficient to determine the energy of a scattered particle from a measured plate position. The excitation energy corresponding to each plate position was determined by its distance from the peak of a strongly populated state with known excitation energy. In principle, the excitation energies can be determined directly if the beam energy and Q-values are well known. From the intensities of the peaks, the relative

Table 3

Experiments Done in the Present Study

Nucleus Studied	Target	(α, t) reaction E = 25 MeV	($^3\text{He}, d$) reaction E = 24 MeV
^{153}Eu	^{152}Sm	$\theta = 60^\circ, 40^\circ$ + $6^\circ, 15^\circ, 90^\circ, 120^\circ$	$\theta = 27.5^\circ$
^{155}Eu	^{154}Sm	$\theta = 60^\circ, 45^\circ$ + $20^\circ, 30^\circ, 75^\circ, 90^\circ, 120^\circ$	$\theta = 45^\circ$
^{155}Tb	^{154}Gd	$\theta = 60^\circ, 30^\circ$	$\theta = 30^\circ, 40^\circ$
^{157}Tb	^{156}Gd	$\theta = 60^\circ, 45^\circ$	$\theta = 30^\circ, 50^\circ$
^{159}Tb	^{158}Gd	$\theta = 60^\circ, 45^\circ$	$\theta = 30^\circ, 50^\circ$
^{161}Tb	^{160}Gd	$\theta = 60^\circ, 45^\circ$	$\theta = 30^\circ, 50^\circ$
^{163}Ho	^{162}Dy	$\theta = 60^\circ, 45^\circ$	$\theta = 30^\circ, 50^\circ$

+ experiments used in angular distributions only.

Figure 11

The spectra obtained from the $^{154}\text{Gd}(\alpha, t)^{155}\text{Tb}$ reaction at $\theta = 60^\circ$ and the $^{154}\text{Gd}({}^3\text{He}, d)^{155}\text{Tb}$ reaction at $\theta = 30^\circ$. The previous and proposed assignments are shown. The broad peak labelled ${}^{14}\text{N}^*$ is due to the ${}^{13}\text{C}({}^3\text{He}, d){}^{14}\text{N}$ (2.3 MeV) reaction. The $1/2^+[411]^*$ label is to identify the $1/2^+[411]$ orbital fragment referred to in section IV.1g. The $(5/2^-[532])$ and $(7/2^-[523])$ labels identify the strongly mixed negative parity orbitals.

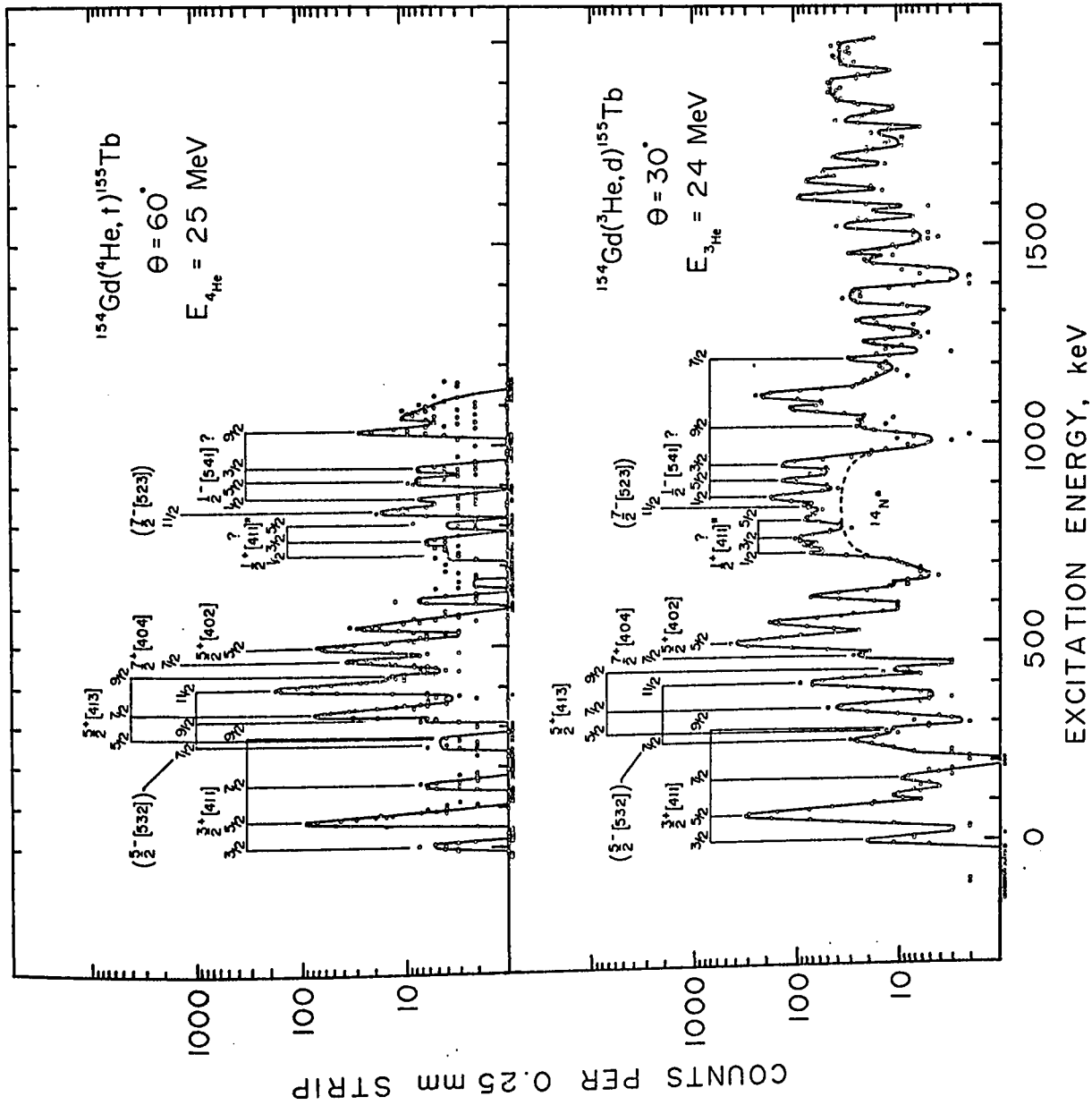


Figure 12

The spectra obtained from the $^{156}\text{Gd}(\alpha,t)^{157}\text{Tb}$ reaction at $\theta = 60^\circ$ and the $^{156}\text{Gd}({}^3\text{He},d)^{157}\text{Tb}$ reaction at $\theta = 30^\circ$. See also the caption for Fig. 11. The broken lines are for tentative multiple assignments of peaks. The broad peak near the ground state in the $({}^3\text{He},d)$ spectrum is probably due to a light impurity in the target.

Figure 13

The spectra obtained from the $^{158}\text{Gd}(\alpha, t)^{159}\text{Tb}$ reaction at $\theta = 60^\circ$ and the $^{158}\text{Gd}({}^3\text{He}, d)^{159}\text{Tb}$ reaction at $\theta = 30^\circ$. See also the caption for Fig. 12. The peak labelled ^{14}N is due to the $^{13}\text{C}({}^3\text{He}, d)^{14}\text{N}$ (g.s) reaction.

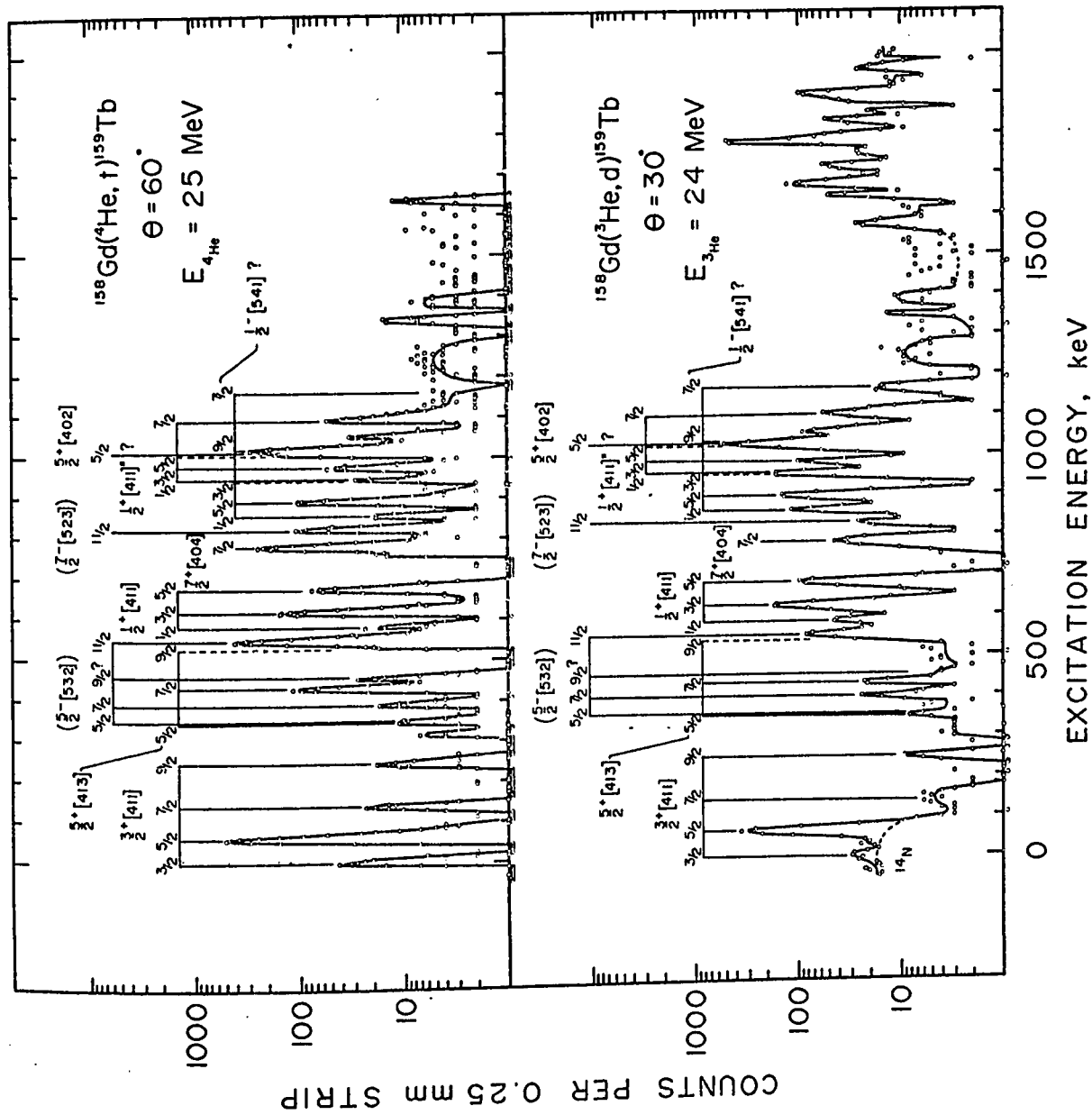


Figure 14

The spectra obtained from the $^{160}\text{Gd}(\alpha, t)^{161}\text{Tb}$ reaction at $\theta = 60^\circ$ and the $^{160}\text{Gd}({}^3\text{He}, d)^{161}\text{Tb}$ reaction at $\theta = 50^\circ$. See also the caption for Fig. 13.

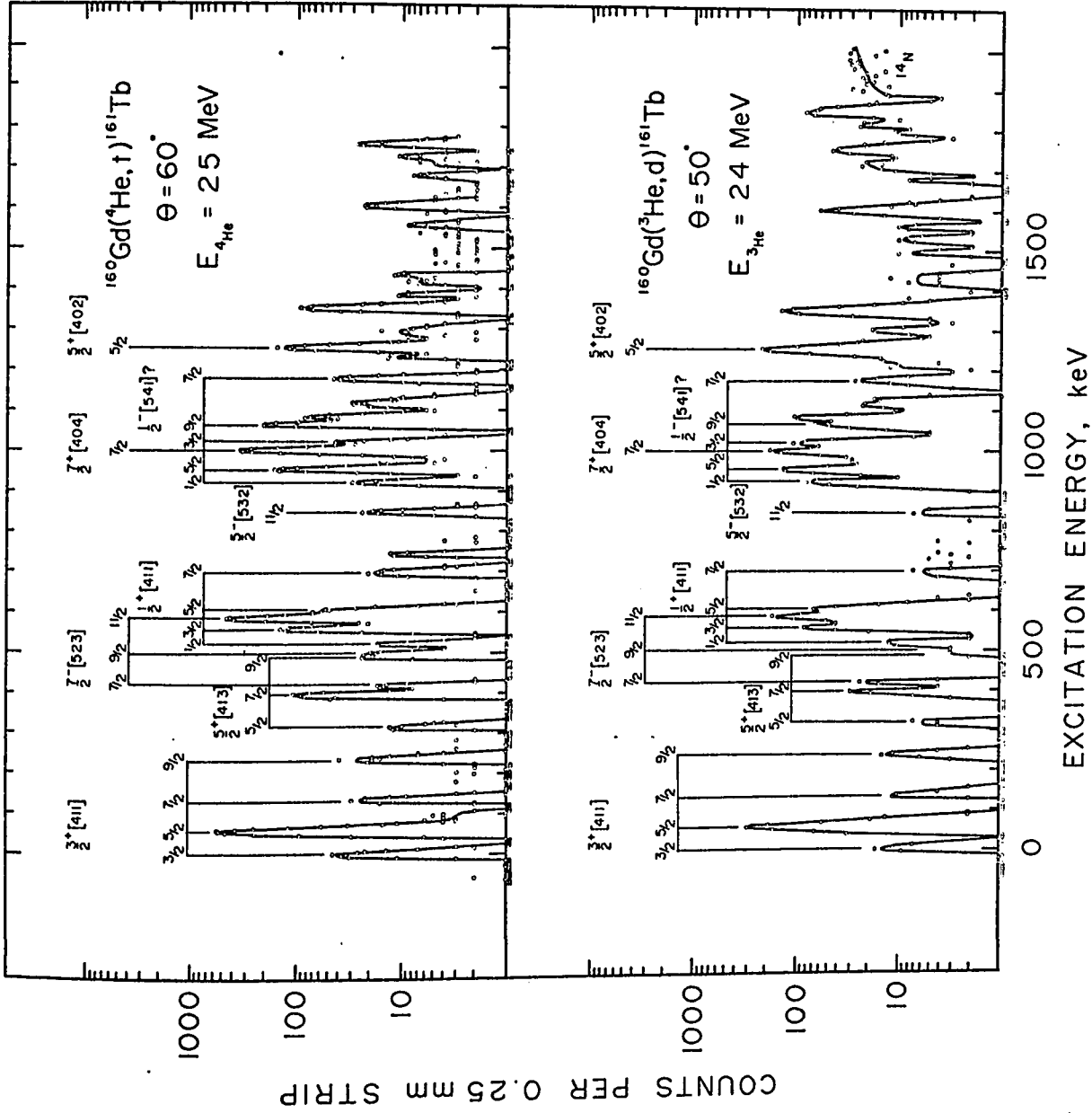


Figure 15

The spectra obtained from the $^{162}\text{Dy}(\alpha, t)^{163}\text{Ho}$ reaction at $\theta = 60^\circ$ and the $^{162}\text{Dy}({}^3\text{He}, d)^{163}\text{Ho}$ reaction at $\theta = 30^\circ$. The previous and proposed assignments are shown. The broad peak labelled $^{14}\text{N}^*$ is due to the $^{13}\text{C}({}^3\text{He}, d)^{14}\text{N}$ (2.3 MeV) reaction

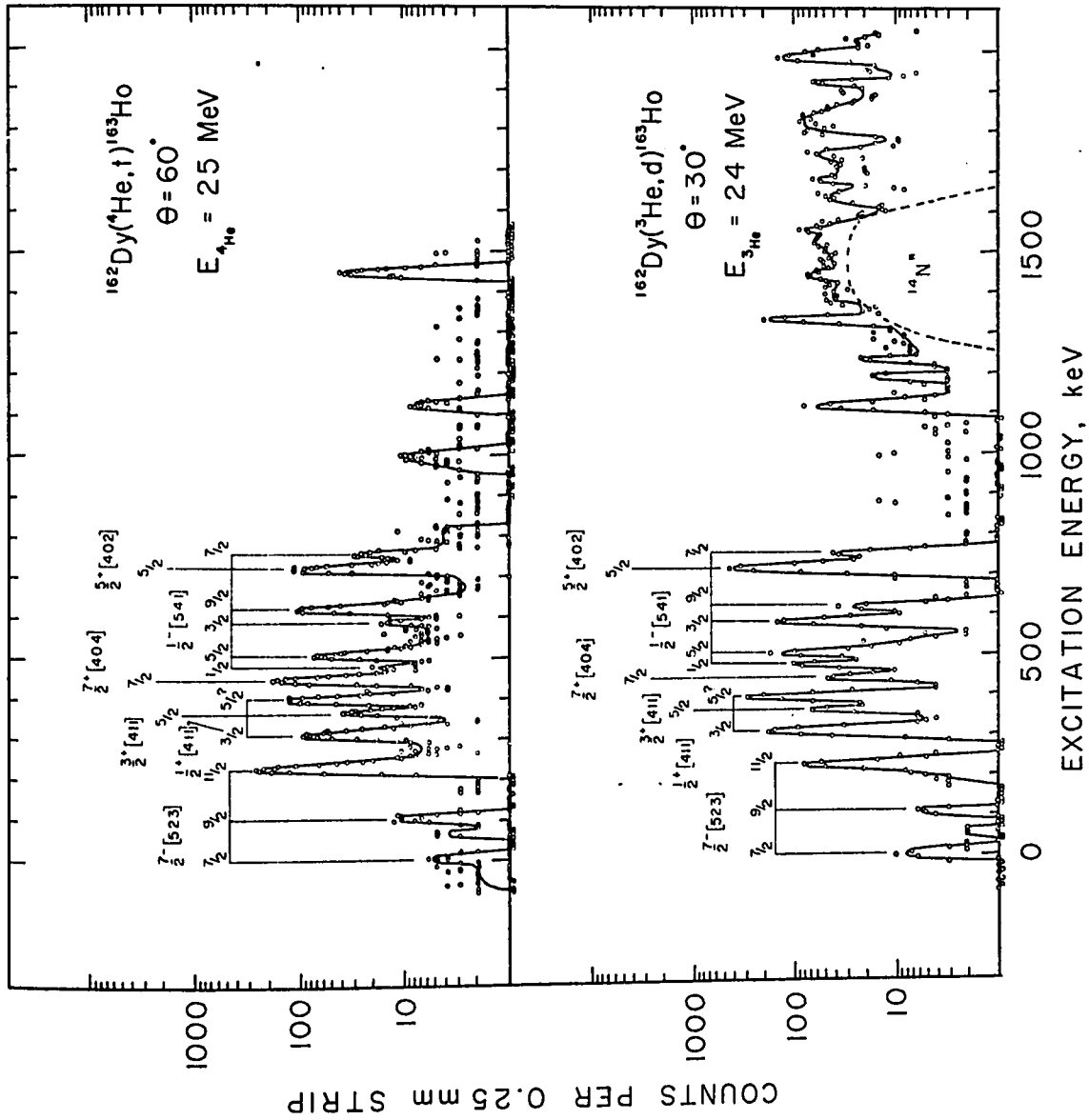


Figure 16

The spectra obtained from the $^{152}\text{Sm}(\alpha, t)^{153}\text{Eu}$ reaction at $\theta = 60^\circ$ and the $^{152}\text{Sm}(^3\text{He}, d)^{153}\text{Eu}$ reaction at $\theta = 27.5^\circ$ ($E = 24$ MeV). The previous and proposed assignments are shown.

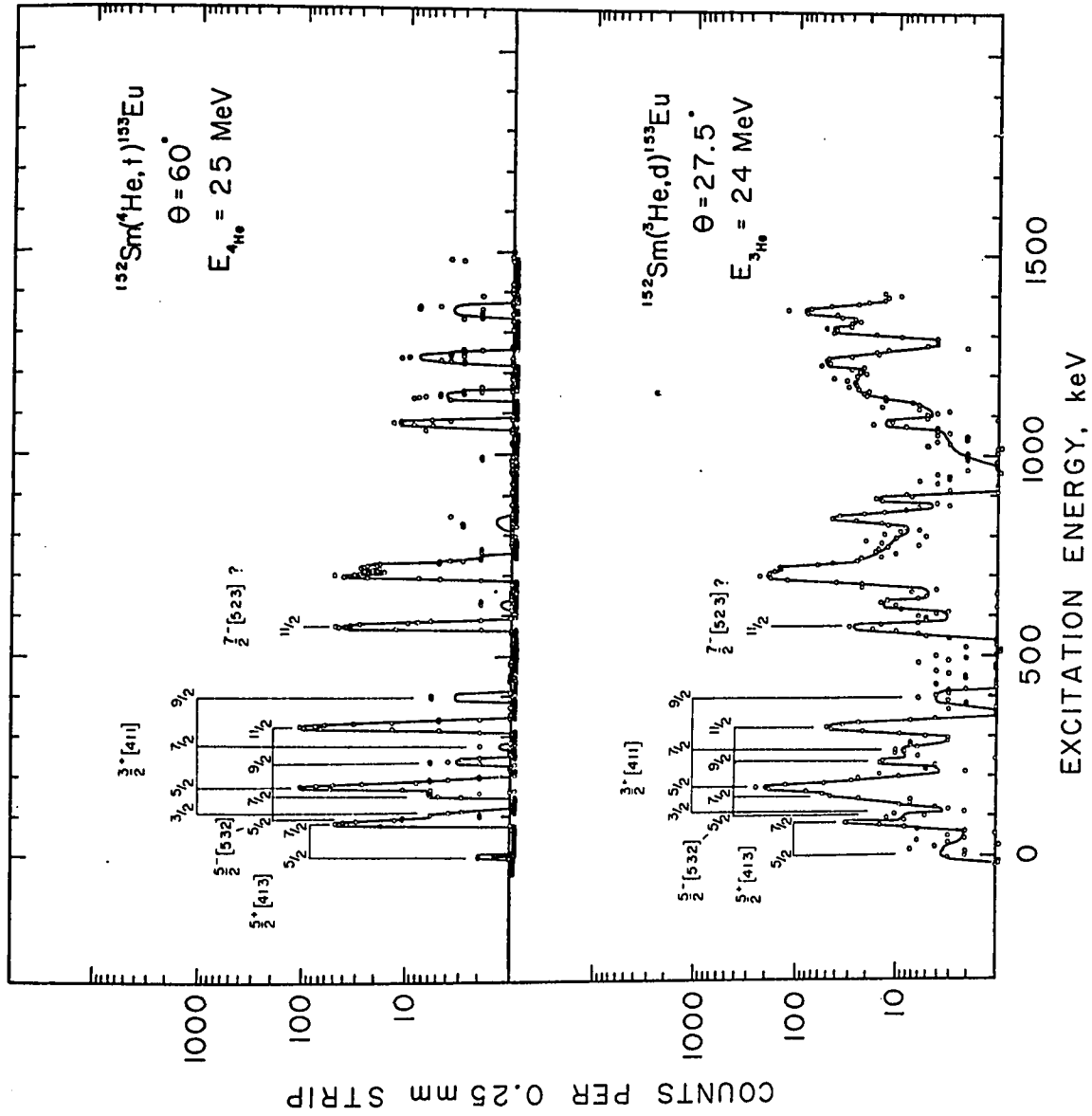
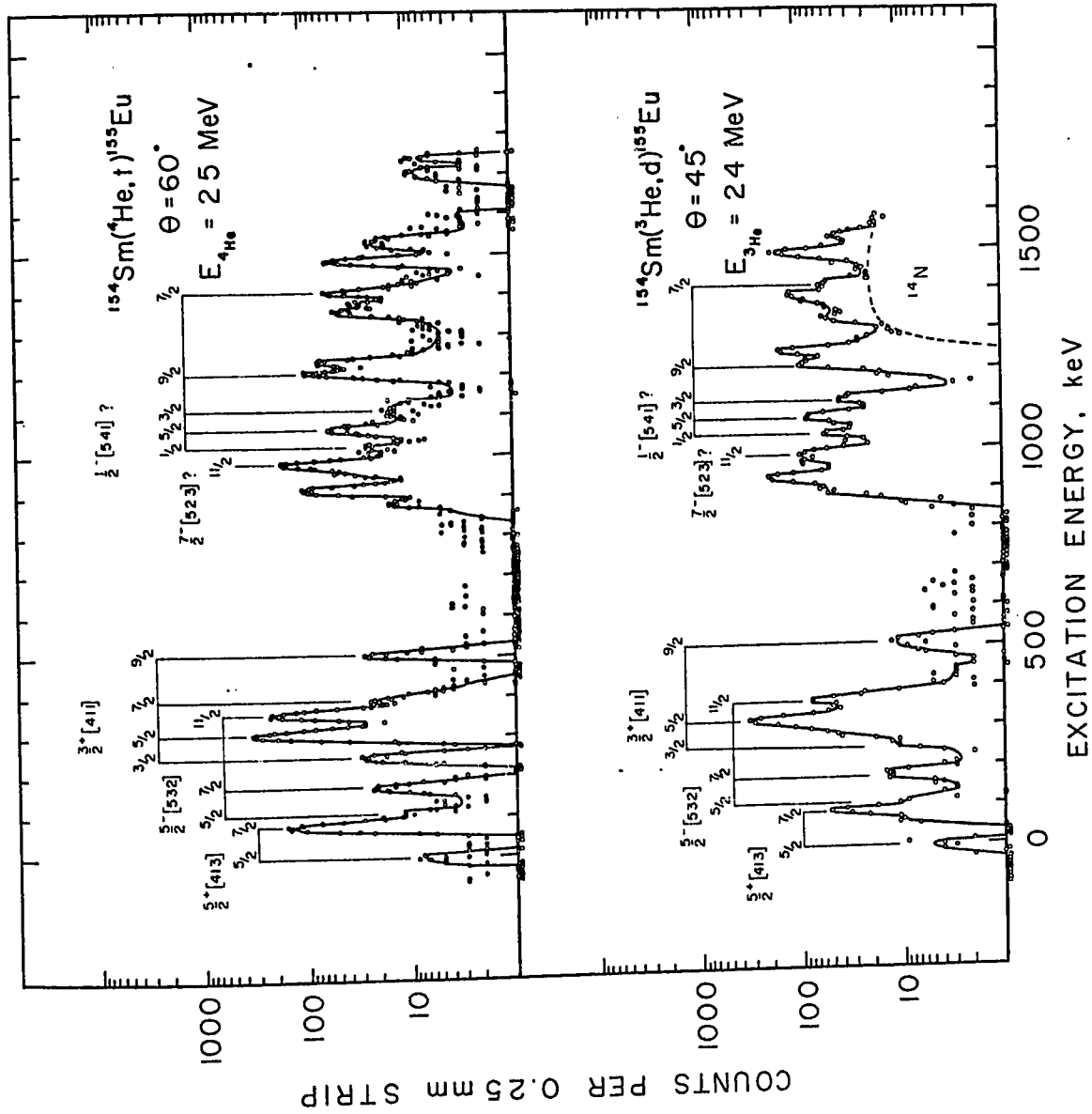


Figure 17

The spectra obtained from the $^{154}\text{Sm}(\alpha, t)^{155}\text{Eu}$ reaction at $\theta = 60^\circ$ and the $^{154}\text{Sm}(^3\text{He}, d)^{155}\text{Eu}$ reaction at $\theta = 45^\circ$ ($E = 24$ MeV). The previous and proposed assignments are shown. The broad peak labelled ^{14}N is due to the $^{13}\text{C}(^3\text{He}, d)^{14}\text{N}$ (g.s.) reaction.



differential cross sections were calculated. A lithium-drifted silicon detector was placed in the target chamber at $\theta=30^\circ$ from the incident beam direction. The number of particles scattered into the detector was measured, and by using the solid angles subtended by the detector and the spectrograph, and the elastic scattering cross section for the incident beam at $\theta=30^\circ$, the absolute cross sections of the peaks observed in the spectra were calculated. The elastic scattering cross sections for $\theta=30^\circ$ were taken to be 100% of the Rutherford cross section, as predicted by the DWBA calculations for both the ^3He at $E = 24$ MeV and α at $E = 25$ MeV. As discussed in section III.2, the gadolinium targets had $\sim 5\%$ thorium impurity. For experiments with these targets, a correction was made to the number of particles measured by the monitor.

The energies and intensities of the levels populated in the reactions are shown in tables 5 to 11. For the typical spectrograph solid angle of $\sim 2\text{msr.}$, the resolution was usually ~ 12 keV FWHM for the (α,t) reaction and ~ 16 keV FWHM for the $(^3\text{He},d)$ reactions. For the strong peaks, the excitation energies have uncertainties of ~ 3 keV and the relative intensities, uncertainties of $\sim 10\%$. For the absolute cross sections, which are very sensitive to the angle at which the monitor was placed as well as the solid angle subtended, uncertainties of $\sim 25\%$ are estimated.

In the (α,t) reactions, the elastically scattered alphas were detected at positions near the triton spectra on the photographic plates. From the positions of the alpha peak and the peaks in the triton spectra, the ground state Q values were determined. Table 4

Table 4

Reaction Q-values

<u>Reaction</u>	<u>1971 Mass Table</u> a)	<u>1972 Mass Table</u> b)	<u>This Work</u>
$^{154}\text{Gd}(\alpha, t)^{155}\text{Tb}$	-14.997 ± 0.02	-14.971 ± 0.012	-14.96 ± 0.03
$^{156}\text{Gd}(\alpha, t)^{157}\text{Tb}$	-14.293 ± 0.006	-14.297 ± 0.005	-14.28 ± 0.02
$^{158}\text{Gd}(\alpha, t)^{159}\text{Tb}$	-13.702 ± 0.008	-13.677 ± 0.002	-13.66 ± 0.02
$^{160}\text{Gd}(\alpha, t)^{161}\text{Tb}$	-13.015 ± 0.011	-12.998 ± 0.005	-12.98 ± 0.02
$^{162}\text{Dy}(\alpha, t)^{163}\text{Ho}$	-14.336 ± 0.003	-14.331 ± 0.003	-14.32 ± 0.02
$^{152}\text{Sm}(\alpha, t)^{153}\text{Eu}$	-13.928 ± 0.004	-13.918 ± 0.003	-13.92 ± 0.015
$^{154}\text{Sm}(\alpha, t)^{155}\text{Eu}$	-13.158 ± 0.006	-13.161 ± 0.004	-13.14 ± 0.02
a)	Wapstra and Gove (1971)		
b)	Meredith and Barber (1972)		

Table 5

Levels in ^{155}Tb

Energy (keV)			$d\sigma/d\Omega$ ($\mu\text{b}/\text{sr}$)				Interpretation
(prev.)	(α, t)	($^3\text{He}, d$)	($^3\text{He}, d$)	($^3\text{He}, d$)	(α, t)	(α, t)	
			$\theta=30^\circ$	$\theta=40^\circ$	$\theta=60^\circ$	$\theta=30^\circ$	
0	0	0	3.1	4.7	1.0	0.4	$3/2\ 3/2^+[411]$
65.4	65	65	110	101	20	2.7	$5/2\ 3/2^+[411]$
155.8	155	152	4.9	2.2	1.3	<0.4	$7/2\ 3/2^+[411]$
250.0	~ 250	252	~ 12	7.8	1.2	0.8	$7/2^-\{5/2^-[532]\}^a$
271.2							$5/2\ 5/2^+[413]$
274.1		272	~ 4.5	6.8	0.8	<0.4	$9/2\ 3/2^+[411]$
317.0	318		<2	<1	1	<0.4	$9/2^-\{5/2^-[532]\}$
335.0	335	334	17	18.5	18.3	4.8	$7/2\ 5/2^+[413]$
397.4	398	397	34	36	45	19	$11/2^-\{5/2^-[532]\}$
452.6	~ 450		2	<0.8	1.5	<0.4	$9/2\ 5/2^+[413]$
466.9	467	466	7.7	8	7.6	2.5	$7/2\ 7/2^+[404]$
498.8	499	501	157	161	16.5	2.7	$5/2\ 5/2^+[402]$
549.9	550	548	66	56	6.9	0.4	$3/2\ 1/2^+[411]$
	614	616	27	21	1.2	0.3	
652.0	~ 645	~ 651	~ 5	~ 1.5	0.5	0.4	$5/2\ 1/2^+[411]$
		727	~ 10	20	~ 0.4		$1/2\ 1/2^+[411]^*b$
743.9	~ 747	745	~ 11	12	0.4		
760.5	~ 762	761	~ 22	26	1		$3/2\ 1/2^+[411]^*$
811	806	810	~ 15	11	~ 0.8		$5/2\ 1/2^+[411]^*$
	836	834	~ 10	9.3	3.3		$11/2^-\ 7/2^-[523]$
		863	~ 58	57	~ 0.4		$1/2\ 1/2^-[541]$
		907	29	29	~ 0.4		$5/2\ 1/2^-[541]$
		926	~ 7	12.5	~ 0.4		
		950	36	45	~ 0.4		$3/2\ 1/2^-[541]$
	1035	1041	~ 10	10.5	3.7		$9/2\ 1/2^-[541]$
		1085	42	40	0.4		
		1189	83	89	<0.5		
		1218	9	7.8			$7/2\ 1/2^-[541]$

Table 5 (continued)

Levels in ^{155}Tb

Energy (keV)			$d\sigma/d\Omega$ ($\mu\text{b}/\text{sr}$)				Interpretation
(prev.)	(α, t)	($^3\text{He}, d$)	($^3\text{He}, d$) $\theta=30^\circ$	($^3\text{He}, d$) $\theta=40^\circ$	(α, t) $\theta=60^\circ$	(α, t) $\theta=30^\circ$	
		1251	7	2.3			
		1307	9.4	6.3			
		\sim 1368	21.5	19			
1452.1		1455	7.8	5.4			
1479.4		1480	8.1	8.7			
		1548	11.5	20			
1575.1		1581	6.2	\sim 4			
		1616	37	43			
		1658	\sim 28	33			
		1685	\sim 21	15.5			
		1721	19.4	12.5			

MCMASTER UNIVERSITY LIBRARY

- a This level and the others with the assigned Nilsson orbital enclosed in pointed brackets are from the strongly mixed negative parity orbitals discussed in section IV(3).
- b The asterisk denotes the fragment of the $1/2^+[411]$ orbital as discussed in section IV(7).

Table 6

Levels in ^{157}Tb

Energy (keV)			$d\sigma/d\Omega$ ($\mu\text{b}/\text{sr}$)				Interpretation
(prev.)	(α, t)	($^3\text{He}, d$)	($^3\text{He}, d$) $\theta=30^\circ$	($^3\text{He}, d$) $\theta=50^\circ$	(α, t) $\theta=60^\circ$	(α, t) $\theta=45^\circ$	
0	0	0	~ 6	21.5	3.1	6.1	$3/2\ 3/2^+[411]$
60.8	61	61	123	94	48	39	$5/2\ 3/2^+[411]$
143.8	145	146	3.5	~ 3	2.6	2.4	$7/2\ 3/2^+[411]$
252.4	254	249	6	~ 6	1.3	~ 0.9	$9/2\ 3/2^+[411]$
327.6	320	325	3.5	~ 2	~ 1.5	~ 1	$5/2\ 5/2^+[413]$
357.6		357	6.7	5.4	~ 0.4	~ 0.8	$7/2^-\{5/2^-[532]\}^a$
407.9	407	407	15	11.5	13	13	$7/2\ 5/2^+[413]$
425.9	428	423	3.6		3.8		$9/2^-\{5/2^-[532]\}$
517.6	519	518	21	27	54	53	$11/2^-\{5/2\ [532]\}$
597.5	595	596	18.5	31.5	~ 2.4	~ 0.8	$1/2\ 1/2^+[411]$
637.2	639	636	51	56	17	10.2	$3/2\ 1/2^+[411]$
658.6	659	660	19	33	29	19	$7/2\ 7/2^+[404]$
697.4	698	696	30	30	5.2	2.6	$5/2\ 1/2^+[411]$
795	795	796	3.9	~ 10	1.9	3.7	$7/2\ 1/2^+[411]$
	840	839	180	147	23	16.5	$5/2\ 5/2^+[402]$
860.6	861	860	~ 10	c	12	8.2	$11/2^-\{7/2^-[523]\}$
		887	50	~ 15	~ 1.5	~ 1.5	$1/2\ 1/2^-[541]$
	926	926	81	52	11.5	9.5	$5/2\ 1/2^-[541]$
		969	52	32	0.7	< 0.3	$1/2\ 1/2^+[411]^*{}^b$
							$3/2\ 1/2^-[541]$
	1007	1005	35	29	2.8	2.6	$3/2\ 1/2^+[411]^*$
	1051	1052	12	15	12	13	$9/2\ 1/2^-[541]$
	~ 1083	1077	9	8	0.6	< 0.3	$5/2\ 1/2^+[411]^*$
	1122	1100	16	15	1.2	~ 0.8	
		1119	13				

Table 6 (continued)

Levels in ^{157}Tb

Energy (keV)			$d\sigma/d\Omega$ ($\mu\text{b}/\text{sr}$)				Interpretation
(prev.)	(α, t)	($^3\text{He}, d$)	($^3\text{He}, d$) $\theta=30^\circ$	($^3\text{He}, d$) $\theta=50^\circ$	(α, t) $\theta=60^\circ$	(α, t) $\theta=45^\circ$	
		1164	7	c			$7/2\ 1/2^- [541]$
		1190	15.5	7.4			
		1454	33	35			
		1562	68	61			

- a This level and the others with the assigned Nilsson orbital enclosed in pointed brackets are from the strongly mixed negative parity orbitals discussed in section IV(3).
- b The asterisk denotes the fragment of the $1/2^+ [411]$ orbital as discussed in section IV(7).
- c Obscured or not observed.

Table 7

Levels in ^{159}Tb

Energy (keV)			$d\sigma/d\Omega$ ($\mu\text{b}/\text{sr}$)				Interpretation
(prev.)	(α, t)	($^3\text{He}, d$)	($^3\text{He}, d$) $\theta=30^\circ$	($^3\text{He}, d$) $\theta=50^\circ$	(α, t) $\theta=60^\circ$	(α, t) $\theta=45^\circ$	
0	0	0	c	3.6	7.5	6.7	$3/2\ 3/2^+[411]$
58.0	58	58	132	92	102	78	$5/2\ 3/2^+[411]$
137.6	137	136	5	2.2	4.1	2.1	$7/2\ 3/2^+[411]$
	242	244	3.2	3.7	3.5	~ 1.5	$9/2\ 3/2^+[411]$
348.2	348	346	3.7	2.9	2.0	~ 2	$5/2\ 5/2^+[413]$
	388	392	7.5	7.6	3.2	~ 2	$7/2^-\{5/2^-[532]\}^a$
	429	430	8.3	11.5	23	18	$7/2\ 5/2^+[413]$
	455	~ 462	~ 1.2	~ 3.5	4.0	5.1	$9/2^-\{5/2^-[532]\}$
	534	536	~ 6		~ 4		$9/2\ 5/2^+[413]$
581.1	546	547	38	32	86	74	$11/2^-\{5/2^-[532]\}$
		582	22	11.3	~ 3	~ 2	$1/2\ 1/2^+[411]$
	617.9	618	76	42	32	23	$3/2\ 1/2^+[411]$
674.3	673	677	42	24	15	8.6	$5/2\ 1/2^+[411]$
	762	765	~ 8		3, 8		
854.5	778	778	23	27	49	33	$7/2\ 7/2^+[404]$
	823	825	12	9.5	21	16	$11/2^-\{7/2^-[523]\}$
		858	40	24	~ 4	~ 1.5	$1/2\ 1/2^-[541]$
	892	893	60	44	21	18	$5/2\ 1/2^-[541]$
							$1/2\ 1/2^+[411]^*b$
	945	949	65	40	4.3	2.1	$3/2\ 1/2^-[541]$
	975	977	34	25	11.5	5.3	$3/2\ 1/2^+[411]^*$
1016	1021	205	153	79	53	$5/2\ 1/2^+[411]^*$ $5/2\ 5/2^+[402]$ $9/2\ 1/2^-[541]$	
	1049	1054	39	27	6.7	4	
	1099	1098	29	14	11	6.8	$7/2\ 1/2^+[411]^*$
	1154	1158	8.4	4.7	0.8	~ 0.4	$7/2\ 1/2^-[541]$

Table 7 (continued)

Levels in ^{159}Tb

Energy (keV)			$d\sigma/d\Omega$ ($\mu\text{b}/\text{sr}$)				Interpretation
(prev.)	(α, t)	($^3\text{He}, d$)	($^3\text{He}, d$) $\theta=30^\circ$	($^3\text{He}, d$) $\theta=50^\circ$	(α, t) $\theta=60^\circ$	(α, t) $\theta=45^\circ$	
	1214	1217	~ 4	7.3	c	1.7	
	1257	1255	6	16.5	~ 1	1.2	
	1338	1346	3.5	~ 3	3.5	3.5	
	1572	1570	12.5	8	1.0		
	1642	1643	16	~ 11	2.6		
		1670	56	36			
		1715	26	7			

- a This level and the others with the assigned Nilsson orbital enclosed in pointed brackets are from the strongly mixed negative parity orbitals discussed in section IV(3).
- b The asterisk denotes the fragment of the $1/2^+[411]$ orbital as discussed in section IV(7).
- c Obscured or not observed.

Table 8

Levels in ^{161}Tb

Energy (keV)			$d\sigma/d\Omega$ ($\mu\text{b}/\text{sr}$)				Interpretation	
(prev.)	(α, t)	($^3\text{He}, d$)	($^3\text{He}, d$) $\theta=30^\circ$	($^3\text{He}, d$) $\theta=50^\circ$	(α, t) $\theta=60^\circ$	(α, t) $\theta=45^\circ$		
0	0	0	7.1	3.3	11	14	$3/2$ $3/2^+$ [411]	
56.2	57	57	96	61	134	143	$5/2$ $3/2^+$ [411]	
133.7	134	135	1.4	1.9	6.4	3.1	$7/2$ $3/2^+$ [411]	
	235	236	2.2	3.1	7.3	2.4	$9/2$ $3/2^+$ [411]	
314.8	315	318	} <i>a</i>	1.2	2.6	2.2	$5/2$ $5/2^+$ [413]	
394.4	395	394		5	24	38	$7/2$ $5/2^+$ [413]	
417	416	418		3.1	3.9	~ 3.5	$7/2$ $7/2^-$ [523]	
	489			~ 0.8	3.5	9.2	{ $9/2$ $5/2^+$ [413] $9/2$ $7/2^-$ [523]	
	499							
	518	517			3.2	3.1	2.8	$1/2$ $1/2^+$ [411]
	559	557			16.5	34	32	$3/2$ $1/2^+$ [411]
585.6	585	583			30	105	120	$11/2$ $7/2^-$ [523]
	603	603			14	17.5	15	$5/2$ $1/2^+$ [411]
	698	697			1.6	6.5	4.8	$7/2$ $1/2^+$ [411]
	743	~ 740		0.8	2.6	1.5		
	847	~ 848	3.4	0.8	5.7	8.1	$11/2$ $5/2^-$ [532]	
	921	922	26	17	6.1	3.0	$1/2$ $1/2^-$ [541]	
	951	952	45	32	38	34	$5/2$ $1/2^-$ [541]	
	998	998	52	24	84	76	$7/2$ $7/2^+$ [404]	
1020	1020	40	22		7.9	~ 4	$3/2$ $1/2^-$ [541]	
1063	1064	12.5	14		43	54	$9/2$ $1/2^-$ [541]	
1083	1082	26	21		20	12		
	1113	1118	6.4	6.7	{ 5.4 2.3	10		
	1128							
	1176	1176	9.8	5.9	11.5	11	$7/2$ $1/2^-$ [541]	
	1232				2.1	2.5		
	1254	1256	80	52	38	30	$5/2$ $5/2^+$ [402]	

Table 8 (continued)

Levels in ^{161}Tb

Energy (keV)			$d\sigma/d\Omega$ ($\mu\text{b}/\text{sr}$)				Interpretation
(prev.)	(α, t)	($^3\text{He}, d$)	($^3\text{He}, d$) $\theta=30^\circ$	($^3\text{He}, d$) $\theta=50^\circ$	(α, t) $\theta=60^\circ$	(α, t) $\theta=45^\circ$	
	1303	1302	~ 4.7	4.7	2.5	2.6	
	1354	1351	50	34	~ 24	16.5	
	1386	~ 1375		~ 13	1.9	2.5	
		1402	9.8	< 1			
	1419				2.2	2.0	
	1433	1433	3.1	3	2.3	2.8	
	~ 1499	1498	2.8	1.9	~ 0.9	1	
		1530	4.7	2.5	< 0.6	< 1	
	1560	1561	4.3	2	2.5	< 2	
	1607	1603	17	12	7.5	7.4	
	1680	~ 1676		1	2	11	
	1726	1711		4.4	2.7		
	1756	1755	17	14.5	6.4		
		1851	35	23			

a Obscured by the $\text{C}^{13}({}^3\text{He}, d){}^{14}\text{N}(\text{g.s.})$ reaction.

Table 9

Levels in ^{163}Ho

Energy (keV)			d σ /d Ω ($\mu\text{b}/\text{sr}$)				Interpretation
(prev.)	($^3\text{He}, \text{d}$)	(α, t)	($^3\text{He}, \text{d}$) $\theta=30^\circ$	($^3\text{He}, \text{d}$) $\theta=50^\circ$	(α, t) $\theta=60^\circ$	(α, t) $\theta=45^\circ$	
0	0	0	4	5	1.5	1.	7/2 7/2 ⁻ [523]
	60	~60	0.8	2.9	0.5	~2	b
100	103	100	2.1	0.9	2.4	4.3	9/2 7/2 ⁻ [523]
224	223	222	26.	33.	50.	44	11/2 7/2 ⁻ [523]
	307	307	60	59	20	13	3/2 1/2 ⁺ [411]
	361	361	17	18	5.4	5.4	5/2 3/2 ⁺ [411]?
	393	392	80	97	24	15	5/2 1/2 ⁺ [411]?
440	440	440	16	31	32	24	7/2 7/2 ⁺ [404]
	473	468	29	29	1.7	0.8	1/2 1/2 ⁻ [541]
	503	501	35	43	11	9.8	5/2 1/2 ⁻ [541]
	580	580	45	46	2	a	3/2 1/2 ⁻ [541]
	617	613	9.9	17	21	19	9/2 1/2 ⁻ [541]
	713	711	129	151	14	22	5/2 5/2 ⁺ [402]
	749	747	13	12	5.6	5.1	7/2 1/2 ⁻ [541]
	879		2.8	5.5	a	a	
	992	~985	3.4	5.7	~1.5		
	1117	1114	18	19	1.8		
	1189		~1.5	4.1	~0.1		
	1230	1228	~4.2	8.5	0.6		
	1330		43	53	~0.3		
	1440	1442	~10	27	8.3		11/2 9/2 ⁻ [514] ?

a obscured or not observed

b may be due to a reaction due to a target impurity of ^{163}Dy or ^{164}Dy (see table 2).

Table 10

Levels in ^{153}Eu

Energy (keV)		$d\sigma/d\Omega$ ($\mu\text{b}/\text{sr}$)					Interpretation
(α, t)	$(^3\text{He}, d)$	$(^3\text{He}, d)$	$(^3\text{He}, d)$	$(^3\text{He}, d)$	(α, t)	(α, t)	
	b	$\theta=27.5^\circ$	$\theta=30^\circ$ b	$\theta=40^\circ$ b	$\theta=60^\circ$	$\theta=40^\circ$	
0	0	a	2	a	1	~ 2	$5/2$ $5/2^+$ [413]
85	90	18	17	24	37	31	$7/2$ $5/2^+$ [413]
(97) c							$5/2$ $5/2^-$ [532]
104						2.9	$3/2$ $3/2^+$ [411]
150	(152) c	~ 5			4.1	~ 2	$7/2$ $5/2^-$ [532]
173	173	160	231	168	76	50	$5/2$ $3/2^+$ [411]
235		9			3.9	~ 2	$9/2$ $5/2^-$ [532]
	265	~ 10	a	2	<1	~ 0.8	$7/2$ $3/2^+$ [411]
322	321	43	47	54	85	80	$11/2$ $5/2^-$ [532]
395	397	4	8.5	10	2.4	1.5	$9/2$ $3/2^+$ [411]
570	568	20	21	26	41	26	$11/2$ $7/2^-$ [523]?
	635	10	12	7.5	~ 1		
696		~ 98			32	~ 22	
705		~ 100	398	297	15		
718		~ 80			20	~ 18	
733					2.9		
~ 840	842	30	57	35	~ 0.9		
1071	1074	12	9.5	7.	11		
1138	1141		83	54	8		
1235	1228	35	78	61	11		
1358	1357	88	150	116	6		

a obscured or not observed

b reaction data from Ungrin et. al. (1969)for $E_{^3\text{He}} = 28 \text{ MeV}$ c energies from decay scheme study, Ungrin et. al. (1969)

MCMASTER UNIVERSITY LIBRARY

Table 11
Levels in ^{155}Eu

Energy (keV)		$d\sigma/d\Omega$ ($\mu\text{b/sr}$)					Interpretation
(α, t)	($^3\text{He}, d$)	($^3\text{He}, d$) $\theta=45^\circ$	($^3\text{He}, d$) $\theta=30^\circ$ b	($^3\text{He}, d$) $\theta=50^\circ$ b	(α, t) $\theta=60^\circ$	(α, t) $\theta=45^\circ$	
0	0	1.7	4	0.5	1.6	2.5	$5/2$ $5/2^+$ [413]
78	78	~15	~8	~7	49	45	$7/2$ $5/2^+$ [413]
	104		~4	~2	~3	~1	$5/2$ $5/2^-$ [532]
169	169	6.5	8	4.5	6.7	6.7	$7/2$ $5/2^-$ [532]
247	251	3.4	15	2.5	9.6	10	$3/2$ $3/2^+$ [411]
307	307	116	178	76	109	93	$5/2$ $3/2^+$ [411]
356	357	22	28	21	77	77	$11/2$ $5/2^-$ [532]
388	392	a	a	3	5.5	7.9	$7/2$ $3/2^+$ [411]
501	502	3.5	9.8	5.4	6.6	3	$9/2$ $3/2^+$ [411]
~875	876	10	12	4.2	~4	~4	
912	~910	60	84	66	35	25	
952	955	25	34	19	11	10.2	
976	978	22	33	22	52	40	$11/2$ $7/2^-$ [523]?
	1024	13	24	11	~2	<2	$1/2$ $1/2^-$ [541]?
1062	1067	~25	48	31	23	9.5	$5/2$ $1/2^-$ [541]?
	1109	~10	27	29	<10	a	$3/2$ $1/2^-$ [541]?
1202	1201	25	23	16	21	27	$9/2$ $1/2^-$ [541]?
1230	1233	36	70	52	19	22	
	1318	12	29	11	<3	~2	
1353		<10		<5	9	15	
1375	1374	24	58	22	~6	~9	
1401	1402	7	17	13	12	12	$7/2$ $1/2^-$ [541]?
1480	1482	40	69	43	16	11	

a obscured or not observed
 b reaction data from Ungrin et. al. (1969)
 for $E_{^3\text{He}} = 28 \text{ MeV}$

displays the results for the present study and shows them to be consistent with those calculated from two recent mass tables.

III.7 Energy Resolution Considerations

For the experiments done in the present study, high energy resolution is of great importance. In the nuclei investigated, the average energy density of the strongly populated states is about twenty per MeV. Thus, peak widths considerably less than 50 keV FWHM (Full Width, Half Maximum) are desired. There are a number of different factors which affect the total resolution. These are mainly target thickness effects, aberrations and energy spread in the incident beam, and the resolution of the spectrograph. Efforts were made to optimise the total resolution within the practical limitations (such as the length of time for the experiment).

In the target, the two principal effects are due to energy loss and straggling. The former concerns the average energy lost by a beam of charged particles passing through a thin foil. This energy loss is different for the various kinds of particles. Thus the energy of the reaction product will generally depend on whether the reaction occurs near the front or near the back of the target. For example, 25 MeV α particles will lose an average of ~ 11 keV passing through a $100 \mu\text{g}/\text{cm}^2$ foil of samarium, whereas 10 MeV tritons (which have approximately the energy expected for a typical (α, t) reaction) will lose only ~ 4 keV. (These values are based on calculations by Williamson, Boujot and Picard, 1966.) Thus, if the (α, t) reaction on such a foil is studied in transmission geometry (the reaction products detected on the side of the foil opposite

to the α beam), an average energy spread of ~ 7 keV due to the differential energy loss is expected in the reaction products. As the energy loss for a particle passing through material is a statistical process, a spread in the energy (straggling) of the particles about their average energy is also expected. A calculation of this energy spread (Clarke, 1971) for 25 MeV α particles on a $100 \mu\text{g}/\text{cm}^2$ foil of samarium gives a FWHM of ~ 7 keV. The effect of straggling due to the carbon backings is also important. A $30 \mu\text{g}/\text{cm}^2$ thick carbon foil would contribute ~ 5 keV FWHM for the α and ^3He particles and ~ 2 keV for deuterons and protons. The net effect on the resolution due to a typical target for the experiments is expected to be ~ 7 keV FWHM. This of course varies from target to target and also depends on the angles at which the spectrograph and target are placed. These angles determine the effective thickness of the target to the incident and scattered particles.

The effect on the resolution of the aberrations and energy spread in the incident beam is also important. In principle, due to the dispersion of the analyzing and switching magnets, the energy spread in the beam (attributed to effects from the ion source and stripper foil as well as fluctuations in the terminal voltage) results in a wide beam spot on the target. It was mentioned earlier that this effect could be compensated for, with the dispersion of the spectrograph. However, this will not work if the width of the beam on the target is due to aberrations in the beam optics. Assuming the width of the beam spot is due to these aberrations, and is about 1 mm on the target, as 'seen' by the spectrograph, the image size of

this spot on the focal plane of the spectrograph would be about 0.5 mm (determined by the focal plane magnification). For the (α, t) reactions, this would result in an energy width of ~ 6 keV, and for $(^3\text{He}, d)$ reactions, ~ 13 keV.

Aberrations in the focussing properties of the spectrograph also affect the total resolution. For the solid angles used in the present study, these aberrations were not believed to be serious. It was found that for reactions done with larger solid angles, 'shoulders' on the low energy side of the peaks were observed, although the FWHM of the peaks were not appreciably affected. This effect made the analysis of such spectra difficult.

The total magnitude expected for all these effects is in agreement with the observed resolution.

CHAPTER IV

INTERPRETATION

In the following sections, the low lying levels of the nuclei studied are identified in terms of the Unified Model. In some cases, the results of complementary investigations are used to provide strong arguments for these model assignments. Because the proton states in the isotopes of an element are expected to have similar properties, the four terbium nuclei are discussed together. Following the discussion of ^{163}Ho , the two europium isotopes are also considered together.

IV.1 ^{155}Tb , ^{157}Tb , ^{159}Tb and ^{161}Tb

A number of decay scheme studies have been made on these nuclei, including works by Blichert-Toft et al. (1967), Brown et al. (1969), Zylicz et al. (1966), Seaman et al. (1967), Funke et al. (1966) and Hill and Wiedenbeck (1968). In addition, Coulomb excitation experiments on ^{159}Tb by Diamond et al. (1963), (p,t) experiments on ^{159}Tb by Goles (1971), and ($\alpha,2n$), (d,2n) and (p,n) experiments to study levels in ^{155}Tb and ^{157}Tb by Winter et al. (1971) have been performed. In general, efforts were made to interpret the observed excitations in terms of the Unified Model. In several cases, the importance of Coriolis coupling and particle-vibrational mixing was recognized.

The analysis of the terbium isotopes in this investigation, is also presented in a paper by Tippett and Burke (1972). A similar but independent investigation has recently been made by Boyno and Huizenga (1972). A comparative discussion of the two works is presented in section IV.1h.

IV.1a The $3/2^+[411]$ orbital

The spins and parities of the ground state and first three excited states for each of the terbium nuclei studied had previously been determined as $3/2^+$, $5/2^+$, $7/2^+$ and $9/2^+$ respectively. These states had been assigned as rotational members of the $3/2^+[411]$ orbital. As this orbital comes from the $2d_{5/2}$ shell, the spectroscopic factor for the $I=5/2$ member of the band is expected to be the largest. In the present work, this is found to be the case, and the measured values of $U_{j\lambda}^2 C_{j\lambda}^2$ agree well with those predicted. A comparison of these values is found in table 12. All the states discussed above are seen clearly, except the $9/2$ $3/2^+[411]$ level in ^{155}Tb which is not resolved from the $5/2$ $5/2^+[413]$ state. The present results offer strong confirmation for the previous assignments of these bands.

IV.1b The $5/2^+[413]$ orbital

The $I=5/2$ and $I=7/2$ members of bands based on this orbital had been assigned in all four nuclei, as well as rotational members up to $I=13/2$ in ^{155}Tb and $I=11/2$ in ^{157}Tb (see Bunker and Reich (1971) and Winter et al. (1971)). As this state appears below the $3/2^+[411]$ orbital in the Nilsson diagram, it is expected to have a small U^2 for the present reactions. The $I=7/2$ member should contain most of the spectroscopic strength (the theoretical $C_{j\lambda}^2$ is ~ 0.94) and the observed fingerprint for the band, as well as the (α, t) to $(^3\text{He}, d)$ cross section ratio for the $I=7/2$ member confirms the previous assignment. The results are displayed in table 13. The differences between the measured and calculated values of

Table 12

Spectroscopic information for the $3/2^+$ [411] and $5/2^+$ [402] bands in Tb isotopes

	$3/2^+$ [411] Orbital				Rotational Parameter	$5/2^+$ [402] Orbital
	I=3/2	I=5/2	I=7/2	I=9/2		
^{155}Tb						
Energy (keV)	0	65	152	270	12.9	500
$U^2C_{j\lambda}^2$	0.04	0.57	0.04	0.04 ^a		0.95
($^3\text{He}, d$)	0.03	0.58	0.10	0.15		0.80
Calc.	0.01	0.53	0.11	0.03		0.74
^{157}Tb						
Energy (keV)	0	61	145	254	12.0	840
$U^2C_{j\lambda}^2$	0.12	0.85	0.07	0.03		1.3
($^3\text{He}, d$)	0.2	0.78	0.14	0.18		0.9
Calc.	0.02	0.66	0.11	0.05		0.81
^{159}Tb						
Energy (keV)	0	58	137	242	11.5	1020
$U^2C_{j\lambda}^2$	0.08	0.95	0.07	0.03		$\sim 1^a$
($^3\text{He}, d$)	0.04	0.92	0.17	0.13		0.84
Calc.	0.02	0.61	0.10	0.06		
^{161}Tb						
Energy (keV)	0	57	135	236	11	1256
$U^2C_{j\lambda}^2$	0.08	0.90	0.06	0.05		0.6
($^3\text{He}, d$)	0.06	0.84	0.10	0.11		0.5
Calc.	0.01	0.61	0.10	0.06		0.85

^a Multiple assignment

AGN001 11/10/2011 08:15:55 PM

Table 13

Spectroscopic Information for the $5/2^+$ [413] and $7/2^+$ [404] orbitals in Tb isotopes

	$5/2^+$ [413] Orbital			Rotational Parameter, keV	$7/2^+$ [404] Orbital I=7/2
	I=5/2	I=7/2	I=9/2		
^{155}Tb Energy (keV)	272	334	450	10.3	467
^{155}Tb $U^2C_{j\lambda}^2$ (α, t)	<0.04 ^b	1.0	0.1		0.40
^{155}Tb $U^2C_{j\lambda}^2$ ($^3\text{He}, d$)	<0.04	0.55	0.03		0.25
Calc.	0.02	0.63	0.02		0.37
^{157}Tb Energy (keV)	320	409	\sim 510	11.4	659
^{157}Tb $U^2C_{j\lambda}^2$ (α, t)	0.02	0.51	a		1.1
^{157}Tb $U^2C_{j\lambda}^2$ ($^3\text{He}, d$)	0.02	0.55			1.0
Calc.	0.01	0.21	0.01		0.81
^{159}Tb Energy (keV)	348	429	\sim 540	12	778
^{159}Tb $U^2C_{j\lambda}^2$ (α, t)	0.03	0.37	a		1.2
^{159}Tb $U^2C_{j\lambda}^2$ ($^3\text{He}, d$)	0.03	0.42			1.1
Calc.	0.01	0.15	0.01		0.88
^{161}Tb Energy (keV)	318	394	492	11.4	998
^{161}Tb $U^2C_{j\lambda}^2$ (α, t)	0.02	0.44	\sim 0.04 ^b		1.6
^{161}Tb $U^2C_{j\lambda}^2$ ($^3\text{He}, d$)	0.02	0.29			1.7
Calc.	0.01	0.11	0.01		0.94

a Obscured or not observed

b Multiple assignment

$U^2 C_{j\lambda}^2$ can be attributed partly to the underestimate of the DWBA normalization, discussed in section II.3, but more significantly to the estimate of the U^2 in the Coriolis calculation. Adjustment of the Fermi level and the diffuseness parameter may give better agreement with the observed strength. The large spectroscopic strength for the $7/2 \ 5/2^+[413]$ state in ^{155}Tb is attributed to strong mixing with the $7/2^+[404]$ state assigned by Winter et al. (1971) at 467 keV. The relative strengths of these two states can be reproduced by the Coriolis calculation. The discrepancy between the $U^2 C_{j\lambda}^2$ values measured in the (α, t) and in the $(^3\text{He}, d)$ reactions may be due to an inaccurate prediction of the intensity by the DWBA calculation for the (α, t) reactions at such negative Q values. The $I=5/2$ and $I=9/2$ members of the $5/2^+[413]$ bands are expected to be populated weakly. Evidence for the band head is seen in the reactions on all four nuclei. As well, the $I=9/2$ state in ^{161}Tb is located in the 490 keV doublet with the weak $9/2 \ 7/2^-[523]$ state. Evidence for the $I=9/2$ state is seen at 450 keV in ^{155}Tb , and in ^{159}Tb this member is tentatively assigned to a level at ≈ 530 keV that appears as a shoulder on the 546 keV peak in the (α, t) spectra.

IV.1c The $5/2^- [532]$ and $7/2^- [523]$ orbitals

In the terbium isotopes, a number of rotational members of the $5/2^- [532]$ and $7/2^- [523]$ Nilsson orbitals have been previously identified. (See Bunker and Reich (1971)). In ^{157}Tb the band head of the $5/2^- [532]$ orbital had been located at 326 keV excitation. A state at 358 keV was assigned by Funke et al. (1966) as the $7/2^- [523]$ band head, and by Blichert-Toft et al. (1967) as the $I=7/2$ member of the $5/2^- [532]$ orbital. Winter et al. (1971) studied the γ de-excitation of this nucleus following

(d,2n) and (p,n) reactions, and identified rotational members up to $I=11/2$ for the $7/2^- [523]$ orbital, for which they placed the band head at 571 keV. They also analysed the energies of the two distorted rotational bands considering the Coriolis coupling between them.

In the present work, identification of the orbitals or confirmation of earlier assignments is generally made by locating the $I=11/2$ member of the rotational bands. The $5/2^- [532]$ and $7/2^- [523]$ orbitals, which both come from the $1h_{11/2}$ spherical shell model state, have most of their spectroscopic strengths in the $I=11/2$ member and should mix strongly. This is especially true for the terbium isotopes, where the $5/2^- [532]$ orbital is expected to appear as a hole state, and the $7/2^- [523]$ orbital as a particle state, both with excitation energies less than one-half MeV. As well as distorting the rotational level spacings, the strong mixing is expected to cause the intensity of the lower $I=11/2$ member to be considerably larger than that predicted without mixing. In ^{157}Tb as well as the other terbium isotopes, there are only four strongly populated low-lying states with high ℓ -values ($\ell \approx 5$). The $7/2 \ 5/2^+ [413]$ state which is found at 409 keV in ^{157}Tb was discussed previously. States at 518 and 659 keV both have $U_{j\ell}^2 C_{j\ell}^2$ near unity, and the state at 861 keV has $U_{j\ell}^2 C_{j\ell}^2 \approx 0.4$. The presence of these three states in the present work is consistent with Winters assignments of the $11/2 \ 5/2^- [532]$, $7/2 \ 7/2^+ [404]$ and the $11/2 \ 7/2^- [523]$ states respectively. However, the predicted relative spectroscopic strengths of the $I=11/2$ states by a Coriolis mixing calculation, using the parameters of Winter et al., does not agree with the experimental measurements. The relative intensity of the lower $I=11/2$ state to the upper $I=11/2$ state is ≈ 3 by measurement and 1.2 by

calculation. In the present work, the parameters of the Coriolis mixing calculation are adjusted, and with an unmixed band head energy of about 150 keV less than that used by Winter for the $7/2^- [523]$ orbital, a value of 2.3 for the ratio of these spectroscopic strengths is obtained. It is clear from the calculated mixing amplitudes of these states that the asymptotic quantum numbers are no longer valid for these strongly mixed levels. The experimental and calculated values of $U^2 C_{j\ell}^2$ for these bands are displayed in Table 14.

In ^{155}Tb the levels at 227 keV and 250 keV had been assigned as the $5/2^- [532]$ and $7/2^- [523]$ intrinsic states respectively by Jursik (1969). However, Winter et al. (1971) assigned two members of the $7/2^- [523]$ orbital with a band head at 545 keV. They also assigned the $5/2^- [523]$ orbital with the band head at 227 keV and found rotational members up to $I=23/2$. The level at 250 keV was assigned as the $7/2^- 5/2^- [532]$ state. Two of the levels populated with high ℓ -values in the present work, at 398 keV and 467 keV, had been assigned by Winter et al. as the $11/2^- 5/2^- [532]$ and $7/2^- 7/2^+ [404]$ states respectively. In view of these assignments, the level at 836 keV populated with a high- ℓ transition is labelled as the $11/2^- 7/2^- [523]$ state. As in ^{157}Tb the relative spectroscopic strengths calculated using Winter's parameters for the Coriolis mixing does not agree with those measured. Again, variation of these parameters in the present work results in better agreement with the experimental measurements.

Levels at 417 keV, 480 keV and 586 keV in ^{161}Tb have been assigned to the $7/2^- 7/2^- [523]$, $5/2^- 5/2^- [532]$ and $7/2^- 5/2^- [532]$ states respectively, by Zylicz et al. (1966). In the $(^3\text{He},d)$ and (α,t) spectra, peaks corresponding to the first of these states are clearly seen, but the

Table 14

Spectroscopic information for the mixed $5/2^- [532]$ and $7/2^- [523]$ Orbitals in Tb isotopes

	I=5/2	I=7/2	i=7/2	I=9/2	I=9/2	I=11/2	I=11/2
^{155}Tb Energy (keV)	227	250	545	318	688	398	835
$U^2C_{j\ell}^2$ (α, t)		0.06		0.04		1.7	0.22
$(^3\text{He}, d)$	α	0.06	α		α	1.5	0.37
Calc.	0.0001	0.02	0.002	0.01	0.004	0.91	0.39
^{157}Tb Energy (keV)	326	357	572	426	709	517	861
$U^2C_{j\ell}^2$ (α, t)		~ 0.01				1.4	0.4
$(^3\text{He}, d)$	α	0.04	α	α	α	1.2	0.3
Calc.	0.0001	0.02	0.002	0.01	0.004	0.85	0.36
^{159}Tb Energy (keV)	363	389	$(\sim 520)^b$	455	$(\sim 670)^b$	546	823
$U^2C_{j\ell}^2$ (α, t)		0.02		0.08		1.3	0.37
$(^3\text{He}, d)$	α	0.07		~ 0.12		1.6	0.49
Calc.	0.0001	0.02	0.002	0.01	0.004	0.82	0.34
^{161}Tb Energy (keV)	480	418	586	~ 495	$(\sim 700)^b$	584	847
$U^2C_{j\ell}^2$ (α, t)		0.02		0.04		1.3	0.10
$(^3\text{He}, d)$	α	0.04	α			1.6	0.13
Calc.	0.0001	0.026	0.0001	0.01	0.001	0.96	0.16

 α Obscured or not observed. b The state has not been observed and its energy is based on the calculations.

remaining ones are obscured by large peaks due to neighbouring states. The high ℓ states at 584 keV and 846 keV are assigned to the $I=11/2$ members of the $7/2^- [523]$ and $5/2^- [532]$ orbitals respectively. The relative spectroscopic strengths of these levels are in agreement with the Coriolis mixing calculation for the $7/2^- [523]$ and $5/2^- [532]$ orbitals. The $9/2$ $7/2^- [523]$ rotational member may be located in the multiplet at 495 keV, consistent with the rotational parameter and expected $U^2 C_{j\ell}^2$.

Only the band head of the $5/2^- [532]$ orbital had been identified in ^{159}Tb (Bunker and Reich (1971)). States populated by high ℓ transitions are found at 429 keV, 455 keV, 545 keV, 779 keV and 823 keV with $U^2 C_{j\ell}^2$ values of approximately 0.4, 0.1, 1.3, 1.2 and 0.4 respectively. The level at 429 keV has been previously assigned as the $7/2$ $5/2^+ [413]$ state. (See section IV.1b). By analogy with the spectroscopic strengths and excitation energies observed in ^{155}Tb and ^{157}Tb , the levels at 546 keV and 823 keV are assigned as the $I=11/2$ members of the $7/2^- [523]$ and $5/2^- [532]$ orbitals. The Coriolis calculation is able to reproduce the experimental results. The weakly populated level at 390 keV has an intensity and energy consistent with its assignment as the lower $I=7/2$ state of the mixed $7/2^- [523]$ and $5/2^- [532]$ orbitals. The level at 455 keV has approximately the appropriate energy for the lower $I=9/2$ state, and appears to have a high ℓ value, but its intensity is larger than expected.

IV.1d The $1/2^+ [411]$ orbital

As this orbital is coupled with a large theoretical E2 matrix element to the $3/2^+ [411]$ orbital, it is likely that strong mixing with the gamma vibration based on the ground state may cause the single particle strength of the $1/2^+ [411]$ orbital to fragment. A number of authors (see

Bunker and Reich (1971)) have assigned levels with $I=1/2$, $3/2$ and $5/2$ at 597 keV, 637 keV and 698 keV in ^{157}Tb and at 581 keV, 618 keV and 674 keV in ^{159}Tb as members of either the $1/2^+[411]$ band or of a gamma vibrational band based on the ground state. The decoupling parameter expected for the single particle orbital is ~ -1.0 . The observed values of $\sim +0.05$ are considered evidence for the states being largely vibrational in nature. Calculations by Soloviev and Vogel (1967) however, indicate that these states should consist mainly of the gamma vibration based on the $3/2^+[411]$ orbital with an admixture of about 60% of the $1/2^+[411]$ single particle state. In the present work, the first three rotational members of these previously assigned bands are seen in both nuclei, as well as the $I=7/2$ member in ^{157}Tb which has been identified by Goles (1971). The fingerprint is consistent with that expected for the $1/2^+[411]$ band. The results are shown in table 15. The summed $U^2 C_{J\ell}^2$ of each band is ~ 0.8 , which, in view of the fact that the extracted spectroscopic strengths are in general about 30% larger than expected, is consistent with the reduced strengths predicted by Soloviev. Possible assignments for other fragments of the $1/2^+[411]$ orbital will be discussed in a later section.

In the present work, a sequence of levels in ^{161}Tb is found to have properties similar to those of the bands in ^{157}Tb and ^{159}Tb . The ℓ -values determined by the (α, t) to $(^3\text{He}, d)$ cross section ratios, the relative spectroscopic factors and the energy spacings suggest that the levels at 517 keV, 559 keV, 602 keV and 698 keV are the $I=1/2$, $3/2$, $5/2$ and $7/2$ members respectively, of a band containing a large $1/2^+[411]$ admixture. The decoupling and rotational parameters of the band are 0.2 and 11.2 keV respectively. The summed $U^2 C_{j\ell}^2$ of the band is ~ 0.5 , which

Table 15

Spectroscopic information for the $1/2^+ [411]$ orbital and $1/2^+ [411]$ fragment in Tb isotopes

	$1/2^+ [411]$ Orbital			Rotational Parameter (keV)	a	$1/2^+ [411]$ Fragment			Rotational Parameter (keV)	a
	I=1/2	I=3/2	I=5/2			I=1/2	I=3/2	I=5/2		
^{155}Tb Energy (keV)	508 ^d	548 ^d	650 ^d	17.2	-0.2	725	761	810	10.6	0.07
$U^2C_{j\ell}^2$ (α, t)	a	0.33	0.06			~0.04	0.1	0.04		
$^3\text{He, d}$	0.3	0.01				0.04	0.12	0.06		
^{157}Tb Energy (keV)	595	639	698	13.2	0.1	969 ^b	1007	1080	13.6	-0.07
$U^2C_{j\ell}^2$ (α, t)	0.1	0.7	0.18	0.2		0.04	0.06	0.03		
$^3\text{He, d}$	0.1	0.38	0.15	0.2		0.14	0.17			
^{159}Tb Energy (keV)	582	620	675	11.8	0.07	949 ^b	979	1022	9.3	0.07
$U^2C_{j\ell}^2$ (α, t)	0.07	0.57	0.22	a		0.3	0.3	a		
$^3\text{He, d}$	0.07	0.48	0.2			0.2	0.2			
^{161}Tb Energy (keV)	517	559	602	11.2	0.02					
$U^2C_{j\ell}^2$ (α, t)	0.02	0.33	0.14	0.1						
$^3\text{He, d}$	0.03	0.19	0.13	0.09						
$U^2C_{j\ell}^2$ Calculation ^c	0.1	0.5	0.2	0.15						~1

a Obscured or not observed

b Multiple assignment

c The results of the Nilsson calculation with Coriolis mixing differed only slightly for the different isotopes.

d Assignment proposed by Harmatz (1972), see text.

is slightly less than that of the corresponding bands in ^{157}Tb and ^{159}Tb .

Evidence for the $1/2^+[411]$ orbital in ^{155}Tb is not strong.

Persson and Ryde (1964), studying the electromagnetic transitions following the decay of ^{155}Dy , tentatively assigned the bands to levels placed at ~ 0.8 MeV. In a similar study by Blichert-Toft et al. (1967) no assignment was made for the $1/2^+[411]$ orbital. They proposed levels at 500 keV and 550 keV and tentatively assigned them to the first two members of the $3/2^+[422]$ orbital. Harmatz (1972) in a study of the electromagnetic transitions following the beta decay of ^{155}Dy , assigned spin values of $1/2$, $3/2$ and $5/2$ to levels at 508 keV, 550 keV and 652 keV respectively, and suggested that these were members of the mixed gamma vibration and $1/2^+[411]$ single particle band, similar to those seen in ^{157}Tb and ^{159}Tb . In the present study of ^{155}Tb , an intense peak is seen at 550 keV and a weaker one at about 645 keV. A very strong peak at 500 keV, seen in both the (α, t) and the $(^3\text{He}, d)$ reactions, which is probably due to the level at 498.7 keV identified by Harmatz (1972) and Blichert-Toft (1967), is likely to obscure a weakly populated state at 508 keV. The observed strengths in the (α, t) and $(^3\text{He}, d)$ reactions are consistent with $\ell=2$ for both the 550 keV and 650 keV states. The summed $U^2 C_{j\ell}^2$ for these states is ~ 0.35 which is not unreasonable for a single particle admixture into a γ -vibration, but the spectroscopic strength of the 650 keV state is about $1/5$ that expected relative to the 550 keV state for the $1/2^+[411]$ fingerprint. The rotational parameter calculated for this band would be 17.2 keV which is rather large. The decoupling parameter of -0.2 differs from those of other terbium nuclei, which have values of $\sim +0.05$. This may be considered evidence for a larger admixture of the $1/2^+[411]$ orbital than

in the other nuclei, even though the single particle strengths do not indicate this. On the basis of the present experimental evidence, the assignment of levels at 508 keV, 550 keV and 650 keV to a γ -vibration based on the ground state, mixed with the $1/2^+[411]$ single particle orbital as proposed by Harmatz, cannot be confirmed. It is possible that these states, while containing a large $1/2^+[411]$ single particle strength, may have a more complex structure than a simple γ -vibrational mixture.

Some alternative assignments have been considered for the $1/2^+[411]$ orbital in ^{155}Tb . If it does not mix with the $K=1/2$ gamma vibration based on the $3/2^+[411]$ orbital, the $I=1/2$ and $I=3/2$ members of the $1/2^+[411]$ orbital are expected to fall very close to each other. The expected spectroscopic strengths are consistent with the assignment of the peak at 500 keV excitation as the unresolved $I=1/2$ and $I=3/2$ members and the peak at 550 keV as the $I=5/2$ and $I=7/2$ members of the band, but the rotational parameter for this case would be ~ 5 keV. If the state at 615 keV were assigned to be the $I=5/2$ and $7/2$ members a more reasonable rotational parameter of ~ 11.5 keV would result, but the population of the 615 keV state is too weak for this interpretation. Other possible evidence of the $1/2^+[411]$ orbital as well as a tentative assignment of the level at 499 keV from the present studies will be discussed in later sections.

IV.1e The $7/2^+[404]$ orbital

For a nuclear deformation, $\delta \sim 0.3$, the Nilsson model predicts that the $7/2^+[404]$ orbital should fall within the first two MeV of excitation for $Z=65$ nuclei. This orbital is difficult to identify firmly in the present work, as almost all of its spectroscopic strength is in

the $I=7/2$ rotational member. Winter et al. (1971), assigned the $7/2\ 7/2^+[404]$ state to levels at 467 keV in ^{155}Tb and 659 keV in ^{157}Tb . In the present work, states at these energies are populated with (α, t) to $(^3\text{He}, d)$ cross section ratios consistent with the assignment of $\ell=4$, and have $U^2 C_{j\ell}^2$ values that are in agreement with expectations as shown in table 13. Levels at 778 keV in ^{159}Tb and 998 keV in ^{161}Tb are assigned as the $7/2\ 7/2^+[404]$ states as they appear to have $\ell \approx 4$ and reasonable spectroscopic strength. Also they exhibit the systematic rise in excitation energy expected for this orbital with the increasing deformation that is observed for increasing masses of isotopes in this region.

Other Nilsson orbitals that are considered for assignment to the strongly populated high spin levels in ^{159}Tb and ^{161}Tb are the $9/2^- [514]$, $1/2^+ [660]$ and $1/2^- [541]$ states. The $9/2^- [514]$ orbital appears above the $7/2^+ [404]$ orbital in the Nilsson diagram and as it mixes strongly with the $7/2^- [523]$ band, its intensity, according to the Coriolis mixing calculation, should be considerably less than that observed for the levels in question. As the $1/2^+ [660]$ orbital has not been identified in any $Z=67$, $Z=69$ or $Z=71$ nuclei, it is unlikely that it appears at ~ 1 MeV in ^{159}Tb and ^{161}Tb . The $1/2^- [541]$ orbital has an expected $U^2 C_{j\ell}^2$ of ~ 0.5 for the $I=9/2$ member as well as one of ~ 0.3 for the $I=5/2$ rotational member. Its tentative assignment will be discussed in a later section.

IV.1f The $5/2^+ [402]$ orbital

The fingerprint for this orbital is characterized by a strong $\ell=2$ population for the $I=5/2$ member of the rotational band. The other band members are expected to be populated too weakly to be observed. In the

present work, strong transitions with ($^3\text{He},d$) to (α,t) cross section ratios consistent with $\ell=2$ are observed for states at 500 keV in ^{155}Tb , 840 keV in ^{157}Tb , about 1020 keV in ^{159}Tb and at 1256 keV in ^{161}Tb . The $5/2^+[402]$ state appears above the $7/2^+[404]$ orbital in the Nilsson diagram and both have the same slope with changing deformation. Thus it would be expected that as one goes to the heavier terbium nuclei, and the deformation increases, the excitation energy of the $5/2^+[402]$ state should increase, as it does for the $7/2^+[404]$ state. The levels mentioned above satisfy all these expectations and in addition are about the only unassigned states with absolute cross sections as large as those expected for the $5/2^+[402]$ orbital. Hence it is reasonable to assign them as the $5/2$ $5/2^+[402]$ states as shown in table 12. In ^{161}Tb , the $U^2C_{j\ell}^2$ for the 1256 keV state is ~ 0.5 , which is weaker than the $U^2C_{j\ell}^2$ for the other nuclei, but it is the strongest unassigned state in the first 2 MeV of excitation. In ^{159}Tb , the $5/2$ $5/2^+[402]$ state was assigned within a multiplet which has a centroid energy of 1021 keV in the ($^3\text{He},d$) spectra and 1016 keV in the (α,t) spectra. The multiplet is very strong in both reactions, and the observed strength is consistent with at least two states in the peak, with ℓ -values ~ 2 and ~ 5 each with $U^2C_{j\ell}^2$ near unity. An alternative assignment of the 500 keV level in ^{155}Tb to the $1/2^+[411]$ orbital was discussed earlier. Although this state is considerably closer to the $7/2^+[404]$ orbital than for the other nuclei, there are no unassigned states within the first 1200 keV of excitation having intensities greater than half that expected for the $5/2$ $5/2^+[402]$ state. This level was observed previously by Blichert-Toft *et al.* (1967) and Harmatz (1972), and was assigned a spin of $I=3/2$, although a spin value of $5/2$ would be

consistent with the multipolarities of the 499 keV and 433 keV electromagnetic transitions to the ground and first excited states. For the $I=5/2$ assignment, the calculated relative intensity of these transitions agrees with that measured by Harmatz, although there is little evidence of a transition from this state to the $I=7/2$ member of the ground state band.

IV.1g The $1/2^- [541]$ orbital and fragments of the $1/2^+ [411]$ orbital

In the region of one MeV excitation in each of the terbium nuclei studied, there is a number of unassigned states with l -values both ≈ 2 and ≈ 5 with $U^2 C_{j l}^2$ (assuming these approximate l -values) of about 0.3. On the basis of the present work alone, the character of these states cannot be determined with certainty. The tentative assignments proposed in this section for the $1/2^- [541]$ orbital and fragments of the $1/2^+ [411]$ orbital are based largely on the similarities in structure among the spectra for the four terbium isotopes.

Diamond et al. (1963), in a study of the coulomb excitation of ^{159}Tb observed electromagnetic transitions with energies of 920 keV, 949 keV, 969 keV and 978 keV and fitted them into a $K=1/2^+$ band with $I=3/2$ and $I=5/2$ members at 979 keV and 1087 keV, respectively. The $I=1/2$ band head was not observed in that study. Recent calculations by Soloviev and Fedotov (1971) predict a second fragment of the $1/2^+ [411]$ orbital (the first one was discussed in section IV.1d) to appear at about 1.6 MeV in a state with about 30% of the single particle strength. In the present work, levels were observed at 949 keV and 979 keV and a multiplet at 1021 keV. The transitions observed by Diamond et al. are re-assigned to ones depopulating these levels. The cross section ratios for the 949 and 979 keV states are consistent

with l -values of 0 and 2 respectively. Assignment of $I=1/2$ and $3/2$ to these two states, with an $I=5/2$ state at 1022 keV gives a rotational parameter of ~ 10 keV and a decoupling parameter of approximately zero. The interpretation of these states as a fragment of the $1/2^+[411]$ orbital is tentative as the $U^2 C_{j\ell}^2$ for both the $I=1/2$ and $3/2$ states is ~ 0.25 . This is not characteristic of the $1/2^+[411]$ orbital as the $I=1/2$ member is usually considerably weaker than the $I=3/2$ member. This assignment places a second $I=5/2^+$ state in the multiplet at 1020 keV, as the $5/2 \ 5/2^+[402]$ state has been tentatively assigned there as well. The latter level would contribute most of the $l \sim 2$ strength to the multiplet as assumed in section IV.1f above, as the expected $U^2 C_{j\ell}^2$ of the $5/2 \ 1/2^+[411]$ state is ~ 0.2 .

A level at 855 keV in ^{159}Tb had previously been identified (Bunker and Reich (1971)) as a $I=1/2$ state, but the parity was not known. In the present studies it is suggested that the levels at 858 keV, 892 keV and the high l strength observed in the multiplet at 1016 keV are the $I=1/2$, $5/2$ and $9/2$ members of the $1/2^-[541]$ band respectively. On the basis of these energies, the rotational parameter and decoupling parameter are calculated to be $\frac{\hbar^2}{2\mathcal{J}} = 10.75$ keV and $a=2.2$, respectively. These are reasonable values for this orbital. The spectroscopic fingerprint also agrees well with the predicted one as can be seen in table 16. From the energy spacings listed above, the $I=3/2$ member of this band would be expected to be found at 961 keV. It is likely that the particle groups corresponding to an excitation energy of 949 keV are partly due to this state, in addition to the $1/2 \ 1/2^+[411]$ strength discussed earlier in this section. The observed cross sections are considerably larger than

Table 16

Spectroscopic information for the $1/2^- [541]$ Orbital in Tb isotopes

	I=1/2	I=3/2	I=5/2	I=7/2	I=9/2	Rotational Parameter (keV)	Decoupling Parameter
155 Tb Energy (keV)	863	949	907	1218	1041	11.25	2.0
$U^2C_{j\lambda}^2$ (α, t)	0.07	<0.1	0.1		0.4		
$U^2C_{j\lambda}^2$ ($^3\text{He}, d$)	0.11	0.08	0.2	0.05	0.6		
157 Tb Energy (keV)	887	969 ^a	926	1164	1051	10.75	2.2
$U^2C_{j\lambda}^2$ (α, t)	0.12		0.43		0.80		
$U^2C_{j\lambda}^2$ ($^3\text{He}, d$)	0.09		0.52	0.04	0.77		
159 Tb Energy (keV)	858	949 ^a	892	1152	1016	10.75	2.2
$U^2C_{j\lambda}^2$ (α, t)	0.05		0.32	0.01	^a		
$U^2C_{j\lambda}^2$ ($^3\text{He}, d$)	0.13		0.47	0.05			
161 Tb Energy (keV)	921	1021	951	1179	1064	9.6	2.3
$U^2C_{j\lambda}^2$ (α, t)	0.06	.08	0.32	0.09	0.95		
$U^2C_{j\lambda}^2$ ($^3\text{He}, d$)	0.09	.11	0.41	0.07	0.90		
$U^2C_{j\lambda}^2$ Calc. ^b	0.05	0.06	0.25	0.04	0.50		2.8

^a Multiple assignment^b The results of the Nilsson calculation with Coriolis mixing differed only slightly for different isotopes.

expected for either of these two states alone, but are consistent with the sum expected if the two states were unresolved.

In ^{157}Tb states with $\ell=0$ or 1 are found at 887 and 969 keV. These two levels as well as ones at 926 keV and 1052 keV are tentatively assigned to the $I=1/2, 3/2, 5/2$ and $9/2$ members respectively, of the $1/2^- [541]$ orbital. As seen in table 16, the spectroscopic fingerprint and rotational parameters are similar to those of the band observed in ^{159}Tb . A fragment of the $1/2^+ [411]$ orbital is also tentatively assigned to states at 969 keV, 1001 keV and 1077 keV for the $I=1/2, 3/2$ and $5/2$ members respectively. As in ^{159}Tb , the $1/2, 1/2^+ [411]$ and the $3/2, 1/2^- [541]$ states are not resolved. Alternatively, the levels at 889 keV, 926 keV and 1006 keV could be assigned to the fragment of the $1/2^+ [411]$ orbital. Such an assignment would give a rotational parameter of 14.5 keV, a decoupling parameter of $a=-0.1$ and $U^2 C_{j\ell}^2$ of the first three members of about 0.1, 0.4 and 0.2 respectively, compared to $U^2 C_{j\ell}^2$ of the other fragment of the band at 595 keV of 0.1, 0.5 and 0.2 respectively. However, this would prevent the assignment of the $1/2^- [541]$ orbital, especially the strongly populated high ℓ state at 1052 keV. The two other possible Nilsson orbitals with high ℓ strength, the $1/2^+ [660]$ and $9/2^- [514]$ orbitals, are both unlikely sources for the observed intensity of the peak, from considerations outlined earlier in the discussion of the $7/2^+ [404]$ orbital.

On the basis of similar spectroscopic fingerprints and level spacings to the states in ^{157}Tb and ^{159}Tb , the $1/2^- [541]$ orbital is tentatively assigned in ^{155}Tb with a band head at 863 keV and in ^{161}Tb at 921 keV. These assignments of the $1/2^- [541]$ orbital in the four terbium isotopes do not exhibit the excitation energy systematics expected for the

$1/2^- [541]$ orbital. From the Nilsson diagram, the relative excitation energy should decrease with increasing deformation and thus with increasing mass. According to the present assignments the total spread in excitation energies is 63 keV and there is no monotonic trend. As in ^{157}Tb an alternative assignment was considered possible for some of these states at about one MeV excitation. In ^{155}Tb the levels at 907 keV, 926 keV and 950 keV could be assigned to the $I=1/2, 3/2$ and $5/2$ members of a fragment of the $1/2^+ [411]$ orbital. This would give a fingerprint with $U^2 C_{j\ell}^2$ values of $\sim 0.1, 0.2$ and 0.05 respectively for the $I=1/2, 3/2$ and $5/2$ members, and rotational and decoupling parameters of 9.2 keV and 0.6 . Such an assignment has a rather low rotational parameter and again leaves the strongly populated high ℓ state unassigned. Hence the first interpretation discussed above is preferred although one cannot be certain on the basis of the present data alone. Persson and Ryde (1964), had suggested the assignment of the first three members of the $1/2^+ [411]$ orbitals to levels at 761 keV, 811 keV and 879 keV in ^{155}Tb as mentioned in a previous section. Harmatz (1972) assigned the $I=1/2, 3/2$ and $5/2$ members of the $1/2^+ [411]$ orbital to levels at 761 keV, 744 keV and 937 keV respectively. In the present study, only the states at 745 keV, 761 keV and 811 keV were observed. These are not clearly seen in the $\theta=30^\circ$ ($^3\text{He},d$) spectrum, shown in Fig. 11, due to the reaction from ^{13}C , but were well resolved in the ($^3\text{He},d$) spectrum measured at $\theta=40^\circ$. The proposed assignment of the 761 keV and 745 keV states to the first two members of the $1/2^+ [411]$ band is not consistent with the expected spectroscopic fingerprint or the rotational spacing expected from other terbium nuclei, as well as the high internal conversion coefficient of the 761 keV transition measured by

Harmatz. Assignment of the 761 keV and 810 keV states as the $I=3/2$ and $I=5/2$ members of the orbital, respectively, and the state found at 725 keV as the $I=1/2$ member, which is consistent with the (α, t) to $(^3\text{He}, d)$ cross section ratio, gives an acceptable fingerprint and a rotational spacing similar to those of the $1/2^+[411]$ orbital fragments observed in ^{157}Tb and ^{159}Tb . This tentative assignment is displayed in table 15. The spin values assigned to the 761 keV and 810 keV levels appear to be consistent with the high internal conversion coefficients observed by Harmatz for the 760 keV transition, and for the 744 keV transition, which is re-assigned between the 810 keV and 65 keV levels. In ^{161}Tb no levels near one MeV excitation are found to exhibit similar strengths and spacings to those tentatively assigned as fragments of the $1/2^+[411]$ orbital in the other three terbium nuclei. If, however, the band exhibits a rotational spacing characteristic of the unperturbed $1/2^+[411]$ orbital, with a decoupling parameter $a \sim -1.0$, the 953 keV level could possibly be a multiplet of the $I=1/2$ and $3/2$ members of the band, and the 1083 keV level a multiplet of the $I=5/2$ and $7/2$ members of the band. From the present work, it appears that the properties of the $1/2^+[411]$ orbital found at about 0.5 MeV excitation in all the isotopes studied, and that which has been called the $1/2^+[411]$ fragment, found at about 0.9 MeV, are not vastly different. Both contain appreciable single particle strength, although the decoupling parameters generally are near zero, characteristic of collective excitations.

On the basis of the Unified Model, fragmentation of the single quasi-particle states above about one MeV is expected, due to the mixing of single quasi-particle and three quasi-particle states, as well as more complicated forms of excitation which are normally neglected in the simple model description of the low lying states. This expectation is consistent with the increased density of states which is observed above about one MeV excitation. Thus the assignments of the $1/2^- [541]$ orbital and the fragment of the $1/2^+ [411]$ orbital at about one MeV excitation in the terbium isotopes must in general be considered tentative.

IV.1h Proton Studies of Terbium

A comparison of the interpretations from the reaction study of terbium presented here, with the interpretations presented by Boyno and Huizenga (1972) in a similar study, reveal two important features.

The first, which is recognized in any spectroscopic investigation, is the value of good resolution. The resolution in the present experiments is ~ 14 keV, compared with an estimated value of ~ 20 keV in the study by Boyno and Huizenga (1972). A number of levels which are important in the interpretation are not resolved by Boyno and Huizenga (1972). These include the 861 keV level in ^{157}Tb (fig. 12), the 518 keV, 1020 keV and 1063 keV levels in ^{161}Tb (fig. 14), and the 348 keV level and the multiple nature of the 1020 keV level in ^{159}Tb (fig. 13).

The other feature is that a study of the differences in the interpretations from these two independent works can reveal just how much confidence should be placed in the assignments. If the spins and parities

of some levels are previously assigned from a complementary investigation (e.g. a decay scheme study), the interpretation of these levels is generally the same for the two reaction studies. In particular, the assignments of the $3/2^+[411]$ and $5/2^+[413]$ orbitals in the four isotopes, as well as the $1/2^+[411]$ orbital in ^{157}Tb and ^{159}Tb , the $7/2^+[404]$ orbital in ^{155}Tb and ^{157}Tb , and the mixed $5/2^- [532]$ and $7/2^- [523]$ orbitals in ^{155}Tb , ^{157}Tb and ^{159}Tb are the same in the two studies. For the cases in which the population of a level is very strong, such as the $5/2^- [402]$ state in the four isotopes, the interpretations from the two investigations are also in agreement. This should apply to the $7/2^- [404]$ state in ^{159}Tb and ^{161}Tb . However, in ^{161}Tb , Boyno and Huizenga (1972) assigned this state to the level at 951 keV. The level at 998 keV was assigned as a multiplet containing the $I=1/2$ and $I=3/2$ members of the $1/2^+[411]$ orbital. In the present work, these two levels are assigned to the $5/2^- [541]$ and $7/2^- [404]$ states respectively (see table 8). The cross section ratios from both investigations strongly favour the present assignments. The major differences between the two works are in the consideration of the $1/2^- [541]$ orbital and the $1/2^+[411]$ orbital fragment. The reasons for the tentative assignments of these two bands in the present study, are presented in the previous section. Only the $I=1/2$ and $I=5/2$ states of the $1/2^- [541]$ orbital have the same assignment in both works, and this is mainly attributed to the previous assignment of the $I=1/2$ state to the level at 855 keV (section IV.1g). It is the opinion of the author that the distinction between the $1/2^+[411]$ orbital (with an expected decoupling parameter of $a \approx -0.8$) and the $1/2^+[411]$ mixed

vibrational state (a_0), proposed by Boyno and Huizenga (1972), is not realistic. If the single particle state is to fragment, it is likely to split into two strongly mixed states (as indicated by Soloviev and Fedotov, 1971). Thus their assignment of the levels at 923 keV in ^{157}Tb , 974 keV in ^{159}Tb and 990 keV in ^{161}Tb to multiplets containing the $I=1/2$ and $I=3/2$ members of the $1/2^+[411]$ single particle orbital is felt to be very questionable. Nevertheless, the differences in the interpretation of the $1/2^-[541]$ orbital and the $1/2^+[411]$ orbital fragment between the two investigations, clearly demonstrates the tentative nature of these particular assignments.

IV.2 ^{163}Ho

The most recent investigations of the states in ^{163}Ho are those by Funke et al. (1966) with a decay scheme study from the beta decay of ^{163}Er , by Geiger and Graham (1967) studying the isomeric transitions resulting from proton bombardment of dysprosium, and by Goles (1971) with the $^{165}\text{Ho}(p,t)^{163}\text{Ho}$ reaction.

The excitation energies of the levels observed in a reaction study are generally determined relative to a strongly populated member of the ground state rotational band that has also been identified in a decay scheme study. This makes use of the higher precision with which the electromagnetic transitions are measured. For ^{163}Ho , only the first two states in the ground state rotational band have been assigned by Funké et al. (1966), and they are both weakly populated in the present work. Moreover, the proposed energy of the first excited

state of 92 keV, by Funke et al., is not in agreement with that measured by Goles (1971), of 100 keV. In the present studies, the level at 440 keV which is assigned by Funke et al. (1966) as the $7/2^- 7/2^+[404]$ state, is strongly populated and is used to normalize the energies. The energies of the first and second excited states from the present work are in agreement with those measured by Goles (1971), as shown in table 9. A simple rearrangement of the transitions in the level scheme proposed by Funke et al. (1966), results in a scheme that is consistent with their experimental information, and with the energies of the levels observed in the present work.

IV.2a The $7/2^- [523]$ Orbital

This orbital has been assigned previously to the ground states of ^{163}Ho , ^{161}Ho and ^{165}Ho (Bunker and Reich, 1971). The present work confirms the assignments by Goles (1971) of the ground state and levels at 100 keV and 222 keV in ^{163}Ho to the $7/2^-$, $9/2^-$ and $11/2^-$ members of the $7/2^- [523]$ orbital respectively. The 222 keV level has a cross section ratio consistent with an $\ell=5$ transfer. As expected for the $11/2^- 7/2^- [523]$ state, the level is strongly populated. However, its intensity is appreciably larger than the calculation predicts, even when the usual Coriolis mixing with the other states from the $h_{11/2}$ shell is included. The results are shown in table 17 and will be discussed in a later section.

IV.2b The $7/2^+ [404]$ Orbital

This orbital was assigned by Funke et al. (1966) at 440 keV. As discussed in section IV.2, this state is used to normalize the energies

Table 17

Spectroscopic information for ^{163}Ho

Orbital	I=1/2	I=3/2	I=5/2	I=7/2	I=9/2	I=11/2	Rotational Parameter	Decoupling Parameter
$7/2^- [523]$ E (keV)				0	100	222	11	
$U^2 C_{j\lambda}^2$ (α, t)				~ 0.02	0.1	1.1		
${}^3\text{He, d}$				0.04	0.15	1.8		
(calc. a)				0.01	0.01	0.48		
(calc. b)				0.01	0.01	0.84		
$1/2^+ [411]$ E (keV)	299	307	393?	?			~ 9.2	-0.7
$U^2 C_{j\lambda}^2$ (α, t)	c	0.6	0.7					
${}^3\text{He, d}$		0.55	0.7					
(calc)	0.08	0.46	0.19	0.15				
$3/2^+ [411]$ E (keV)			361					
$U^2 C_{j\lambda}^2$ (α, t)			0.2					
${}^3\text{He, d}$			0.15					
(calc)		0.003	0.1	0.01				
$7/2^+ [404]$ E (keV)				440	?			
$U^2 C_{j\lambda}^2$ (α, t)				1.2				
${}^3\text{He, d}$				1.1				
(calc)				0.9	0.01			

Table 17 (continued)
Spectroscopic information for ¹⁶³Ho

Rotational
Parameter
(keV)

I=11/2

I=9/2

I=7/2

I=5/2

I=3/2

I=1/2

2.5

10.5

Orbital

5/2⁺ [402] E (keV)
U²C_j² (α,t)
(³He,d)
(calc)
712
1.2
1.0
0.89

1/2⁻ [541] E (keV)
U²C_j² (α,t)
(³He,d)
(calc)
473 580 500 748 615
0.1 0.07 0.3 0.13 0.9
0.1 0.17 0.45 0.11 1.1
0.05 0.06 0.25 0.05 0.64

9/2⁻ [541] E (keV)
U²C_j² (α,t)
(³He,d)
(calc)
1442
0.9
1.1
0.8

(calc a)
(calc b)
c
unmixed 7/2⁻ [523] orbital
mixing with 9/2⁻ [514] orbital included (see text)
level assigned from previous work, Geiger and Graham (1967)

measured from the present reactions. The cross section ratio of the 440 keV level is consistent with an $\ell=4$ transition, and the measured $U^2C_{j\ell}^2$ of 1.1 is in agreement with the expected value of 0.9.

IV.2c The $1/2^+[411]$ and $3/2^+[411]$ Orbitals

An isomeric state at 299 keV has previously been assigned to the $I=1/2$ member of the $1/2^+[411]$ orbital (Geiger and Graham, 1967). In the present study, only a strongly populated state at 307 keV is seen, and it has a cross section ratio consistent with an $\ell=2$ transfer. This level is assigned to the $I=3/2$ member of the $1/2^+[411]$ orbital. The observed $U^2C_{j\ell}^2$ is consistent with that expected (~ 0.5), and the theoretical decoupling parameter predicts that the $I=1/2$ and $I=3/2$ members of the band should be close together. The $I=1/2$ member, which is expected to be weakly populated, would be obscured by the 307 keV state. The $I=5/2$ and $I=7/2$ members of the orbital are expected to fall ~ 100 keV higher in excitation energy. The level at 393 keV appears to have $\ell \sim 2$, but its intensity is about three times that expected. It is possible that the level is a multiplet. The assignment of the $5/2$ $1/2^+[411]$ state to this level is still very tentative.

A state with an ℓ transfer of ~ 2 is seen at 361 keV. It is too close to the $I=3/2$ member of the $1/2^+[411]$ orbital to be the $I=5/2$ member of the band, and is tentatively assigned to the $5/2$ $3/2^+[411]$ state which is expected to appear as a hole state at ~ 300 keV excitation (the band head of the $3/2^+[411]$ orbital in ^{165}Ho appears at 363 keV, 67 keV below the $1/2^+[411]$ orbital). An alternative assignment of the $5/2$ $3/2^+[411]$

state (the only member of the $3/2^+[411]$ orbital expected to have an appreciable population in the present study) is to the 393 keV level. This would assume that the level is a multiplet containing both the $5/2\ 1/2^+[411]$ and $5/2\ 3/2^+[411]$ states. The strong Coriolis mixing between these two states would make such an assignment very unlikely.

With the proposed assignments, shown in figure 15 and table 9, the Coriolis mixing between the two orbitals should be appreciable. The situation could be further complicated by the presence of the $7/2^+[404]$ orbital at 440 keV and the $5/2^+[413]$ orbital expected at about 0.5 MeV. Sample Coriolis mixing calculations which have been performed indicate that the $I=7/2$ members of the $1/2^+[411]$ and $3/2^+[411]$ orbitals should mix strongly with the $I=7/2$ states from these other two orbitals. These calculations were not able to describe the observed intensities of the states, in particular, the 393 keV level. Thus, without other corroborating evidence, the assignments of the $I=5/2^+$ states to the levels at 361 keV and 393 keV are considered very tentative.

IV.2d Other Levels

The interpretation of several other levels is based only on the experimental evidence from the present study, and therefore the assignments are not considered definite.

The $1/2^-[541]$ orbital is expected to appear at about 0.5 MeV in ¹⁶³Ho, on the basis of the Nilsson model (see Figure 1), and is the only orbital in the region, other than the $1/2^+[411]$ orbital, expected to have an appreciable population of low spin rotational members in the reactions.

Two levels that are populated with low ℓ transfer are observed at 473 keV and 580 keV. These are assigned to the $I=1/2$ and $I=3/2$ members respectively of the $1/2^- [541]$ orbital. The $I=5/2$, $7/2$ and $9/2$ members are assigned to levels at 500 keV, 748 keV and 615 keV respectively. The levels at 500 keV and 748 keV have cross section ratios consistent with $\ell=3$ transfers, and the 615 keV level, with an $\ell=5$ transfer. The rotational parameter is 10.5 keV and the decoupling parameter, 2.5, which are similar to those observed for the orbital in the terbium isotopes (table 16). As shown in table 17, the $U^2 C_{j\ell}^2$'s are in good agreement with those expected.

A strongly populated state at 712 keV with a cross section ratio consistent with $\ell=2$ is assigned to the $5/2 \ 5/2^+ [402]$ orbital. Arguments similar to those for its assignment in the terbium nuclei apply here: It is expected to appear above the $7/2^+ [404]$ orbital in excitation, and to have a $U^2 C_{j\ell}^2$ near unity (assuming an $\ell=2$ transition). The 712 keV level is the one most intensely populated within the first two MeV of excitation. As shown in table 17, the extracted $U^2 C_{j\ell}^2$ is consistent with that expected for the $5/2 \ 5/2^+ [402]$ state.

A level with $\ell=5$ and a $U^2 C_{j\ell}^2$ (assuming $\ell=5$) near unity, is observed at 1442 keV. This strength could be attributed to either the $9/2^- [514]$ or $1/2^+ [660]$ orbitals. Both states are calculated to fall in the first two MeV of excitation in ^{163}Ho , and as most of the spectroscopic strength is expected to be found in one member of each band, no assignment can be made, based on a characteristic fingerprint. The assignment of the $11/2 \ 9/2^- [514]$ state to the 1442 keV level is preferred as the $1/2^+ [660]$ has not been identified in any $Z=69$ or $Z=71$ nuclei. The $9/2^- [514]$ orbital is

expected to mix strongly with the ground state $7/2^-$ [523] orbital. An attempt was made to describe the intensity of the $11/2$ member of the ground state band by Coriolis mixing, similar to that done in the terbium isotopes (with $\lambda = 0$ MeV and $\Delta = 0.5$ MeV). The calculations did not predict sufficient intensity for the $11/2$ $7/2^-$ [523] state (even when the $9/2^-$ [514] orbital was placed as close as 500 keV excitation). However, if the Fermi surface (λ) is placed at about -0.2 MeV, the calculated spectroscopic strengths are consistent with the tentative assignment of the $11/2$ $9/2^-$ [514] state to the 1442 keV level.

IV.3 ^{153}Eu and ^{155}Eu

The isotopes ^{153}Eu and ^{155}Eu have both been studied by decay scheme techniques by Ungrin et al. (1969a) and Ungrin and Johns (1969). A ($^3\text{He},d$) reaction study into these isotopes has also been done by Ungrin et al. (1969b). Spin assignments from the reaction studies were based mainly on the deuteron angular distributions, and identification of the levels was made in terms of the Nilsson model including pairing effects, but Coriolis mixing was not considered. The present studies with the (α,t) reactions serve to confirm the spin assignments and spectroscopic strengths, especially for the high spin transfers to which the (α,t) reaction is particularly sensitive.

IV.3a The $5/2^+$ [413] Orbital

The ground and first excited states of both the europium isotopes have been identified as the $I=5/2$ and $I=7/2$ members of the $5/2^+$ [413] orbital (see Bunker and Reich, 1971). The extracted $U_{jl}^2 C_{jl}^2$'s from the ($^3\text{He},d$) reactions of Ungrin ($E_{^3\text{He}}=28$ MeV) and from the (α,t)

Table 18
Spectroscopic information for the $5/2^+[413]$ orbital in the Europium isotopes

	I=5/2	I=7/2	I=9/2	Rotational Parameter
^{153}Eu Energy (kev)	0	78		11.1
$U^2C_{j\ell}^2$ (α, t)	0.02	0.6	a	
$(^3\text{He}, d)$	0.01	0.4		
Calc	0.01	0.54	0.01	
^{155}Eu Energy (kev)	0	83		11.8
$U^2C_{j\ell}^2$ (α, t)	0.02	0.65	a	
$(^3\text{He}, d)$	0.01	0.6		
Calc	0.01	0.58	0.01	
	a	not observed		

reactions and ($^3\text{He},d$) reactions of the present work ($E_{^3\text{He}} = 24 \text{ MeV}$) are in good agreement with the Nilsson model prediction, and are displayed in table 18.

IV.3b The $5/2^- [532]$ Orbital

From decay scheme studies (see Bunker and Reich, 1971), the first two rotational members of the $5/2^- [532]$ orbital have been assigned in ^{153}Eu and ^{155}Eu . In the ($^3\text{He},d$) reaction study (Ungrin *et al.*, 1969b), evidence of these members was found, and the $11/2^- 5/2^- [532]$ state, which is expected to be strongly populated, was found at 321 keV in ^{153}Eu and at 357 keV in ^{155}Eu . In the present work, the cross section ratios offer further confirmation of the spin assignments of the $I=11/2$ states, and their spectroscopic strengths agree with those measured by Ungrin *et al.* (1969b). A weakly populated level is found at 235 keV in ^{153}Eu in the (α,t) experiments and the ($^3\text{He},d$) experiment at $E = 24 \text{ MeV}$, and its excitation energy and cross section ratio are consistent with its assignment to the $9/2^- 5/2^- [532]$ state. The spectroscopic information for the orbital is displayed in table 20. In the interpretation, Ungrin (1969b) used an assumed $U^2 \approx 0.7$ for the state to account for the large spectroscopic strengths. This U^2 is too large for the $5/2^- [532]$ orbital, which is expected to be a 'hole' state (it appears below the $5/2^+ [413]$ orbital in the Nilsson diagrams). However, as in the discussion of the terbium isotopes, there should be strong mixing between this orbital and the $7/2^- [523]$ orbital, which is predicted to appear as a particle state within one MeV of excitation. As in ^{155}Tb , ^{157}Tb and ^{159}Tb , this

Table 19
Spectroscopic information for the $3/2^+ [411]$ orbital in the Europium isotopes

	I=3/2	I=5/2	I=7/2	I=9/2	Rotational Parameter
^{153}Eu Energy (keV)	103	173	270	395	13.9
$U^2 C_{j\ell}^2$ (α, t)	0.03	0.95	~ 0.02	0.03	
($^3\text{He}, d$)	a	0.83	0.05	0.2	
calc	0.02	0.69	0.06	0.05	
^{155}Eu Energy (keV)	246	307	391	501	12.1
$U^2 C_{j\ell}^2$ (α, t)	0.07	0.8	0.1	0.06	
($^3\text{He}, d$)	0.05	0.72	0.18	0.24	
calc	0.02	0.66	0.06	0.06	

a obscured

Table 20

Spectroscopic information for the $5/2^- [532]$ and $7/2^- [523]$ orbitals in the Europium isotopes

$7/2^- [523]$ orbital
I=11/2

$5/2^- [532]$ orbital

Rotational
Parameter

I=11/2

I=9/2

I=7/2

I=5/2

^{153}Eu Energy (keV)	98	152	235	321	570
$U^2C_{jl}^2$ (α, t)	a	0.03	0.06	1.2	0.67
$(^3\text{He}, d)$	a	~ 0.04	0.06	1.4	0.6
Calc	0.0002	0.02	0.006	0.63	0.66

8.5

^{155}Eu Energy (keV)	104	169	357	977
$U^2C_{jl}^2$ (α, t)	~ 0.01	0.03	0.77	0.7
$(^3\text{He}, d)$	~ 0.02	0.05	1.	0.85
Calc	0.0001	0.01	0.45	0.7

9.4

a not observed

should result in an increase in strength of the states with the lowest excitation, as well as a compression of the rotational spacing of the lower band. This could account for the rotational parameter of 8 keV and 9 keV for the bands in ^{153}Eu and ^{155}Eu respectively, and the large $U^2C_{j\ell}^2$'s of the $I=11/2$ states in these isotopes. Identification of the $7/2^- [523]$ orbital will be discussed in section IV.3e.

IV.3c The $3/2^+ [411]$ Orbital

The $3/2^+ [411]$ orbital, which is expected to appear as a particle state in the europium isotopes, has been previously assigned in both europium nuclei (Bunker and Reich, 1971). The first three members were seen in the beta decay studies and the $I=9/2$ member was tentatively assigned in the $(^3\text{He},d)$ reactions. The present work serves to confirm these assignments, and the extracted $U^2C_{j\ell}^2$'s from the (α,t) reactions are in agreement with the $(^3\text{He},d)$ measurements for most of the band members. The results are shown in table 19. However, the extracted spectroscopic strengths for the $I=9/2$ member are considerably stronger from the $(^3\text{He},d)$ experiments of Ungrin et al., (1969), than from the (α,t) and $(^3\text{He},d)$ experiments done for the present study. It is possible that this discrepancy may be caused by reactions from impurities in the targets used by Ungrin.

IV.3d The $1/2^+ [411]$ Orbital

The $1/2^+ [411]$ orbital is expected to appear at about 0.5 MeV in both europium isotopes. Prior to the $(^3\text{He},d)$ reaction studies by Ungrin et al. (1969b), the band head had been assigned to levels at 635 keV in ^{153}Eu and 768 keV in ^{155}Eu , but the weak population

of these states by the proton transfer reaction forced a rejection of these assignments. The proposals for the assignment of the $1/2^+[411]$ orbital made by Ungrin *et al.* (1969b) at 700 keV in ^{153}Eu and 910 keV in ^{155}Eu require further discussion.

In ^{153}Eu , an intense wide peak is seen from the $(^3\text{He},d)$ reaction at 0.7 MeV. From the peak shape, it is apparent that it contains at least two states, one at ~ 700 keV and the other at ~ 715 keV. In the (α,t) reactions it appears to be resolved into four states with energies (± 3 keV) of 696 keV, 705 keV, 718 keV and 733 keV. From the cross section ratio, the " ℓ -value of the multiplet" is ~ 2 , and as the peak shape is similar in both reactions, little can be said about the placement of states of different spins within the multiplet. As mentioned by Ungrin *et al.* (1969), the intensity expected from the $I=1/2$ and $I=3/2$ members of the $1/2^+[411]$ orbital is not sufficient to account for all of the intensity in the peak. Moreover, the 842 keV level to which the $I=5/2$ member had been tentatively assigned is very weakly populated in the (α,t) study, and on the basis of the cross section ratio, should be $\ell=0$. Thus the assignment of the orbital in ^{153}Eu is very tentative.

In ^{155}Eu , Ungrin proposed that the $I=1/2$ and $3/2$ states could appear at 910 keV, but the intensity of the state is about a third of that expected for members of the pure state. The $I=5/2$ member was very tentatively assigned to a level at 1067 keV which has about half the expected intensity. The (α,t) studies are in agreement with the proposed spins and the measured strengths, but do not help to confirm the tentative interpretation.

As in the terbium nuclei, some mixing of the single particle $1/2^+[411]$ state with vibrational states is expected. For ^{153}Eu , Soloviev and Fedotov (1971) predict a $K=1/2^+$ state for which the structure consists of 48% single particle $1/2^+[411]$ state with 23% gamma vibration based on the $5/2^+[413]$ orbital and 26% gamma vibration based on the $3/2^+[411]$ orbital. It would be consistent with the states seen in the terbium nuclei if the rotational band of such a state has a decoupling parameter near zero. Thus the $I=1/2$ and $3/2$ members would be well separated. Possible levels for the $I=1/2$ state, on the basis of the cross section ratio, are at 635 keV or 842 keV in ^{153}Eu and at 1024 keV or 1109 keV in ^{155}Eu . The decay scheme study of Ungrin argues strongly against the assignment of the 635 keV state to $I=1/2$, and if the 700 keV multiplet is to contain the $I=3/2$ member of the band, there would be no suitable candidate for the $I=5/2$ assignment. The lack of states within 300 keV of the 842 keV state makes its possible assignment to the band head unlikely. The problem of the assignment of the $1/2^+[411]$ single particle orbital mixed with a ground state gamma vibration in ^{153}Eu is even more unlikely, as recent Coulomb excitation experiments by Lewis and Graetzer (1971) failed to populate levels that could be ascribed to a $K=1/2^+$ band. In fact, there seemed to be little overlap between the states studied by Coulomb excitation and those studied by the proton transfer reactions and beta decay studies. However, they did place one level at 711 keV which will be discussed later. In ^{155}Eu , there is a similar lack of levels that could be assigned to the $I=3/2$ and $5/2$ members of the $1/2^+[411]$ orbital, which makes the possible assignment

of the 1024 keV or 1109 keV levels to a $K=1/2^+$ single particle vibrational mixture unlikely.

IV.3e Other Levels

The 570 keV level in ^{153}Eu and the 977 keV level in ^{155}Eu are strongly populated in the reactions and on the basis of the cross section ratio appear to have $\lambda \approx 5$. These levels, as suggested by Ungrin, could be assigned to the $11/2\ 7/2^- [523]$ state or the $7/2\ 7/2^+ [404]$ state. Both orbitals are expected to increase in excitation energy with increasing deformation (^{155}Eu has a larger deformation than ^{153}Eu). On the basis of the deformation calculated from the samarium isotones, the $7/2^- [523]$ Nilsson orbital is expected to appear between 0.5 and 1 MeV, and the $7/2^+ [404]$ orbital, between 1.5 and 2 MeV. Thus the assignment of the $11/2\ 7/2^- [523]$ state to these two levels is preferred. Moreover, as mentioned earlier, the mixing of this orbital with the $5/2^- [532]$ orbital would help to explain the observed intensities. It is expected that the closer that the two orbitals are to each other, the stronger they will mix, and the greater the 'transfer of strength' to the lower lying $5/2^- [532]$ orbital. This is consistent with the assignment of the $11/2\ 7/2^- [523]$ state, 250 keV above the $11/2\ 5/2^- [532]$ state in ^{153}Eu and 620 keV above it in ^{155}Eu . The mixing calculations (with $\lambda = 0$ MeV and $\Delta = 0.5$ MeV) do not predict enough intensity in the lower state, as shown in table 20. As for the $7/2^- [523]$ and $9/2^- [514]$ orbitals in ^{163}Ho , an adjustment of the Fermi level predicts an intensity in better agreement with the observations.

A tentative assignment for the $7/2^+[404]$ orbital is made in the multiplet at 700 keV in ^{153}Eu . This could explain some of the observed intensity in the peak, especially in the (α, t) reactions. Lewis and Gratzner (1971), in the Coulomb excitation of ^{153}Eu , placed a level at 711 keV. Although they proposed that it is the $7/2^+$ member of the beta vibration ($K=5/2^+$) based on the ground state, the reduced gamma ray branching ratio calculated for a $I=7/2^+$, $K=5/2^+$ level decaying to the $I=9/2^+$ and $I=7/2^+$ members of a $K=5/2^+$ band was about one tenth of the observed value of 0.27 ± 0.09 . Assuming that the level is the $7/2^+[404]$ state, a calculation of the reduced gamma ray branching ratio gives a value of 0.33, consistent with the observations of Lewis and Graetzer (1971). The $7/2^+[404]$ orbital could be excited by Coulomb excitation as it is expected to mix strongly with the ground state orbital. In ^{155}Eu , other than the level at 976 keV, which is tentatively assigned to the $11/2^-[523]$ state, the most suitable level within 1.5 MeV of excitation for assignment to the $7/2^+[404]$ orbital would be the one at 1202 keV. For the $I=7/2^+$ state, the $U^2 C_{j\lambda}^2$ would be about 0.4, which is rather small.

A preferred assignment of the high spin level at 1202 keV in ^{155}Eu as well as the low spin levels at 1024 keV and 1109 keV, could be to the $1/2^-[541]$ orbital. This orbital is expected to appear within two MeV excitation in ^{155}Eu . If the levels at 1024 keV, 1060 keV and 1200 keV are the $I=1/2$, $5/2$ and $9/2$ members of this orbital, the calculated rotational parameter is 13.5 keV and the decoupling parameter is 2.7. The rotational parameter is larger than expected, but the decoupling parameter is consistent with those

observed in the terbium isotopes. On the basis of these parameters, the $I=7/2$ state could be the level at 1402 keV. The $I=3/2$ member which, on this basis is expected to appear at about 1170 keV, could be the level at 1109 keV. Assuming the proposed assignments, the $U^2C_{j\ell}^2$'s for the $I=1/2$ to $I=9/2$ states are 0.05, 0.07, 0.2, 0.1 and 0.6 respectively, compared with the calculated values of 0.05, 0.06, 0.24, 0.05 and 0.55 respectively. The assignment of this orbital in ^{155}Eu is very tentative.

V Summary

In this study of the proton states of deformed nuclei with $A=153$ to $A=163$, the description of the observed low lying states in terms of the Unified Model has generally been quite successful.

The results confirm the previous assignments of the $3/2^+[411]$ and $5/2^+[413]$ single particle orbitals in the four terbium and two europium isotopes, and a possible assignment is considered for the $3/2^+[411]$ orbital in ^{163}Ho . The $I=11/2$ members of the $5/2^-[532]$ and $7/2^-[523]$ orbitals are identified in ^{161}Tb and ^{159}Tb and the assignments confirmed in ^{155}Tb and ^{157}Tb . In the europium isotopes, the assignment of the $5/2^-[532]$ orbital is confirmed and the $I=11/2$ member of the $7/2^-[523]$ is identified. In ^{163}Ho , confirmation is made for the $7/2^-[523]$ orbital. The assignment of the $7/2^+[404]$ orbital is confirmed in ^{155}Tb , ^{157}Tb , ^{163}Ho , is made in ^{159}Tb and ^{161}Tb , and is tentatively proposed in ^{153}Eu . Previous assignments of the $1/2^+[411]$ orbital are confirmed in ^{157}Tb , ^{159}Tb and ^{163}Ho , and it is identified in ^{161}Tb . For the holmium and terbium isotopes, assignment of the $5/2^+[402]$ orbital is made, and the tentative assignment of the $1/2^-[541]$ orbital is proposed. The $1/2^-[541]$ orbital is very tentatively assigned in ^{155}Eu .

In this study, it has been found necessary to consider the effects of the mixing phenomena in order to interpret the observed states in terms of the model. Most seriously affected by Coriolis mixing are the rotational members of the $5/2^-[532]$ and $7/2^-[523]$

orbitals, whose energies and spectroscopic strengths are greatly perturbed. A level diagram of these states is shown in fig. 18 for the nuclei considered. The energy perturbations are the most serious for the terbium isotopes where the band heads of the orbitals fall the closest to each other. Perturbations in the energy due to the Coriolis mixing for other orbitals appear to be quite small as seen from the level diagrams in figures 19 to 22, and only for the $5/2^+[413]$ and $7/2^+[404]$ orbitals in ^{155}Tb is the shift in spectroscopic strength appreciable.

The importance of the vibrational quasi-particle mixing is demonstrated by the character of the $1/2^+[411]$ orbital. The expected rotational spacing which is observed between the $I=1/2$ and $I=3/2$ members in ^{163}Ho , is not found in the terbium isotopes. Moreover, a second $K=1/2^+$ band is assigned in the present work for several of the terbium isotopes, and is attributed to a fragment of the $1/2^+[411]$ orbital which is also mixed with a vibration. The unsatisfactory theoretical description of these second bands (Soloviev and Fedotov 1971), as well as the difficulty of making any assignment of this orbital in the europium isotopes, suggest that the single particle vibrational mixing is not well understood. This may particularly apply to the $1/2^+[411]$ orbital which can mix strongly with gamma vibrations based on either the $5/2^+[413]$ or the $3/2^+[411]$ orbitals, both of which appear at low excitation in the europium and terbium isotopes, and can also Coriolis mix with the $3/2^+[411]$ orbital and with its own time reversed state (the decoupling effect).

Of the orbitals identified in the present study, it is only

Figure 18

Energies of the assigned band members of the $5/2^-$ [532] and $7/2^-$ [523] orbitals in the nuclei studied.

The label: a refers to the $5/2^-$ [532] orbital
 b refers to the $7/2^-$ [523] orbital

The broken lines represent the strongly mixed levels in the terbium isotopes, discussed in section IV.1c.

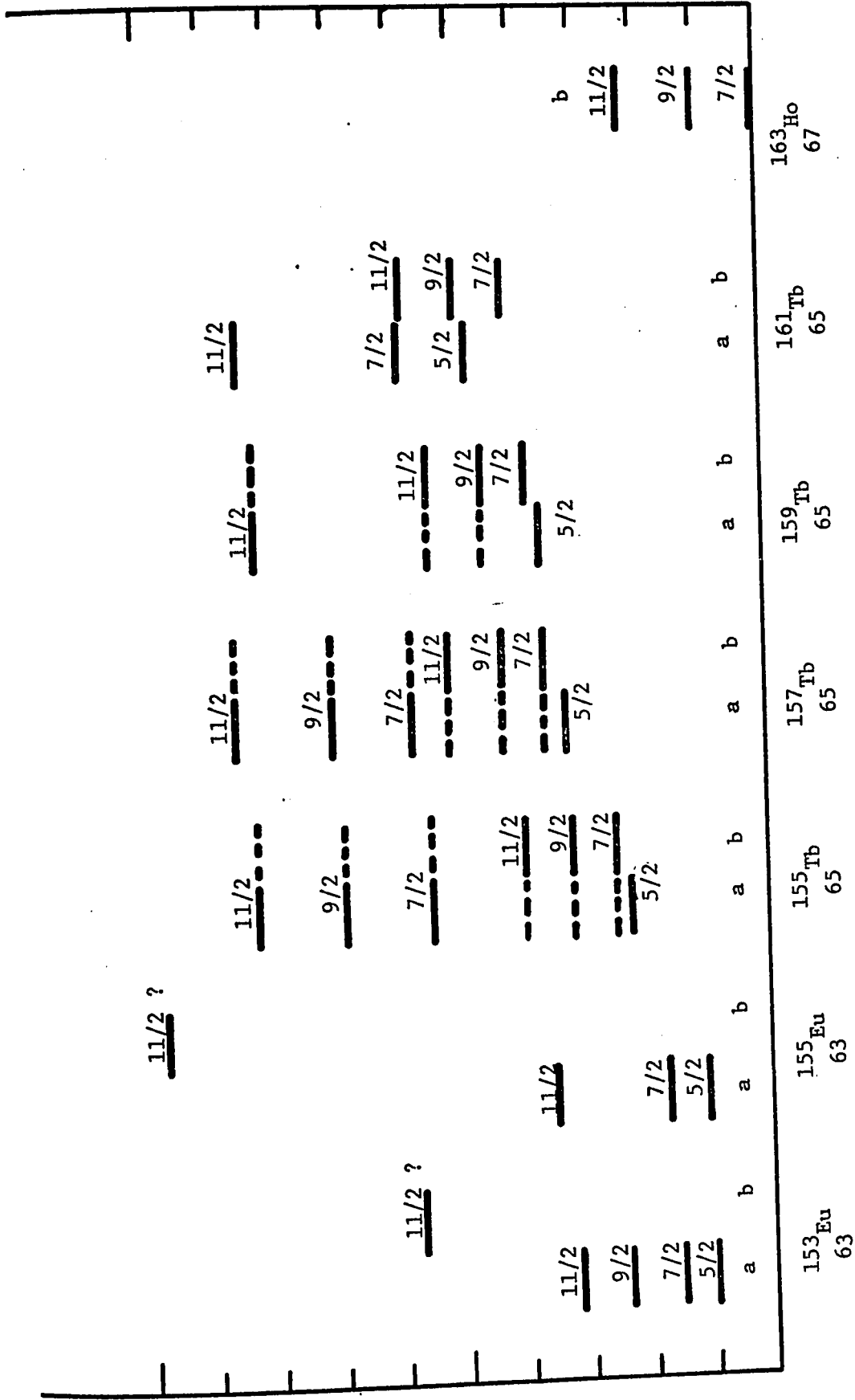
ENERGY (keV)

1000

500

0

117



$5/2^- [532]$ and $7/2^- [523]$ Orbitals

Figure 19

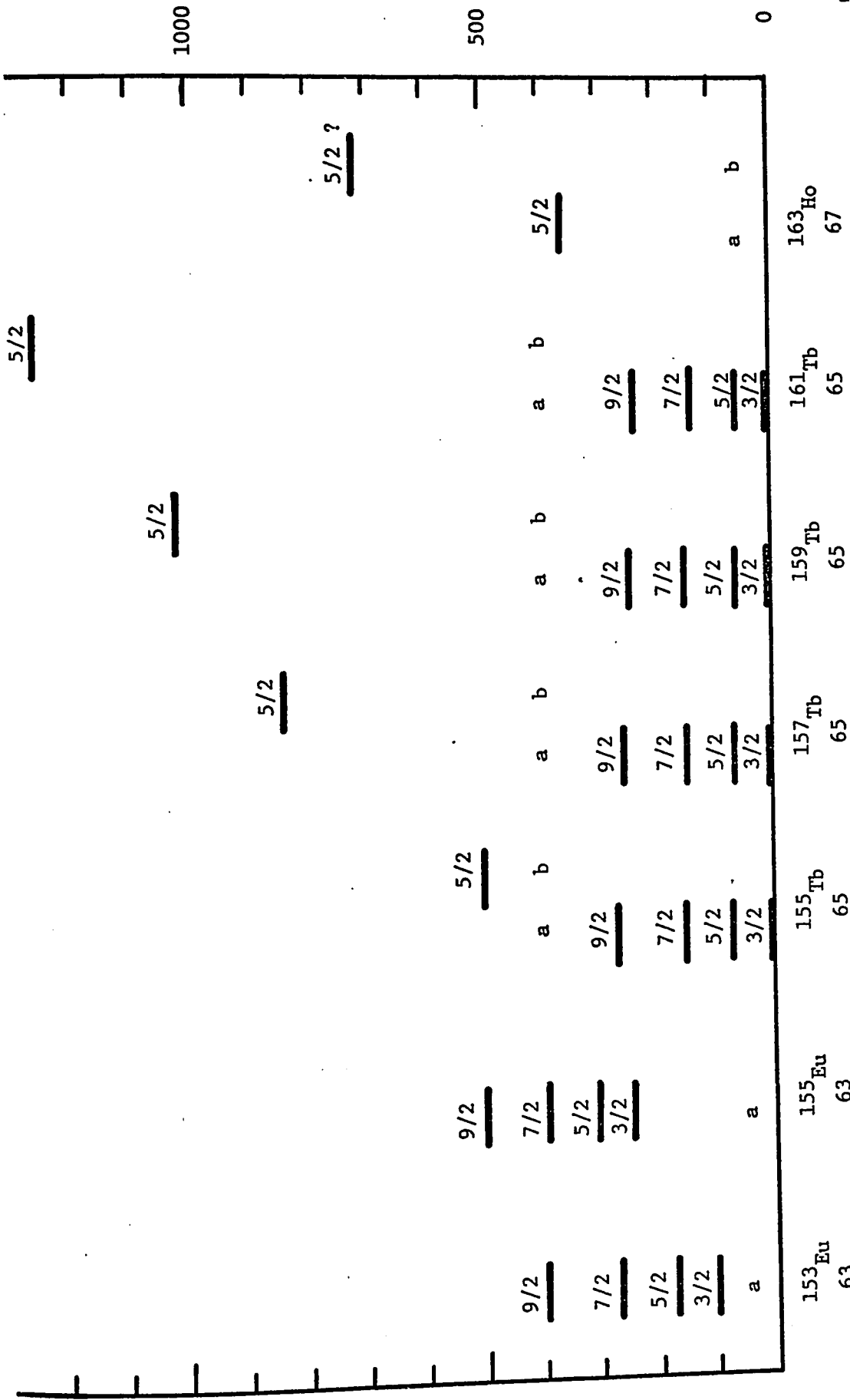
Energies of the assigned band members of the $5/2^+$ [413] and $7/2^+$ [404] orbitals in the nuclei studied.

The label: a refers to the $5/2^+$ [413] orbital
 b refers to the $7/2^+$ [404] orbital

Figure 20

Energies of the assigned band members of the $3/2^+[411]$ and $5/2^+[402]$ orbitals in the nuclei studied.

The label: a refers to the $3/2^+[411]$ orbital
 b refers to the $5/2^+[402]$ orbital



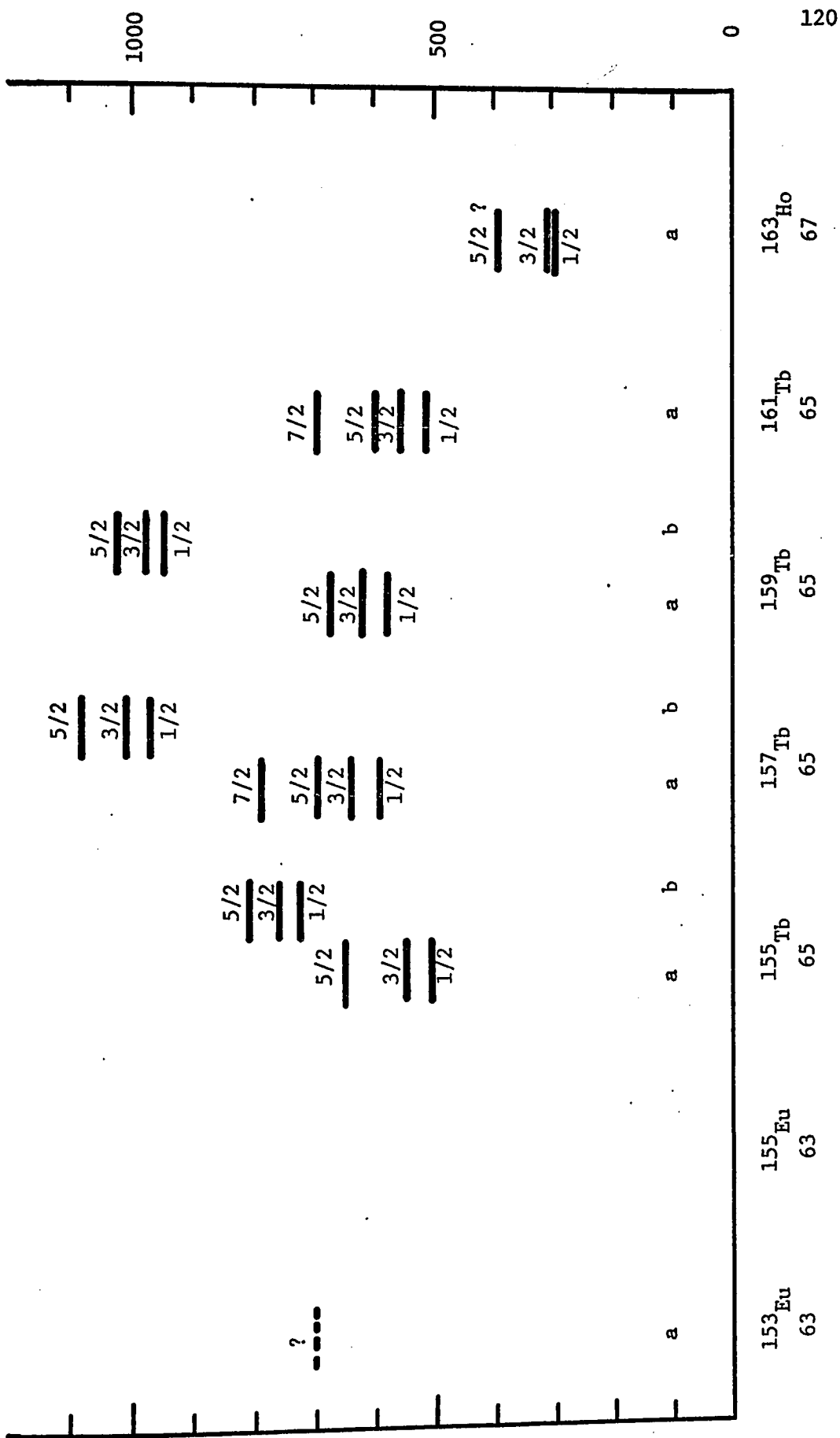
$3/2^+ [411]$ and $5/2^+ [402]$ Orbitals

Figure 21

Energies of the assigned band members of the $1/2^+[411]$ orbital and fragment.

The label: a refers to the $1/2^+[411]$ orbital
 b refers to the $1/2^+[411]$ fragment observed
 in some of the terbium isotopes (see
 section IV.1g)

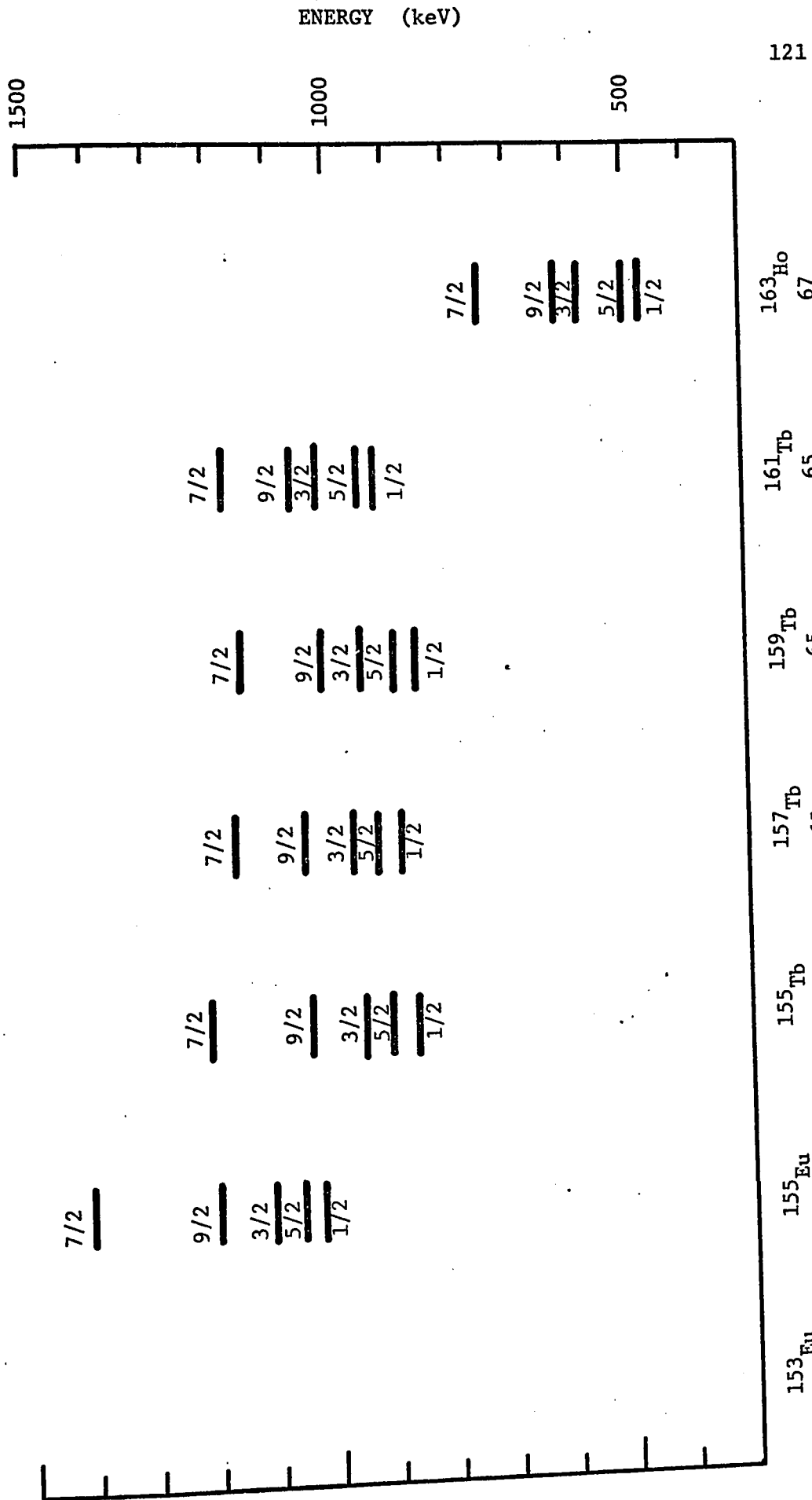
ENERGY (keV)



$1/2^+ [411]$ Orbital and Fragment

Figure 22

Energies of the assigned band members of the $1/2^- [541]$ orbital.



$1/2^- [541]$ Orbital

the appearance of the $1/2^- [541]$ orbital in the lighter terbium isotopes that is contrary to the expectations of the Unified Model. The rapid change in energy with deformation that is calculated from the Nilsson model, is not observed in the terbium isotopes. It is for this reason that the assignment of the $1/2^- [541]$ orbital in ^{155}Tb and ^{157}Tb is considered tentative. Certainly, the rotational spacings (fig. 22) and the fingerprints (table 16) are very reasonable. In general the character of the states above ~ 1 MeV excitation is not well described by the Unified Model. These excitations are influenced by effects that are neglected in the model, and it is possible that these effects have perturbed the position of the $1/2^- [541]$ orbital in the terbium nuclei.

APPENDIX

DWBA Theory

In this section, the theory of the Distorted Wave Born Approximation for the calculation of reaction cross sections is outlined. The discussion will be directed toward single particle stripping reactions. No detailed mathematical developments will be undertaken; these can be found in the references cited.

The differential cross section to be calculated by the DWBA theory is defined in terms of the measurable quantities:

$N_b(\Omega)$ the number of particles b, scattering into solid angle Ω per sec.,

J_a the number of incident particles a per sec.,

N the number of scattering centers (nuclei) per square centimeter,

$$\text{as } \frac{d\sigma}{d\Omega} \equiv \frac{N_b}{NJ_a} \tag{A.1}$$

The exact expression for the differential cross section of a reaction from an initial system with incident particles a, to a final system with particles b scattered into solid angle Ω_b is given in terms of the quantum mechanical transition amplitude T_{ab} by:

$$\frac{d\sigma}{d\Omega} = \frac{\mu_a \mu_b k_a}{(2\pi\hbar^2)^2 k_b} T_{ab}^2 \tag{A.2}$$

where $\mu_a = M_a M_A / (M_a + M_A)$ and $k_a = \mu_a v_a / \hbar$

M_a is the mass of the incident particle

M_A is the mass of the target nucleus

v_a is the velocity of particle a in the center of mass system

A similar definition applies to μ_b and k_b .

(See Messiah, 1966, Chap. XIX.)

The exact expression for the transition amplitude T_{ab} is given by:

$$T_{ab} = \langle \phi_b | V | \psi_a^{(+)} \rangle \quad \text{A.3}$$

where $H \psi_a^{(+)} = E \psi_a^{(+)}$ and $(H-V) \phi_b = E \phi_b$

H is the total Hamiltonian of the system including all channels of the reaction (a,b etc.). $\psi_a^{(+)}$ is the eigenfunction of H with incident plane waves and outgoing spherical waves at infinity. ϕ_b is a solution of the Hamiltonian after the reaction (plane waves at infinity scattered into solid angle Ω_b).

Intuitively, this may not be apparent. The transition amplitude should depend on the rate of change in the overlap of the total time dependent wavefunction with that of the final state:

$$T_{ab} \propto \frac{d}{dt} \langle \phi_b(t) | \psi_a(t) \rangle$$

This has been shown by Gell-Mann and Goldberger (1953) to reduce exactly to A.3 (which contains only the time independent wavefunctions).

The potential in A.3 is the interaction of the particles of b with all the particles of the residual nucleus. This can be separated into an average potential \bar{V}_b and the residual v . The Distorted Wave Born Approximation consists of replacing A.3 by:

$$T_{ab} = \langle \chi_b^- | v | \chi_a^+ \rangle \quad \text{A.4}$$

where χ_b^- is a solution of the Hamiltonian with the average potential \bar{V}_b , and has incoming spherical waves at infinity. This is the distorted wavefunction of particle b. Similarly, χ_a^+ is the distorted wavefunction of the initial system and is a solution of the Hamiltonian with the potential \bar{V}_a .

A fairly clear description of the steps between A.3 and A.4 is given by Glendenning, 1963.

Basically, the Born Approximation consists of the replacement of the exact wavefunction for scattering by potential V , by a known wavefunction which is a solution for scattering by potential \bar{V} ($\approx V$). This is valid when $V-\bar{V}$ is small compared with the particle energy over most of space, and should be true for the expected short range residual nuclear potential. (See Messiah, 1966, Chap. X).

Necessary also in the approximation of T_{ab} (A.4) for the present considerations, is that coupling with other channels is small (i.e. the wavefunctions of channel a and b are not strongly affected by any other channel). This is sometimes not valid for the incident channel which can couple strongly to inelastic excitations of the target. Some coupled channel calculations have been done, but are too complicated to be considered here.

The nature of the transition is assumed to be a direct reaction. This is a process in which only a few particles are involved. Thus, the residual interaction between the core nucleons (those that are not directly involved in the reaction) and the unbound particles can be neglected. For a stripping reaction, the interaction in question is that between the scattered particle and the target nucleus. Such an interaction

could cause collective excitation of the nucleus. Thus, the potential V used for stripping in (A.4) would be that between the transferred and outgoing particles.

There are two other important assumptions. First, the exchange effects which are expected to be small between the bound and free particles, are neglected. Secondly, the nucleus and the potentials are assumed to be spherical. The latter is generally not of importance for deformed nuclei as the ensemble is not aligned, and the aspherical effects will be averaged out for the distorted waves. For a particle transfer reaction, the effect of a deformed potential for the transferred particle was studied by Rost (1967) using a coupled channel calculation and for heavy nuclei was not found to be significant.

The case of single particle stripping will now be considered. Analysis of pick-up reactions and inelastic scattering which can also be treated using a DWBA calculation can be found, for example, in Bassel *et al.* (1962). As well, only spin independent nuclear potentials will be considered. Spin dependent potentials can be treated if the distorted wavefunctions are replaced by spin matrices, but the discussion becomes obscured with the mathematics (See Satchler, 1964).

The conservation of angular momentum and the symmetry of the reaction system require that the particle transferred have a good total angular momentum j and parity π . Thus it will be found in a state $\phi_{j\ell}$ (with good total and orbital angular momentum) which is assumed to be determined by the average potential exhibited by the target nucleons. (Since this bound particle has a good ℓ and j , unlike the distorted waves which are composed of many ℓ 's and j 's, it is trivial to treat the spin

dependence of this potential,

There are two further assumptions about the initial and final channels. The distorting potentials (the nuclear optical potentials) are assumed to be local (momentum independent). Realistically, the potentials are non-local, and correction for this effect can be made in the local energy approximation by multiplying the local wavefunction by $[1 - \beta^2 m V(r)/(2\hbar^2)]^{1/2}$ where β is the range of the non-locality and $V(r)$ is the local optical potential (see Stock et al., 1967). The wavefunctions are also assumed to be separable such that for the reaction $A(a,b)B$ where $a = b + x$ and x is the stripped particle:

$$\chi_a^{(+)} = \psi_a^{(+)} \phi_a^{J_a M_a} \phi_A^{J_A M_A} \quad \text{and} \quad \chi_b^{(-)} = \psi_b^{(-)} \phi_b^{J_b M_b} \phi_B^{J_B M_B} \quad \text{A.5}$$

where ψ is the solution to the Optical Model potential and ϕ is the internal wavefunction of the particle.

As mentioned earlier, the exchange contributions of the wavefunctions are expected to be small between the bound and free particles and are therefore neglected. Thus one has:

$$T_{ab} = \langle \psi_b^{(-)} \phi_b^{J_b M_b} \phi_B^{J_B M_B} | V_{bx} | \psi_a^{(+)} \phi_a^{J_a M_a} \phi_A^{J_A M_A} \rangle \quad \text{A.6}$$

From the nature of the direct reaction process, the final wavefunction of the nucleus $\phi_B^{J_B M_B}$ can be expanded in terms of the target and stripped particle wavefunctions:

$$\phi_B^{J_B M_B} = \sum_{M_A m} \langle J_A M_A \ jm | J_B M_B \rangle \beta_{j\ell} \phi_x^{j\ell m} \phi_A^{J_A M_A} \quad \text{A.7}$$

where $\beta_{j\ell}$ is the coefficient of the overlap of the states and is the square root of the spectroscopic factor for stripping

into a state $\phi_x^{j\ell m}$. This wavefunction can be written:

$$\begin{aligned}\phi_x^{j\ell m} &= \sum_{m_s m_\ell} \langle \ell m_\ell m_s | jm \rangle \phi_x^{j\ell m} \chi_{s_x}^{m_s} \\ &= \sum_{m_s m_\ell} \langle \ell m_\ell m_s | jm \rangle U_x^{j\ell} Y_x^{\ell m_\ell} \chi_{s_x}^{m_s}\end{aligned}\quad \text{A.8}$$

where $U_x^{j\ell}$ is the radial wave equation for particle x in nucleus A, Y is the spherical harmonic and χ_x^{sm} is the spin function of the transferred particle. Similarly the wavefunction of particle a can be written in terms of particles x and b :

$$\phi_a^{J M} = \sum_{M_b m} \langle J_b M_b m | J_a M_a \rangle v_x \phi_x^{s_x m} \phi_b^{J_b M_b}\quad \text{A.9}$$

In this case, $\phi_x^{s_x m} = \phi_{bx} \chi_x^{s_x m}$, as particle x is assumed to be in a relative S state of motion with respect to particle b (i.e. $\phi_{bx} = \phi_{bx}(\ell=0)$). This, for example, neglects the D state admixture to the S state in the deuteron ground state wavefunction. $\chi_x^{s_x m}$ is the spin wavefunction of particle x in particle a. ϕ_{bx} is the solution to the Hamiltonian $(T_{bx} + V_{bx}) \phi_{bx} = E \phi_{bx}$ where V_{bx} is the potential between particles b and x, and it is found also in A.6, the transition matrix element. The coefficient v_x is a measure of the overlap of the wavefunction of b and x with a.

If the expressions A.7, A.8 and A.9 are placed in A.6, one obtains:

$$\begin{aligned}T_{ab} &= \sum_{j\ell} \beta_{j\ell} v_x \sum_{m, m_s, m_\ell} \langle J_a M_a jm | J_b M_b \rangle \langle \ell m_\ell m_s | jm \rangle \\ &\times \langle J_b M_b m | J_a M_a \rangle \int \psi_b^{(-)}(\vec{r}_b) U_x^{j\ell}(\vec{r}_x) Y^{\ell m_\ell}(\theta_x) v_{bx}(\vec{r}_b - \vec{r}_x) \\ &\quad \phi_{bx}(\vec{r}_b - \vec{r}_x) \psi_a^{(+)}(\vec{r}_a)\end{aligned}\quad \text{A.10}$$

The orthogonality of the internal wavefunctions χ_x^{sm} , $\phi_a^{J_a M_a}$ and $\phi_b^{J_b M_b}$ has been used to eliminate them from the expression. The sum over

j and l in A.10 is required as the state into which particle x is stripped may not be one of good j and l as assumed by eqn. A.7.

To obtain the differential cross section using A.1 and A.10, it must be noted that the transition has been calculated between particular magnetic substates of the initial and final nuclei. As the initial population of the magnetic substates (M_A) should be totally random, the cross section must be averaged over these initial states, i.e. $\frac{d\sigma}{d\Omega} \propto \sum_{M_A} T^2 / (2J_A + 1)$. It must also be summed over the final substates (M_B) since the reaction may lead to any one of them. A similar argument applies to the substates of the projectile and scattered particle. Thus:

$$\frac{d\sigma}{d\Omega} = \frac{\mu_a \mu_b k_a}{(2\pi\hbar^2)^2 k_b} \sum_{M_A M_B m_a m_b} \frac{T_{ab}^2}{(2J_A + 1)(2J_a + 1)} \quad \text{A.10'}$$

From the orthogonality property of the Clebsh-Gordan coefficients (see Messiah, 1966, Appendix C):

$$\sum_{M_A M_B} \langle J_A M_A j m | J_B M_B \rangle \langle J_A M_A j' m' | J_B M_B \rangle = (-1)^{j - J_B - M_A} \frac{(2J_B + 1)}{(2j + 1)} \delta_{j'j} \delta_{m'm}$$

the cross terms expected from the square of the transition amplitude with different j , l , s or m are eliminated, and the sum over m_s and m of the second Clebsh-Gordan coefficient in A.10 gives $(-1)^{s_x - j - m} (2j + 1) / (2l + 1)$.

Thus:

$$\frac{d\sigma}{d\Omega} = \frac{\mu_a \mu_b k_a}{(2\pi\hbar^2)^2 k_b} v_x^2 \sum_{j \ l \ m_l} \beta_{j\ell}^2 \frac{(2J_B + 1)}{(2J_A + 1)(2s + 1)(2l + 1)} S_{lsj}^{m_l} \quad \text{A.11}$$

$$\text{and } S_{lsj}^{m_l} = \int \psi_b^{(-)}(\vec{r}_b) U_x^{j\ell}(\vec{r}_x) Y^{\ell m_\ell}(\theta_x) V_{bx}(\vec{r}_{bx}) \phi_{bx}(\vec{r}_{bx}) \psi_a^{(+)}(\vec{r}_a) \quad \text{A.12}$$

One should note that had the spin dependence been included in the distorted waves, the major difference would be that the sum over the magnetic substates m_a and m_b could not have been calculated as simply, but would depend on $\mathcal{S} = \mathcal{S}_{lsj}^{m_a m_b}$. The terms used in this development are not necessarily the same as those used by others. They generally differ in the grouping of the statistical factors and reaction constants.

This next section concerns the evaluation of $\mathcal{S}_{lsj}^{m_l}$ (A.12). The distorted waves $\psi_b^{(-)}$ and $\psi_a^{(+)}$ are the solutions of the Optical Model potentials. These potentials as used in DWUCK (Kunz, 1967) are written:

$$U(r) = U_c(r) + V (e^{x+1})^{-1} + i W_d \frac{d}{dx'} (e^{x+1})^{-1} \quad \text{A.13}$$

where $U_c(r)$ is the Coulomb potential and is

$$\begin{aligned} &= Z_A Z_a e^2 / r \quad \text{for } r > r_{oc} A^{1/3} \\ &= \frac{Z_A Z_a e^2}{(2r_{oc} A^{1/3})} \left[3 - \frac{r^2}{(r_{oc} A^{1/3})^2} \right] \quad \text{for } r < r_{oc} A^{1/3}, \end{aligned}$$

$$x = (r - r_o A^{1/3}) / a \quad \text{a is the diffuseness of the nuclear surface at radius } r_o A^{1/3},$$

W_d is the imaginary surface potential,

V is the volume potential (the maximum depth of the Wood-Saxon potential).

The Hamiltonian with the Optical Model potential (A.13) can be solved for the distorted wavefunctions by using a partial wave expansion:

$$\psi_a^{(\pm)}(kr) = \frac{4\pi}{k_a r_a} \sum_{L_a M_a} i^{\pm L_a} Y_{L_a M_a}^{L_a M_a}(\hat{r}_a) Y_{L_a M_a}^{L_a M_a^*}(\hat{k}_a) \chi_{L_a}(k_a r_a) \quad \text{A.14}$$

where χ_{L_a} is the radial wavefunction and a solution of:

$$\left[\frac{d^2}{dr^2} + k^2 + U(r) - \frac{L(L+1)}{r^2} \right] \chi_L = 0 \quad \text{A.15}$$

$$\text{and } \hat{r}_a = (\theta_{r_a}, \phi_{r_a}) \quad \hat{k}_a = (\theta_{k_a}, \phi_{k_a})$$

(See Bassel et al., 1962)

For the expansion of the distorted waves with a spin dependent potential, see Satchler (1964).

To evaluate $U_x^{j\ell}$, the bound state radial wavefunction of the transferred particle in the final nucleus (eqn. A.12), it is assumed that the interaction between the particle and the target nucleons can be treated as an average potential (an Extreme Shell Model approach). A Hartree-Fock approach to a self-consistent solution for $U_x^{j\ell}$ (a coupled channel calculation) is discussed by Pinkston and Satchler (1965). This approach was also taken by Rost (1967) to account for a deformed potential. In the usual method, $U_x^{j\ell}$ is evaluated as a solution to a Wood-Saxon potential with a Thomas spin-orbit term. The binding energy of the state in the well is determined from the Q-value of the reaction by:

$$B_{xA} = B_{bx} - Q \quad \text{A.16}$$

where B_{bx} is the binding energy of particle x in the projectile,

The Thomas spin-orbit term is given by $V_0 \frac{\lambda}{45.2} \frac{d}{dr} (e^X + 1) \vec{L} \cdot \vec{S}$

where λ is the factor required to describe the nuclear spin-orbit splitting,

and the other terms are the same as in A.13.

$U_x^{j\ell}$ is determined numerically. The potential well depth is varied until the calculated shape of the wavefunction within the well is matched to

the known exponential shape (determined by the binding energy B_{XA}) of the wavefunction outside the well. An outline of this procedure is found in the article by Buck and Hodgson (1961). N , the major oscillator quantum number (which is assumed to be good) is included in $U_x^{j\ell N}$ in order to determine the number of nodes in the radial wavefunction. It is usually chosen to be the same as that of the Shell Model state expected to be populated by a given j and ℓ transfer.

V_{bx} and ϕ_{bx} still remain to be evaluated in A.12. The usual potential and wavefunction used for the stripped particle in the incident projectile are those proposed by Hulthen and Sugawara (1957) (although the analysis has been done with considerably more sophisticated ones - Lim, 1969):

$$V_{bx}(r) = -\frac{\hbar^2}{2m} (\beta^2 - \alpha^2) e^{-\beta r} / (e^{-\alpha r} - e^{-\beta r}) \quad \text{A.18}$$

$$\phi_{bx}(r) = [(2\alpha\beta(\alpha+\beta))^{1/2} / (\beta-\alpha)] (e^{-\alpha r} - e^{-\beta r}) / r \quad \text{A.19}$$

where β and α are the short and long range parameters respectively of the nuclear potential, and can be determined from the properties of the excited and unbound states of particle a . This is considered in detail by Hering *et al.* (1970).

In principle, equation A.12 can now be evaluated. However, it is a six dimensional integral in r_a and r_b . The conventional simplification is the zero-range approximation, which assumes that for the interaction, the distance between b and x is zero. That is $V_{bx} \phi_{bx} = D \delta(r_{bx})$. Perhaps it is simpler to say that the other terms in A.12 vary sufficiently slowly so that the integral

$$D = \int V_{bx}(\vec{r}_{bx}) \phi_{bx}(\vec{r}_{bx}) d\vec{r}_{bx} \quad \text{A.20}$$

can be extracted to give:

$$S_{\ell sj}^{m_\ell} = D \chi_{\ell sj}^{m_\ell} = D \int \psi_b^{(-)}(\mathbf{r}) Y_{\ell m_\ell}(\theta_x) U_x^{j\ell N}(\mathbf{r}) \psi_a^{(+)}(\mathbf{r}) d\mathbf{r} \quad \text{A.21}$$

When the distorted waves are expressed in terms of the partial waves (A.14), the expression A.21 can be reduced to a number of one dimensional integrals of the form:

$$I_{L_A L_B}^{\ell} = \int \chi_{L_B} U_x^{j\ell N} \chi_{L_A} d\mathbf{r} \quad \text{where the angular terms}$$

which contain θ , the scattering angle, have been evaluated explicitly (Bassel et al., 1962). These expressions can be solved numerically.

A correction to the zero range approximation, which can simulate a finite range calculation (a six dimensional integration), can be made. It is based on the effective mass approximation, and consists of introducing a term $(1 + [(\alpha/\beta)^2/B_{bx}](U_a(\mathbf{r}) - U_b(\mathbf{r}) - U_x(\mathbf{r}) - B_{bx}))^{-1}$ into the integrand of equation A.21 (the U's are the various optical potentials, and B_{bx} , α and β have been defined previously). See Hering et al. (1970).

The cross section from A.11 can now be written:

$$\frac{d\sigma(\theta)}{d\Omega} = N \sum_{\ell s j} \frac{2J_B+1}{2J_A+1} \beta_{j\ell}^2 \frac{\sigma_{DW}^{\ell sj}(\theta) (2s+1)}{(2j+1) 2} \quad \text{A.23}$$

$$\text{where } \sigma_{DW}^{\ell sj}(\theta) = \frac{\mu_a \mu_b \dots k_a^2}{(2h^2)^2 k_b (2s+1)} \sum_{m_\ell} \frac{\chi_{\ell sj}^{m_\ell} (2j+1)}{(2\ell+1) (2s+1)}$$

and is the expression evaluated by DWUCK.

$N = v_x^2 D^2$, the normalization constant for the particular reaction. Its evaluation is discussed by Hering et al. (1970), but there does not seem to be a general agreement on the values obtained for complex particles by the various authors (eg. Kunz (1967) and Hering et al. (1970)).

REFERENCES

- Anderson, B. L., 1968. Nucl. Phys. A112, 443.
- Bardeen, J., Cooper, L. N., and Schrieffer, J. R., 1957. Phys. Rev. 106, 162.
- Bassel, R. H., Drisko, R. M., and Satchler, G. R., 1962. "The Distorted Wave Theory of Direct Nuclear Reactions", ORNL-3240.
- Bes, D. R., and Sorensen, R. A., 1969. Advances in Nuclear Physics. Eds. Baranger and Vogt, Plenum Press, N. Y.
- Blichert-Toft, P. H., Funk, E. G., and Mihelich, J. W., 1967. Nucl. Phys. A100, 369.
- Bohr, N., 1948. Mat. Fys. Medd. Dan. Vid. Selsk. 18, No. 8.
- Boyno, J. S., and Huizenga, J. R., 1972. Submitted to Phys. Rev. See also Annual Report, 1971, Nuclear Structure Research Laboratory, University of Rochester, 119.
- Brown, R. A., Roulston, K. I., Ewan, G. T., and Anderson, G. I., 1969. Can. J. Phys. 47, 1017.
- Bunker, M. E., and Reich, C. W., 1971. Rev. Mod. Phys. 43, #3, 348.
- Butler, S. T., Austern, N., and Pearson, C., 1958. Phys. Rev. 112, 1227.
- Chi, B. E., 1966. Nucl. Phys. 83, 97.
- Clarke, N. M., 1971. Nucl. Inst. and Meth. 96, 497.
- Davydov, A. S., 1966. "Quantum Mechanics", NEO Press, Ann Arbor, Michigan.
- Diamond, R. M., Elbek, B., and Stephens, F. S., 1963. Nucl. Phys. 43, 560.

- Elbek, B., 1963. "Determination of Nuclear Transition Probabilities by Coulomb Excitation", (Copenhagen) Thesis.
- Elbek, B., and Tjøm, P. O., 1969. Advances in Nuclear Physics, Eds. Baranger and Vogt (Plenum Press, N. Y.)
- Evans, R. D. E., 1955. "The Atomic Nucleus", McGraw-Hill, New York.
- French, J. B., Halbert, E. C., McGrory, J. B., and Wong, S. S. M., 1969. Advances in Nuclear Physics, Eds. Baranger and Vogt (Plenum Press, N. Y.)
- Funke, L., Graber, H., Kaun, K.-H., Sodan, H., Werner, L., and Frana, J., 1966. Nucl. Phys. 84, 449. (Levels in ^{157}Tb)
- Funke, L., Graber, H., Kaun, K.-H., Sodan, H., and Frana, J., 1966. Nucl. Phys. 84, 471. (Levels in ^{163}Ho)
- Geiger, J. S., and Graham, R. L., 1967. Can. J. Phys. 45, 2281.
- Gell-Mann, M., and Goldberger, M. L., 1953. Phys. Rev. 124, 1496.
- Glendenning, N. K., 1963. Ann. Rev. Nucl. Science 13, 191.
- Goles, R., 1971. Annual Report of the Michigan State University Cyclotron Laboratory, 55.
- Gustafson, C., Lamm, I. L., Nilsson, B., and Nilsson, S. G., 1967. Ark. Fysik 36, nr. 69.
- Harmatz, B., 1972. Private communication; to be published.
- Hering, W. R., Becker, H., Wiedner, C. A., and Thompson, W. J., 1970. Nucl. Phys. A151, 33.
- Hill, J. C., and Wiedenbeck, M., 1968. Nucl. Phys. 111, 457.
- Hjorth, S. A., Saladin, J. X., and Satchler, G. R., 1965. Phys. Rev. 138, B1425.

- Hooper, M. B., 1966. Nucl. Phys. 76, 449.
- Hulthén, L., and Sugawara, M., 1957. Handb. Physik, Ed. S. Flügge, Springer, 1.
- Jursik, J., Hnatowicz, V., and Zvolsky, J., 1969. Czech. J. Phys. 19B, 870.
- Kunz, P. D., 1967. University of Colorado, Computer Program DWUCK, unpublished.
- Løvholden, G., Hjorth, S. A., Ryde, H., and Harms-Ringdahl, L., 1972 Nucl. Phys. 181, 589.
- Lewis, T., and Graetzer, R., 1971. Nucl. Phys. 162, 145.
- Lim, T. K., 1969. Nucl. Phys. 129, 259.
- Lu, M., and Alford, W. P., 1971. Phys. Rev. C3, 1243.
- Meredith, J. O., and Barber, R. C., 1972. Can. J. Phys. 50, 1195.
- Messiah, A., 1966. "Quantum Mechanics", North-Holland Publishing Company, Amsterdam.
- Nilsson, S. G., 1955. Mat. Fys. Medd. Dan. Vid. Selsk. 29, #16.
- Ogle, W., Wahlborn, S., Piepenbring, R., and Fredriksson, S., 1971. Rev. Mod. Phys. 43, 424.
- O'Neil, R. A., Burke, D. G., and Alford, W. P., 1971. Nucl. Phys. A167, 481.
- O'Neil, R. A., 1970. Private Communication.
- Persson, L., and Ryde, H., 1964. Arkiv Fysik 25, 397.
- Pinkston, W. T., and Satchler, G. R., 1965. Nucl. Phys. 72, 641.
- Preston, 1963. "Physics of the Nucleus", Addison-Wesley, Reading, Mass.
- Price, R. H., Burke, D. G., and Johns, M. W., 1971. Nucl. Phys. A176, 338.

- Rost, E., 1967. Phys. Rev. 154, 994.
- Satchler, G. R., 1964. Nucl. Phys. 55, 1.
- Seaman, G. G., Bernstein, E. M., and Palms, J. M., 1967. Phys. Rev. 161, 1223.
- Smith, W. R., 1967. Nucl. Phys. A94, 550.
- Soloviev, V. G., and Vogel, P., 1967. Nucl. Phys. 92, 449.
- Soloviev, V. G., and Fedotov, S. I., 1971. Preprint E4-6055, Joint Institute for Nuclear Research, Dubna.
- Spencer, J. E., and Enge, H. A., 1966. Nucl. Instr. and Meth. 49, 181.
- Stock, R., Bock, R., David, P., Duhm, H., and Tamura, T., 1967. Nucl. Phys. 104, 136.
- Tippett, J. C., and Burke, D. G., 1972. Submitted to Can. J. Physics.
- Ungrin, J., and Johns, M. W., 1969. Nucl. Phys. A127, 353.
(Decay scheme studies of ^{153}Eu)
- Ungrin, J., Sujkowski, Z., and Johns, M. W., 1969a. Nucl. Phys. A123, 1. (Decay scheme studies of ^{155}Eu)
- Ungrin, J., Burke, D. G., Johns, M. W., and Alford, W. P., 1969b. Nucl. Phys. A132, 322. ($^3\text{He},d$) reaction studies into ^{153}Eu and ^{155}Eu)
- Ungrin, J., 1969. Ph.D. Thesis, McMaster University.
- Wapstra, A. H., and Gove, M. B., 1971. Nuclear Data Tables, Vol. 9, # 4 and 5.
- Westgaard, L., and Bjørnholm, S., 1966. Nucl. Instr. and Meth. 42, 77.
- Williamson, C. F., Boujot, J. P., and Picard, J., 1966. "Tables of Range and Stopping Power of Chemical Elements for Charged

Particles of Energy 0.05 to 500 MeV", Report CEA-R 3042,
Commissariat à l'Energie Atomique - France.

Winter, G., Funke, L., Kaun, K.-H., Kemnitz, P., and Sodan, H.,
1971. Nucl. Phys. A176, 609.

Zylicz, J., Hansen, P. O., Nielsen, H. L., and Wilsky, K., 1966.
Nucl. Phys. 84, 13.